

# Numerical Approximation of Dynamic Models for Special Relativistic Flows



*By*

*Tayabia Ghaffar*

**Department of Mathematics  
Quaid-i-Azam University  
Islamabad, Pakistan  
2019**

# Numerical Approximation of Dynamic Models for Special Relativistic Flows



ISLAMABAD

*By*

*Tayabia Ghaffar*

*Supervised By*

*Prof. Dr. Shamsul Qamar*

Department of Mathematics, COMSATS Institute of Information Technology,  
Park Road, Chak Shahzad, Islamabad, Pakistan

and

*CO-Supervised By*

*Prof. Dr. Muhammad Ayub*

**Department of Mathematics**

**Quaid-i-Azam University**

**Islamabad, Pakistan**

**2019**

# Numerical Approximation of Dynamic Models for Special Relativistic Flows



ISLAMABAD

By  
*Tayabia Ghaffar*

A DISSERTATION SUBMITTED IN THE PARTIAL FULFILLMENT OF THE  
REQUIREMENT FOR THE DEGREE OF  
DOCTOR OF PHILOSOPHY  
IN  
MATHEMATICS

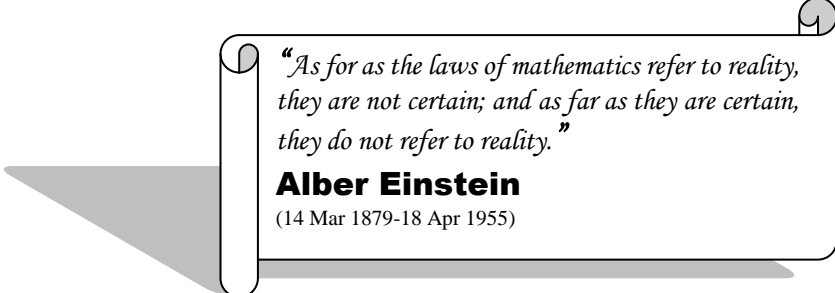
*Supervised By*  
*Prof. Dr. Shamul Qamar*

Department of Mathematics, COMSATS Institute of Information Technology,  
Park Road, Chak Shahzad, Islamabad, Pakistan

and

*Co-Supervised By*  
*Prof. Dr. Muhammad Ayub*

**Department of Mathematics**  
**Quaid-i-Azam University**  
**Islamabad, Pakistan**  
**2019**



*“As for as the laws of mathematics refer to reality,  
they are not certain; and as far as they are certain,  
they do not refer to reality.”*

**Alber Einstein**

(14 Mar 1879-18 Apr 1955)

## Dedication:

This work is dedicated to my husband and teacher.

## **Author's Declaration**

I, **Tayabia Ghaffar** hereby state that my PhD thesis titled "**Numerical Approximation of Dynamic Models for Special Relativistic Flows**" is my own work and has not been submitted previously by me for taking any degree from the Quaid-i-Azam University Islamabad, Pakistan or anywhere else in the country/world.

At any time if my statement is found to be incorrect even after my graduate the university has the right to withdraw my PhD degree.

Name of Student: **Tayabia Ghaffar**

Date: **02-07-2019**

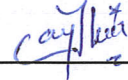
## **Plagiarism Undertaking**

I solemnly declare that research work presented in the thesis titled "**Numerical Approximation of Dynamic Models for Special Relativistic Flows**" is solely my research work with no significant contribution from any other person. Small contribution/help wherever taken has been duly acknowledged and that complete thesis has been written by me.

I understand the zero tolerance policy of the HEC and **Quaid-i-Azam University, Islamabad** towards plagiarism. Therefore, I as an Author of the above titled thesis declare that no portion of my thesis has been plagiarized and any material used as reference is properly referred/cited.

I undertake that if I am found guilty of any formal plagiarism in the above titled thesis even afterward of PhD degree, the University reserves the rights to withdraw/revoke my PhD degree and that HEC and the University has the right to publish my name on the HEC/University Website on which names of students are placed who submitted plagiarized thesis.

Student/Author Signature: \_\_\_\_\_

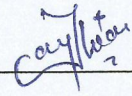


Name: **Tayabia Ghaffar**

## Certificate of Approval

This is to certify that the research work presented in this thesis entitled "Numerical Approximation of Dynamic Models for Special Relativistic Flows" was conducted by Miss. Tayabia Ghaffar under the supervision of Prof. Dr. Shamsul Qamar and co-supervised by Prof. Dr. Muhammad Ayub. No part of this thesis has been submitted anywhere else for any other degree. This thesis is submitted to the Department of Mathematics, Quaid-i-Azam University, Islamabad in partial fulfillment of the requirements for the degree of Doctor of Philosophy in Field of Mathematics from Department of Mathematics, Quaid-i-Azam University Islamabad, Pakistan.

Student Name: Tayabia Ghaffar

Signature: 

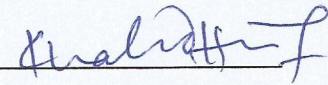
### Viva Voce Examination Committee:

a) External Examiner 1:

Name: Dr. Khalid Hanif

Designation: Assistant Professor

Post-graduate Federal Govt. College (Men) Sector H-8, Islamabad.

Signature: 

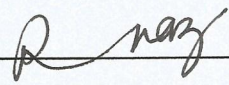
b) External Examiner 2:

Name: Dr. Rahila Naz

Designation: Assistant Professor

Department of Humanities and Sciences,

Institute of Space Technology, Islamabad 44000, Pakistan.

Signature: 

c) Internal Examiner :

Name: Dr. Muhammad Ayub

Designation: Professor

Office Address: Department of Mathematics, QAU Islamabad.

Signature: 

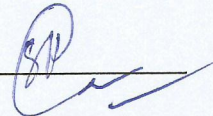
Supervisor Name:

Name: Dr. Shamsul Qamar

Designation: Professor

Office Address: Department of Mathematics,

COMSATS Institute of Information Technology, Chak Shahzad, Islamabad.

Signature: 

Co-Supervisor Name:

Dr. Muhammad Ayub

Signature: 

Name of Dean/ HOD

Prof. Dr. Sohail Nadeem

Signature: 

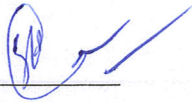
# Numerical Approximation of Dynamic Models for Special Relativistic Flows

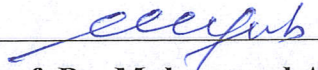
By  
**Tayabia Ghaffar**

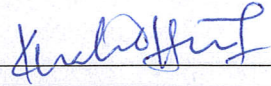
## *Certificate*

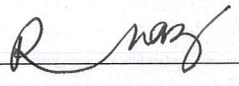
A THESIS SUBMITTED IN THE PARTIAL FULFILLMENT OF THE REQUIREMENT  
FOR THE DEGREE OF THE DOCTOR OF PHILOSOPHY  
IN  
MATHEMATICS

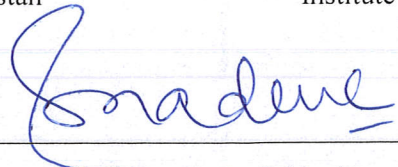
**We accept this dissertation as conforming to the required standard.**

1.   
**Prof. Dr. Shamul Qamar**  
(Supervisor)  
Department of Mathematics,  
COMSATS Institute of Information Technology  
Park Road Chak Shahzad, Islamabad, Pakistan

2.   
**Prof. Dr. Muhammad Ayub**  
(Co-Supervisor)  
Department of Mathematics,  
Quaid-i-Azam University, Islamabad

3.   
**Dr. Khalid Hanif**  
(External Examiner)  
Post-graduate Federal Govt. College (Men)  
Sector H-8, Islamabad, Pakistan

4.   
**Dr. Rahila Naz**  
(External Examiner)  
Department of Humanities and Sciences,  
Institute of Space Technology, Islamabad.

5.   
**Prof. Dr. Sohail Nadeem**  
(Chairman)

**Department of Mathematics  
Quaid-i-Azam University  
Islamabad, Pakistan  
2019**



# *Acknowledgements*

*All the praises and appreciations are for the omnipotent Allah, the most merciful and generous that knows better the hidden truths of the universe, and the Holy Prophet Muhammad (PBUH) who declared it an obligatory duty of every Muslim to seek and acquire knowledge.*

*I am highly obliged to every person who blessed me with knowledge and support for carrying out this research work. My love and wishes for my parents and my family members without whom I would not have been able to carry out this task. No words can express my deepest gratitude for them.*

*I am really thankful to my supervisor Prof. Dr. Shamsul Qamar, Department of Mathematics, COMSATS Institute of Information Technology, Islamabad, for giving me valuable suggestions, extraordinary experience and support with patience throughout the work. He will always be an inspiration for me.*

*I offer my sincerest gratitude to my co-supervisor Prof. Dr. Muhammad Ayub, who has supported me throughout my research work. I am indebted to him more than he knows. My respect and thanks to the chairman of the department Prof. Dr. Tasawar Hayat, for the facilitations and support.*

*I am thankful to Dr. Muhammad Yousaf, Dr. Muhammad Ishtiaq for his sincere guidance to complete this thesis. I am also trying to acknowledge all my fellows for their help and support.*

*In the last but not least, my parents deserve special mention for their inseparable support and prayers. I would like to pay my gratitude and thanks to my husband for love, care and support in one and the other ways, my sisters and brother for their prayers, support and encouragement.*

***May Allah bless all those who pray for me (Aamin)***

*Tayabia Ghaffar*

*Date: July 02, 2019.*

# PREFACE

This thesis is mainly focused on numerical approximations of the special relativistic hydrodynamic flow models using the central upwind scheme. In recent years, relativistic hydrodynamic models have played a pivotal role in many fields such as nuclear collisions of high energy, astrophysics, laser technology, etc. The precise modeling of numerous features of the high energy in astrophysical phenomenon involves the evaluation of the Einstein theory simultaneously with those of special relativistic hydrodynamic (SRHD) equations. Such numerical models seems to be more complex rather than the nonrelativistic because of nonlinearity relation between the conserved and the primitive quantities. The main goal of the thesis project is to establish a very simple, reliable and efficient numerical techniques in order to solve the special relativistic hydrodynamic (SRHD) and the ultra-relativistic hydrodynamic (URHD) equations. Both single and multi-component flows are considered. A high-resolution shock-capturing central upwind schemes are extended and then applied for solving the governing sets of equations. The proposed numerical algorithm utilizes the accurate information of locally propagating speeds to minimize numerical diffusions in the solutions. This scheme provides the second-order accuracy by applying the MUSCL type reconstruction as well as Runge-Kutta (RK) time step method. After discussing the model equations and solution technique employed, a series of one and two-dimensional numerical test problems are conducted. In order to validate the capability of suggested method and its accuracy, the staggered central (NT) and the kinetic flux vector splitting (KFVS) schemes are also implemented on the equations of same model. Where it is observed that the suggested scheme is robust with less error accuracy as compared to those schemes available in the literature having the sooth algorithms, even in the case of highly-relativistic

two-space dimensional numerical test problems. The major part of this thesis is organized by the following approach.

The first chapter of this thesis provided the historical background that inspire me to work on this project. The relativistic hydrodynamics (RHD) simulations have a key role in the astrophysical system to understand the actual mechanism. The importance and uses of these hydrodynamics models which lead towards efficiency and accuracy of various schemes e.g., special relativistic hydrodynamics (SRHD) models are presented in this chapter. The schemes such as the staggered central and central upwind are proposed to numerically execute the special relativistic hydrodynamic model equations. Anticipated numerical achievements of proposed schemes are pointed out in this portion of thesis.

Here, the portion gives a brief overview of the state and the conservative formulation techniques of flow models, weak solutions, hyperbolic systems of conservation laws, Riemann problem and nonrelativistic sets of Euler equations. A brief description of relativistic hydrodynamic models in the historical background is also provided in chapter two.

The backgrounds of special relativistic hydrodynamic(SRHD) flow models are presented in chapter three. The one and two-dimensional central upwind methods are successfully implemented to estimate the flow model equations. Many test problems are provided by this chapter. The numerical solutions of the central upwind scheme are analyzed with the exact solutions as well as with the solutions obtained from central and kinetic flux vectors splitting schemes in details. Graphical results and the error analysis are also presented. The major findings of chapter three have been published in **International journal of *PLOS ONE*, 10 (2015): e0128698.**

Chapter four is deal with the approximate solutions of the ultrarelativistic hydrodynamic

(URHD) models for single and two-space dimension. The scheme of central upwind is proposed in order to approximate the modeled equations. For validation, complicated numerical test cases are carried out. The numerical solutions as well as graphical presentation of the central upwind schemes are analyzed with the available limited results of KFVS and central schemes. The main conclusions of chapter four have been published in *Results in Physics*, **9** (2018) 1161-1169.

In chapter five, we extend the Euler equations for special relativistic flow to multi-component flow. The central (NT) schemes are implemented to solve for single and two space dimensions models of relativistic multi-component flows. Several numerical problems of RHD model are presented to illustrate the higher accuracy, reliability and efficiency of designed schemes are considered here. In order to understand the results various graphical figures are depicted in this chapter. Furthermore, the key points of the current chapter have been published in *Applied Mathematics*, **5** (2014) 1169-1186.

Chapter six finalizes the thesis by summarizing the obtained results and gives outlook to the future work.

Chapter seven contains the cited references that have been published in various authentic international Journals.

# TABLE OF CONTENTS

<b>1</b>	<b>Introduction</b>	<b>1</b>
1.1	Problems and Motivations . . . . .	2
1.2	The RHD Codes Review . . . . .	3
1.3	The Numerical Challenges . . . . .	5
1.4	The Proposed Techniques . . . . .	5
1.4.1	Staggered Central Schemes . . . . .	6
1.4.2	Central Upwind Schemes . . . . .	7
1.4.3	The KFVS Method . . . . .	8
1.5	The Project Achievements . . . . .	9
<b>2</b>	<b>Preliminaries</b>	<b>11</b>
2.1	The Conservation Laws . . . . .	12
2.2	The Hyperbolic Law of Conservation . . . . .	13
2.3	Laws of Conservation for Weak Solution . . . . .	15
2.4	The Non-relativistic Euler Equation . . . . .	16

2.5	The Riemann Problem . . . . .	20
2.6	The Gas Dynamics . . . . .	20
2.6.1	The Perfect Gas . . . . .	21
2.6.2	Compressible Flows . . . . .	21
2.6.3	The Mach Number . . . . .	21
2.7	Special Relativity . . . . .	21
2.7.1	The Metric Tensor . . . . .	22
2.7.2	Lorentz Transformations . . . . .	22
2.7.3	Vectors and Tensors . . . . .	23
2.7.4	Four-Velocity . . . . .	24
2.7.5	The Tensor for Stress Energy . . . . .	24
<b>3</b>	<b>The Central Upwind Scheme for SRHD Model</b>	<b>26</b>
3.1	Derivation of SRHD Equations . . . . .	27
3.1.1	Recovery of Primitive Variables . . . . .	29
3.2	Numerical Scheme . . . . .	31
3.2.1	The One-dimensional Central Upwind Scheme . . . . .	32
3.2.2	The two-dimensional Central Upwind Schemes . . . . .	34
3.3	The Numerical Tests . . . . .	36
3.3.1	The One-dimensional Problems . . . . .	36

3.3.2	The Two-dimensional Problems . . . . .	44
3.4	Summary . . . . .	58
<b>4</b>	<b>The Central Upwind Scheme for URHD Model</b>	<b>59</b>
4.1	The Ultra-relativistic Hydrodynamics (URHD) . . . . .	60
4.2	Central Upwind Schemes . . . . .	62
4.3	Central Schemes(NT) . . . . .	64
4.4	The KFVS Method . . . . .	66
4.5	MUSCL-Type Reconstruction Method . . . . .	68
4.6	Numerical Tests . . . . .	69
4.6.1	One-dimensional Problems . . . . .	69
4.6.2	Two-dimensional Problems . . . . .	78
4.7	Summary . . . . .	88
<b>5</b>	<b>The Central Scheme (NT) for Relativistic Flow Model</b>	<b>89</b>
5.1	Mathematical Formulation . . . . .	91
5.2	Numerical Scheme . . . . .	95
5.2.1	One-dimensional Central Schemes . . . . .	96
5.2.2	Two-dimensional Central Schemes . . . . .	100
5.3	Numerical Tests . . . . .	108

5.3.1	One-dimensional Problems . . . . .	109
5.3.2	Two-dimensional Problems . . . . .	113
5.4	Summary . . . . .	121
<b>6</b>	<b>Conclusions</b>	<b>122</b>
6.1	Evaluation of The Methods . . . . .	123
6.2	Future Considerations . . . . .	125
<b>7</b>	<b>References</b>	<b>126</b>



## List of Figures

3.1	Comparison of $L^1$ -errors. . . . .	38
3.2	Comparison at $t = 0.4$ for the shock problem-I. . . . .	40
3.3	Comparison at $t = 0.35$ for the shock test problem-II. . . . .	41
3.4	Comparison at $t = 0.35$ for the relativistic-shock test problem. . . . .	43
3.5	Comparison of $L^1$ -errors. . . . .	45
3.6	Comparison at $t = 0.4$ for $400 \times 400$ mesh cells. . . . .	47
3.7	Results at $t = 0.4$ for the shock test problem. . . . .	48
3.8	The representation for initial data. . . . .	49
3.9	Results at $t = 1.7$ for diffracting the shock waves test problem. . . . .	50
3.10	Comparison at $t = 1.7$ for $300 \times 300$ mesh cells. . . . .	51
3.11	Comparison at $t = 0.2$ at $200 \times 200$ mesh cells. . . . .	53
3.12	Results at $t = 0.2$ for the cylindrical blast test problem. . . . .	54
3.13	Comparison at $t = 1.0$ for $400 \times 400$ mesh cells. . . . .	55
3.14	The results at $t = 1$ for explosion in the box. . . . .	56
3.15	The results at $t = 2$ for explosion in the box. . . . .	57

4.1	Comparison of $L^1$ -errors. . . . .	71
4.2	Comparison at $t = 0.45$ for the shock test problem-I. . . . .	73
4.3	Comparison at $t = 0.5$ for the shock test problem-II. . . . .	75
4.4	Comparison at $t = 0.5$ for the perturbed relativistic shock test problem. . .	77
4.5	Comparison of $L^1$ -errors. . . . .	79
4.6	Results at $t = 0.20$ for the cylindrical blast problem. . . . .	81
4.7	Comparison at $t = 0.2$ for $200 \times 200$ mesh cells. . . . .	82
4.8	Results at $t = 3.0$ for explosion in the box. . . . .	84
4.9	Comparison at $t = 3.0$ for $300 \times 300$ mesh cells. . . . .	85
4.10	Results at $t = 0.5, 1.0, 2.0$ (from top to bottom) for the shock bubble inter- action. . . . .	87
4.11	Comparison at $t = 1.0$ for $300 \times 300$ mesh cells. . . . .	88
5.1	Second-order reconstruction . . . . .	98
5.2	Floor plane of staggered grid. . . . .	102
5.3	The stencil of staggered central scheme. . . . .	102
5.4	Comparison results at 400. mesh cells (dash line) versus 4000. mesh cells (solid line) when $t = 0.40$ . . . . .	110
5.5	Comparison result on 400. mesh cells (dashed line) versus 4000. mesh cells (solid line) at $t = 0.350$ . . . . .	112

5.6	Result at $t = 0.15$ for the cylindrical blast problem. . . . .	114
5.7	Comparison results on 400. mesh cells (dashed line) versus 4000. mesh cells (solid line) at the time $t = 0.7$ . . . . .	116
5.8	Results of heliumbubble interaction at different times. . . . .	117
5.9	Computational domain for the shock wave. . . . .	118
5.10	Results of explosion in the box at different times. . . . .	120

## List of Tables

3.1	Comparative numerical results of $L^1$ -errors associative with EOC. . . . .	38
3.2	Comparative numerical results of $L^1$ -errors associative with EOC. . . . .	45
4.1	Comparative numerical results of $L^1$ -errors associative with EOC. . . . .	71
4.2	Comparative numerical results of $L^1$ -errors associative with EOC. . . . .	79

## List of Abbreviations

<i>Name with Detail</i>	
BGK	Boltzmann gas kinetic
CE/SE	Conservation element and solution element
CFL	Courant Friedrichs and Lewy
EOC	Experimental order of convergence
EOS	Equation of state
KFVS	Kinetic flux vector splitting method
LxF	Lax-Friedrich
MHD	Magnetohydrodynamics
MM	Min-Mod (a nonlinear limiter)
MUSCL	Monotone upwind-centered scheme for the conservation laws
NT	Nessyahu and Tadmor
PDEs	Partial differential equations
RHD	Relativistic hydrodynamics
RK	Runge-Kutta
SRHD	Special relativistic hydrodynamics
TVD	Total variation diminishing
URHD	Ultra-relativistic hydrodynamic

## List of Symbols

<i>Symbol's name</i>	
$\vec{A}$	Flux vector
$\vec{A}^i$	Components of flux vector
$\mathcal{A}$	Free transport flux function
$\vec{C}$	Vector of conserved variables
$D$	Rest-mass densities
$C_m$	Components of conserved variables
$c$	Speed of light
$c_s$	Sound speed
$E$	Total specific energy
$e$	Specific energy
$\epsilon$	Internal energy
$g_{\mu\nu}$	Metric tensor
$M$	Momentum
$M_a$	Mach number
$N^\mu$	Mass flux vector
$p$	Pressure
$q^\mu$	Four-momentum
$S$	Surface of arbitrary volume
$T$	Temperature
$T^{\mu\nu}$	Energy-momentum tensor
$t$	Time coordinate
$u^\mu$	Four-velocity
$V$	Arbitrary volume
$v$	Velocity
$v^i$	Spatial velocity components
$x^\mu$	Four-vector

<i>Greek</i>	
$\rho$	Density
$\tau$	Energy density
$\omega$	Ratio of the specific heat
$\omega$	Lorentz factor
$\delta^{ij}$	Knocker delta
$\Gamma$	Adiabatic constant
$\lambda$	Eigen value

# Chapter 1

## Introduction

## 1.1 Problems and Motivations

Like climatology and weather prediction, astrophysics is a field of science in which observations are easily done but direct experiments are difficult to perform. Thus, instead of direct experiments, computer simulations are performed to understand the dynamics of different astrophysical phenomena. A relativistic strategy is essential for modeling high-energy astrophysical phenomena, leading to the introduction of relativistic hydrodynamical models to simulate such high-speed flows. These models have been used to study the dynamics of (a) high energy particles, such as gamma ray bursts, accretion flows, and jets flows [1, 2] (b) dynamics of dense stars and movements of objects around the black holes [3], and (c) cosmology [4]. It is important to mention that for the simulation of phenomena in (a) the theory of the special relativity is sufficient, while theory of general relativity is required for the simulation of phenomena in (b) and (c). In a special relativistic fluid dynamic theory follows the Einstein's law for the special relativity, i.e., considered fluid evolves within the Minkowski flat spacetime that ignores the gravitational effects. While on the other hand, in a case of general relativistic hydrodynamics, the contribution of gravitational acceleration has to be incorporated. Special relativistic hydrodynamic (SRHD) models can also be used in order to simulate high-energy particle beam, freely moving electron laser technologies and the heavy ion collision [5]. In the special relativistic hydrodynamics, ultrarelativistic (UR) limit may be acquired in the case of a small rest-mass density, or at high temperature. In this case, the characteristic of a fluid velocities are much nearest to speed of light therefore rest mass density can be ignored. The dynamics of ultrarelativistic code is employed to model the axisymmetric accretion flows around the black hole [6]. Thus, an effective way of improving our knowledge about the actual mechanisms taking place in



these astrophysical systems is due to relativistic hydrodynamics (RHD) simulations. The governing equations of these models are strongly nonlinear, the space and time are intrinsically coupled, and solutions can become singular through the formation of shock waves and geometric singularities. The present study is emphasis onto the numerical approximation of the special relativistic hydrodynamics (SRHD) models only.

The special relativistic hydrodynamic models contain complex systems of nonlinear and strictly hyperbolic partial differential equations (PDEs). For the experimental tests, it is much complicated to resolve these PDEs analytically. Thus, numerical solution techniques are perused. In the literature, several numerical schemes have been reported for solving relativistic hydrodynamic models [7]. All these schemes are usually developed out from the existing authentic numerical schemes for the approximated solutions of the non-relativistic (classical) Euler's equations for fluid (gas) dynamics [8, 9, 10].

## 1.2 The RHD Codes Review

The role of relativistic hydrodynamics (RHD) is very dominant in various disciplines of physics, such as nuclear physics, astrophysics, and cosmology. The necessity to model relativistic flows, which incorporate strong shocks waves, has stimulated the development of RHD codes. The earliest code that provides the solution of relativistic hydrodynamics equations for Eulerian grids was presented by Wilson and his co-workers [7, 11, 12, 13, 14]. This code is build on explicit finite differencing methods (FDM) that discretizes the convection part of RHD equations followed by the monotonic transport procedure. The stability of code across the shocks wave was efficiently handled by Von Neumann and Richtmyer [15] by using the technique of artificial viscosity. This technique has been

extensively utilized in the numerical cosmology, accretion onto compact objects, relativistic stellar core collapse and heavy ions collisions. Despite its popularity, the accuracy of the code decreases when the Lorentz factor becomes higher, i.e. when the flow is extremely relativistic [16]. In order to overcome the numerical complications in the ultra-relativistic limit, Norman and Winkler [16] have presented an implicit treatment for equations. The numerical techniques were designed for the approximations of nonlinear conservative laws [17]. The single-dimensional scheme, that was based on the exact Riemann-solver, firstly introduced very early by Martí with the coordination of Müller [18] for approximating RHD equations which was afterwards extended to multi-dimensional case. Here, the thesis project. it is constructed and analyze numerical solution techniques for the SRHD and URHD models to overcome various numerical complexities that are associated along these model techniques.

The members of our research group have also contributed to the development numerical codes for solving special relativistic hydrodynamic (SRHD) models. They have extended different high resolution central and upwind finite volume schemes for solving SRHD models. In these high value schemes, the cells interface fluxes were obtained by using either gas-kinetic theory, exact Riemman solvers, or approximate Rieman solvers. The investigate numerical schemes include the gas-kinetic schemes [19, 20, 21], the staggered (NT) schemes [22, 23], the central upwind schemes [24, 25], the space time solution elements and the conservative elements methods [26, 27], and the upwind finite-volume schemes [28]. Moreover, they have also used the finite element method for discontinuous Galerkin in order to solve the single dimension special relativistic hydrodynamic and magneto-hydrodynamic models [29, 30]. The current research work further extends the aforementioned studies of our research towards the advancement of efficient, accurate, and reliable numerical schemes for

solving SHRD equations.

### **1.3 The Numerical Challenges**

Numerous challenges can be faced in the procedure for build the robust, precise and efficient numerical algorithms to approximate SRHD equations. Firstly, in a relativistic case, Euler equations are more complex as compared with the nonrelativistic Euler's equations for the gas dynamics due to intrinsic coupling of the space with time. Secondly, the RHD models are highly nonlinear and contain strictly hyperbolic PDEs, leading to the development of strong shock wave. Thirdly, the RHD simulations are even more complex due to the flows that are near to the speed of light and the nonlinear combinations between the conserved and the primitive variables. Thus, to explore the hidden behaviors of relativistic fluid flows, highly robust, accurate and efficient numerical solution techniques are needed. The developed numerical schemes should be stable and robust enough to allow the smooth transition of strong shock waves. The numerical schemes introduced in this thesis project overcome all such difficulties. They have ability to capture the sharp changes efficiently in the numerical solutions and give correct positions of the discontinuities (shocks).

### **1.4 The Proposed Techniques**

Here, in this thesis project, central upwind technique and the central (NT) technique are numerically executed for the approximated solution of special relativistic hydrodynamic model equations. Achievements of proposed numerical schemes are studied through their ability to solve the complicated test problems. Further, the results provided by suggested schemes are analyzed with those results that are available in literature.

### 1.4.1 Staggered Central Schemes

The first ordered (staggered) Lax-Friedrichs (LxF) scheme [31] is developed on piecewise constant approximation. The high resolutions nonoscillatory numerical schemes were presented by the Nessyahu and the Tadmor, named NT schemes [22] and extended by Jiang and Tadmor [23]. These schemes are used to approximate the special relativistic hydrodynamics Euler's equations for single and the two-space dimension. These numerical schemes have implemented to resolve the problems numerically in the fluid mechanics, metrology, astrophysical medeling, shallow flows, semiconductors and as well as multicomponent flows models [20, 25, 32, 33, 34].

The central schemes are developed on predictor-corrector technique that based on two main steps. In the very first step, the algorithm starts with the known values of cell averages then it is applied to the nonoscillatory piecewise (linear) reconstruction in order to predict point values. Whereas in a final corrector step, realizing the evolution of these predicted mid point values of reconstructed polynomial in term of their staggered cell averages. The central schemes does not require characteristic decomposition and Riemann solver which makes them stable, reliable, simple and efficient. The proposed schemes of second-order accuracy are depend on MUSCL-type reconstructions. The numerical results of second-order and staggered central schemes are presented in [22, 23] and will also apply in our RHD models. The staggered central (NT) schemes are formulated to investigate SRHD and URHD models for comparability and validity. Currently, a very few numerical schemes are available to evaluate the relativistic hydrodynamics models equations.

## 1.4.2 Central Upwind Schemes

Here, in this thesis, the central upwind schemes that are introduced and formulated by the Kurganov and the Tadmor [35] for classical Euler equations, are extended to approximate single and two-dimensional (2D) SRHD and the URHD flow models. These model techniques have employed on various problems in the literature to solve different models, for instance to approximate the equations of double layer shallow water [28] and Hamilton Jacobi equations [24]. The central upwind schemes use single-sided local speed of propagation and approximates the solution in the form of computational cell averages. Moreover, the schemes have an upwind behavior, because it deals with the local speeds of propagating flow in one-side that make it universal, simple and more efficient. There is no characteristic decomposition involved and the Riemann solvers is not needed as well. These numerical methods are conservative and serve in a very natural way that provides the characteristics essential for the effectiveness, such as higher order accuracy, efficient to capture the sharp discontinuities with stability, and converge to exact numerical solution. Utilizing the MUSCL type linear reconstruction scheme and the Runge-Kutta (RK) time stepping technique, the second order accuracy of suggested scheme has obtained. This scheme is better in accuracy as compared to other schemes [22, 23]. The robustness and the efficiency of purposed schemes are illustrated by numerically. The approximated evaluation of the central upwind schemes are analyzed by comparing them with the results of central (NT) [22, 23] and as well as with the KFVS schemes [19, 20, 21, 36].

### 1.4.3 The KFVS Method

Statistical mechanics, the branch of physics focuses on equilibrium distribution for the systems having indistinguishable particles. Bose-Einstein, Maxwell-*Boltzman*, Jüttner and Fermi-Dirac distribution are its four basic examples [37, 38]. Among these, Maxwell-*Boltzman* is employed these static for a classical mechanics model, Bose-Einstein and Fermi Dirac are applied for the quantum mechanical model, and Jüttner distribution applies in relativistic models. Being specific about classical gas dynamic theory, Maxwell-*Boltzman* distribution has been most relevant. The moment of the Maxwellian phase densities are the essential elements for the description of constitutive relation, and also for estimating the numerical fluxes at interfaces of cell. This defines the kinetic schemes depend on the transport equations. Deshpande was the pioneer of the KFVS scheme [39, 40]. The scheme was a consequences of kinetic flux theory depends on the fluids in the class scheme for a compressible classical Euler equation. Moreover, Pulline's equilibrium method for flux [41] and the Rietz kinetic technique [42] are two of the variants of this scheme. Parthene [43] extended to modified the scheme by using the characteristic function, rather than distribution of Maxwellian function. The flux function of explicit based on collisionless Boltzmann equation of kinetic scheme makes it similar to van Leer approach. This feature is regarded as one of the important characteristic of this scheme [40]. Croisille *et. al.* formulated a KFVS scheme for an ideal MHD [44]. Further developments were brought to the gas kinetic scheme by Xu [45] and Tang Xu [36], who used BGK type solver, a modified version made up of particle of collisions at the cell interfaces. Kunik [19] emulated this method to effect the ultrarelativistic Euler equation by applying relativistic Jüttner distribution [37]. This technique was later introduced in the field of special relativistic

hydrodynamics by Qamar and Warnecke [21]. In the process, positive numeric values of the pressure and energy density are maintained by kinetic scheme, while approximating the Euler equation for the gas dynamical model [46]. Here, in the thesis KFVS schemes were implemented to demonstrate the nonlinear equations of SRHD and URHD. The schemes have comparable results for discontinuous solutions.

## 1.5 The Project Achievements

The thesis consists of a numerical simulation for the special relativistic hydrodynamic model equations and multi-component flows. The relativity theory of Einstein in which the gravity acceleration effects are ignored is known as the special theory of relativity. In high energy astrophysics, special relativistic flows and shocks have played a major role in the description of the physical aspects and in the analysis of various observed features. The our concern work mainly focuses on the approximation of special relativistic hydrodynamic models simulating single and multi-component astrophysical flows numerically.

In the first part of this thesis, the special relativistic hydrodynamic (SRHD) equations for both one and two-dimension are numerically solve by employing the central upwind schemes. The numerical dissipations present in the original staggered central schemes are reduced by utilizing one-sided local propagation speed of the SRHD equations. Another feature of this technique is simulation of the complex and hard test cases accurately and efficiently. Several case studies are considered, for example one and two-dimension shock tube problems, forward facing step problem, diffracting shock waves, perturbed shock tube flux flow problem, the interactions for two spherically symmetric fields problem, and cylindrical explosion problem. For comparisons and authentication, different numerical

schemes are proposed e.g. the staggered central and KFVS techniques that are implemented to resolve the similar model equations.

The second part extends this numerical study to the solutions of ultra-relativistic hydrodynamics equations in both single and multi-dimensional (2D) space. The same central upwind technique is applied to solve these models. In contrast to the SRHD model, the primitive elements in URHD models are explicitly expressible in form of conserved quantities. The KFVS and the staggered central schemes are implemented to solve URHD equations for the comparison. The numerical results of these schemes are analyzed with the results of central upwind scheme. Furthermore, the accuracy, validity and computational efficiency of the suggested techniques are also analyzed. The distinguish key features of the central upwind scheme makes this scheme a extensive tool for the approximation of a wide range of hyperbolic models.

The third part of this dissertation is deal with the simulation of relativistic multicomponent flows. Higher order staggered central scheme (NT) is extended for the approximated result of multi-component flow models in both single and multi-dimensional (2D) space. The scheme is capable to capture the complicated wave structures in the solutions and do not involve characteristic decomposition of the fluxes.

The piecewise reconstruction of nonlinear polynomial employ by central scheme also utilizing of nonlinear limiters that ensure the complete nonoscillatory behaviour of the estimated numerical solutions. The central scheme is logically straightforward and computationally efficient and simple.



# Chapter 2

## Preliminaries

In the current chapter, some basic terminologies and equations are presented for understanding the research work of this thesis project. To study a physical system associated with space and time, we must have to use a class of equations known as evolution equations. Here, we briefly formulate conservation laws and their weak formulations. Furthermore, some basics about special relativity and gas dynamics are given before presenting the SRHD equations that will be present in the coming chapters.

## 2.1 The Conservation Laws

Transportation properties of the fluids are governed under the conservation laws. The concerning statements that constitute the conservative laws need to be conserved. Considering a fluid enclosed by an arbitrary fixed control volume denoted by  $V$ . A total change observed in conserved variables due to fluid flows over to surface  $S$  through the control volume is zero in the particular interval of time. The vector of conservative variables which are the functions of space with respect to time  $(t, x, y, z)$  that may be expressed as

$$\vec{C}(t, x, y, z) = \begin{pmatrix} C_1(t, x, y, z) \\ C_2(t, x, y, z) \\ \vdots \\ C_N(t, x, y, z) \end{pmatrix},$$

here  $N$  shows the components of the conserved variables and the corresponding vector flux quantities are representing by

$$\vec{A}(\vec{C}) = \begin{pmatrix} A_1(C) \\ A_2(C) \\ \vdots \\ A_N(C) \end{pmatrix}.$$

The fluid flow through the flat surface  $S$  over the control volume  $V$  and the interval of time is  $[t_0, t_0 + dt]$ , provides

$$\int_{t_0}^{t_0+dt} \iint_S \vec{A}(\vec{C}(t, x)) \cdot d\vec{S} dt - \iiint_V [\vec{C}(t_0, x) - \vec{C}(t_0 + dt, x)] dV = 0. \quad (2.1)$$

In a above given integral over the volume is assumed for conserved quantities  $C_i$ , for  $i = 1, 2, \dots, N$  at the initial and the last simulation times, whereas second double integration expresses the number of fluxes that across  $S$  during time interval representing by  $[t_0, t_0 + dt]$ . Here,  $t_0$  is for the starting time while  $dt$  denotes change in time. Apply divergence theorem the first integration and apply the calculus fundamental theorem at the last integral that provides the below formulation, we get

$$\int_{t_0}^{t_0+dt} \iiint_V \left[ \nabla \cdot \vec{A}(\vec{C}) + \frac{\partial \vec{C}}{\partial t} \right] dV dt = 0. \quad (2.2)$$

For an arbitrary control volume, one can get the hyperbolic system of conservation law, shown below

$$\nabla \cdot \vec{A}(\vec{C}) + \frac{\partial \vec{C}}{\partial t} = 0. \quad (2.3)$$

## 2.2 The Hyperbolic Law of Conservation

This dissertation deals with the models formed the non-linear systems of partial differential equation (PDE). The conservation law in Eq. (2.3) is expressed in the single space dimensional form by

$$\frac{\partial \vec{C}}{\partial t} + \frac{\partial \vec{A}(\vec{C})}{\partial x} = 0, \quad (2.4)$$

where

$$\vec{C} = \begin{pmatrix} C_1 \\ C_2 \\ \vdots \\ C_N \end{pmatrix}, \quad \vec{A}(\vec{C}) = \begin{pmatrix} A_1(\vec{C}) \\ A_2(\vec{C}) \\ \vdots \\ A_N(\vec{C}) \end{pmatrix}.$$

Apply chain rule on the last term of Eq.(2.4) and get

$$\frac{\partial \vec{A}(\vec{C})}{\partial x} = \frac{\partial \vec{A}(\vec{C})}{\partial \vec{C}} \frac{\partial \vec{C}}{\partial x}. \quad (2.5)$$

Using Eq. (2.5) in Eq. (2.4), the following is obtained

$$\frac{\partial \vec{C}}{\partial t} + \frac{\partial \vec{A}(\vec{C})}{\partial \vec{C}} \frac{\partial \vec{C}}{\partial x} = 0, \quad (2.6)$$

which named as Quasi linear form. The matrix of Jacobian for the flux functions is expressed by

$$J(\vec{C}) = \frac{\partial \vec{A}(\vec{C})}{\partial \vec{C}} = \begin{pmatrix} \frac{\partial \vec{A}_1(\vec{C})}{\partial C_1} & \frac{\partial \vec{A}_1(\vec{C})}{\partial C_2} & \dots & \frac{\partial \vec{A}_1(\vec{C})}{\partial C_N} \\ \frac{\partial \vec{A}_2(\vec{C})}{\partial C_1} & \frac{\partial \vec{A}_2(\vec{C})}{\partial C_2} & \dots & \frac{\partial \vec{A}_2(\vec{C})}{\partial C_N} \\ \vdots & \vdots & \ddots & \vdots \\ \frac{\partial \vec{A}_N(\vec{C})}{\partial C_1} & \frac{\partial \vec{A}_N(\vec{C})}{\partial C_2} & \dots & \frac{\partial \vec{A}_N(\vec{C})}{\partial C_N} \end{pmatrix}. \quad (2.7)$$

Matrix  $J$  has the eigenvalues represented by  $\lambda_i$ , for  $i = 1, 2, \dots, N$  that is required for the final solution of the characteristic function

$$\det(J - \lambda I) = 0. \quad (2.8)$$

In the above expression,  $I$  is the  $(N \times N)$  size identity matrix. Physically, eigenvalues gives information about the speed of propagation. A system can be declared as hyperbolic over the point  $(x, t)$  if  $J$  consists of  $\lambda_1, \lambda_2, \dots, \lambda_N$ , the  $N$  real eigenvalues and the respective set of all eigenvectors represent by  $k_{(1)}, k_{(2)}, k_{(3)}, \dots, k_{(N)}$ , that can be linearly independent vectors. A system can be categorized as strictly hyperbolic if it has distinct real eigenvalues  $\lambda_i$ .

## 2.3 Laws of Conservation for Weak Solution

Weak formulation can be obtained after taking integration of the conservation laws in Eq. (2.4) and it is used to capture discontinuities in the flows. By applying integration on Eq. (2.4) on  $S_i$ , the surface area having finite volume showed by  $\Delta V_i$  at the interval,  $x \in (x_{i-1/2}, x_{i+1/2})$ , gives

$$\int_{\Delta V_i} \left( \frac{\partial \vec{A}(\vec{C})}{\partial x} + \frac{\partial \vec{C}}{\partial t} \right) dV = 0. \quad (2.9)$$

By employing the Gauss's theorem, one can get following form

$$\int_{\Delta V_i} \frac{\partial \vec{A}(\vec{C})}{\partial x} dV = \oint_{S_i} \vec{A}(\vec{C}) \cdot d\vec{S}. \quad (2.10)$$

Here,  $\Delta V_i$  is the volume enclosed by the surface  $S_i$ . Further, using (2.10) in (2.9), we have

$$\frac{d}{dt} \int_{\Delta V_i} \vec{C} dV + \oint_{S_i} \vec{A}(\vec{C}) \cdot d\vec{S} = 0. \quad (2.11)$$

The above equation shows that a change in small time in the conserved quantity  $\vec{C}$  over the control volume shown as  $\Delta V_i$  which is on the basis of flux across the surface of the problem denoted by  $S_i$ . By taking integral over to the domain  $[t_n, t_{n+1}]$ . Formulation of weak solution can be expressed as

$$\int_{t_n}^{t_{n+1}} \frac{d}{dt} \int_{V_i} \vec{C} dV + \int_{t_n}^{t_{n+1}} \oint_{S_i} \vec{A}(\vec{C}) \cdot d\vec{S} dt = 0. \quad (2.12)$$

Which represents the better appropriate type of conservation laws, as this includes discontinuity of the stat vectors. Note that the discontinuities may be establish at the final solutions of the hyperbolic system even for considering initial data in smooth form. Therefore, to admit discontinuities in the solutions, weak in formulation is much more needed which seems to not possible when the differential form of the same model is used.

## 2.4 The Non-relativistic Euler Equation

System of the Euler equation that describe flow of the perfect fluid especially in the classical hydrodynamics that appears in a smooth way in the integral form for the conservative laws of the mass  $\rho$ , momentum  $M$  and for energy  $E$  [47, 48]. To linear momentum the derivation is presented here only in one spatial dimension, but the approach can be further explored for more than one space dimension. By using suitable transformations, these system of linear equations can transformed by any required coordinate system. For the purpose of simplification, we take only Cartesian coordinates system. Assume that external forces, such as heat conduction or gravity, on the fluid are negligible. First, consider the conservation law for mass. According to this law, the mass of the fluid flow in the restricted domain  $x_0 < x < x_1$  during time  $t \in (t_0, t_1)$  that are equal to net mass of the fluid that pass through within the domain of the system boundaries in the time  $\Delta t = t_1 - t_0$ , i.e. the mass of a system within the boundary  $\Delta x = x_1 - x_0$  is conserved over time  $\Delta t$ . Further, we suppose that the direction of flow is towards the positive  $x$ -axis. Mathematically, the law of conservation of mass for the above system is express in the integral form by

$$\int_{x_0}^{x_1} [\rho(t_1, x) - \rho(t_0, x)] dx = - \int_{t_0}^{t_1} [\rho(t, x_1) v(t, x_1) - \rho(t, x_0) v(t, x_0)] dt, \quad (2.13)$$

where  $\rho$ , denotes density and  $v$  represents velocity. The law of conservation of momentum state that the variation in total momentum flow over the domain  $\Delta x$  is the same and equal to total flow of momentum across the boundary of domain  $\Delta x$  within time  $\Delta t$  and the pressure  $p$  causes change in momentum at the boundaries within the same interval of time.

Therefore,

$$\begin{aligned} \int_{x_0}^{x_1} [M(t_1, x) - M(t_0, x)] dx &= - \int_{t_0}^{t_1} [M(t, x_1) v(t, x_1) - M(t, x_0) v(t, x_0)] dt \\ &\quad - \int_{t_0}^{t_1} [\rho(t, x_1) - \rho(t, x_0)] dt. \end{aligned} \quad (2.14)$$

The law of conservation of energy has an important role for the analysis of the flowing fluids. According to this law the net change in energy of a system having domain  $\Delta x$  is equals to the flow of energy across the boundaries of a system  $\Delta x$  and the change in energy because of the pressure within time  $\Delta t$ . The conservation law for energy can be formulated as

$$\begin{aligned} \int_{x_0}^{x_1} [E(t_1, x) - E(t_0, x)] dx &= - \int_{t_0}^{t_1} [E(t, x_1) v(t, x_1) - E(t, x_0) v(t, x_0)] dt \\ &\quad - \int_{t_0}^{t_1} [\rho(t, x_1) - \rho(t, x_0)] dt. \end{aligned} \quad (2.15)$$

The above equations (2.13) – (2.15) for the laws of conservation form an integrated system, one for the state vector  $\vec{C}$  and the other for the flux vector  $\vec{A}$ . Therefor, this may possible to write the conservation equation in integral formate as

$$\int_{x_0}^{x_1} [\vec{C}(t_1, x) - \vec{C}(t_0, x)] dx = - \int_{t_0}^{t_1} [\vec{A}(t, x_1) v(t, x_1) - \vec{A}(t, x_0) v(t, x_0)] dt. \quad (2.16)$$

Here, the vectors  $\vec{C}$  and  $\vec{A}$  can be indicated as

$$\vec{C} = [\rho \ M \ E]^T \quad (2.17)$$

with

$$\vec{A} = \begin{pmatrix} M \\ Mv + p \\ (E + p)v \end{pmatrix}. \quad (2.18)$$

The conservative quantities  $\vec{C}$  and  $\vec{A}$  are coupled through the primitive variables  $p$ ,  $\rho$ ,  $v$  and  $e$ . Wherein,  $e$  represents the specific (internal) energy. The coupling of these variables with the energy and momentum equations that can be seen by the following

$$E = \rho\left(e + \frac{\mathbf{v}^2}{2}\right), \quad M = \rho\mathbf{v}. \quad (2.19)$$

These primitive variables can be calculated directly in the physical system. Furthermore, they provide the more natural agreement with the behaviour of the fluid in a system. There are only three Eqs. (2.16)–(2.18) for the four quantities that are unknown such as  $p$ ,  $\rho$ ,  $e$  and  $v$ . Therefore, conservation equations defined in Eqs. (2.16)–(2.18) are not closed. The system can be closed by employing equations of state. The typical structure of EOS can be expressed as

$$p = p(\rho, e). \quad (2.20)$$

The EOS for the perfect gas is representing as

$$p = \rho e(\Gamma - 1). \quad (2.21)$$

In the above expression,  $\Gamma$  represent as specific heat ratio. Here, equation (EOS) of state depends on the fluid model under consideration. A vector of primitive variables can be defined after getting an EOS, for example

$$\vec{C} = \begin{pmatrix} \rho \\ v \\ p \end{pmatrix}. \quad (2.22)$$

The conservative Eq. (2.16) can not be written in integral form whereas the partial differential equations may be written, if  $\vec{C}$  is differentiated with respect to time as

$$\vec{C}(x, t_1) - \vec{C}(x, t_0) = \int_{t_0}^{t_1} \frac{\partial \vec{C}}{\partial t} dt \quad (2.23)$$



and, if  $\vec{A}$  is differentiated in space as

$$\vec{A}(x_1, t) - \vec{A}(x_0, t) = \int_{x_0}^{x_1} \frac{\partial \vec{A}}{\partial x} dx. \quad (2.24)$$

The relations in Eqs. (2.23) and (2.24) is inserted in the integral Eq. (2.16), this gives

$$\int_{x_0}^{x_1} \int_{t_0}^{t_1} \frac{\partial \vec{C}}{\partial t} dt dx = - \int_{t_0}^{t_1} \int_{x_0}^{x_1} \frac{\partial \vec{A}}{\partial x} dx dt. \quad (2.25)$$

Here, we assume that the integration is reversible in order. It is noted that the limits of integration defined in Eq. (2.25) are arbitrary. Therefore, the constants of integration that arises must be zero. Then after simplification, we can get

$$\frac{\partial \vec{C}}{\partial t} + \frac{\partial \vec{A}}{\partial x} = 0, \quad (2.26)$$

representing the Newtonian hyperbolic system of conservative form. conserved quantities  $\vec{C}$  and flux vector  $\vec{A}$  are defined in Eqs. (2.17) and (2.18), respectively. The Eq. (2.26) can be extended to the three dimensional space through the same procedure. The resulting equations can be seen as

$$\frac{\partial \vec{C}}{\partial t} + \sum_{i=1}^3 \frac{\partial \vec{A}^i}{\partial x^i} = 0. \quad (2.27)$$

Here,  $(x^1, x^2, x^3) = (x, y, z)$ . The momentum  $M_i$  for  $i = 1, 2, 3$  has three components in each direction. Therefore, Eq. (2.17) can be written as

$$\vec{C} = \begin{pmatrix} \rho \\ M_1 \\ M_2 \\ M_3 \\ E \end{pmatrix}, \quad (2.28)$$

where

$$M_i = \rho v^i, \quad \text{for } i = 1, 2, 3, \quad (2.29)$$

with

$$E = \rho\left(\frac{\mathbf{v}^2}{2} + e\right). \quad (2.30)$$

Here,  $\mathbf{v} = (v^1, v^2, v^3)^T$ . The flux  $\vec{A}$  in the each directions  $x_i$  is express as

$$\vec{A}^i = \begin{pmatrix} M_i \\ M_1 v^i + \delta^{i1} p \\ M_2 v^i + \delta^{i2} p \\ M_3 v^i + \delta^{i3} p \\ (p + E) v^i \end{pmatrix}, \quad i = 1, 2, 3. \quad (2.31)$$

Where,  $\delta^{ij}$  is the Knocker delta with  $i, j = 1, 2, 3$ .

## 2.5 The Riemann Problem

A Riemann problem is depend on piecewise initial data consisting of two states, a right  $\vec{C}^R$  and a left  $\vec{C}^L$  separated by a single jump discontinuity for at least one field, i.e.  $C_i^L \neq C_i^R$  for at least one  $i$ . For example

$$\frac{\partial \vec{C}}{\partial t} + \frac{\partial \vec{A}(\vec{C})}{\partial x} = 0, \quad (2.32)$$

piecewise initial value

$$\vec{C}(x, 0) = \begin{cases} \vec{C}^R, & \text{if } x > 0, \\ \vec{C}^L, & \text{if } x < 0. \end{cases} \quad (2.33)$$

The above general expression of Riemann problem enable us to explore the behavior of conservational laws in integral form (weak solutions).

## 2.6 The Gas Dynamics

The branch of Gas Dynamics indeed is a pure scientific area that primarily deal with the structure of the gasses flow wherein the compressibility and the temperature changes become significant.

### 2.6.1 The Perfect Gas

The main characteristic of a perfect gas means that the gas must be thermally and the calorically perfect whenever its own internal energy along with enthalpy are the function of the temperature alone. Moreover, the calorically perfect gas have to thermally perfect and the thermally perfect is not necessarily be the calorically perfect.

### 2.6.2 Compressible Flows

Compressibility indeed is the phenomenon by that virtue in which flow of a fluid change the density by which compressibility may also be identify as the define bulk modulus elasticity of a pressure. Then flow with significant compressibility are called compressible flows.

### 2.6.3 The Mach Number

The sound waves propagation are immensely small in the pressure interferences. Speed in which the sound waves propagates within a physical medium is known as speed of the sound, representing by  $c$ . That is why, the Mach number can be defined by ratio of a locally fluid flow speed by the local sound speed in that fluid,i.e.  $M = V/c$ .

## 2.7 Special Relativity

Albert Einstein published the special relativity theory in 1905 [49]. Special Relativity theory is the one of special case for the relativity theory of Einstein. In a theory of special relativity, all effects of gravity and acceleration can be neglected. As the result, Newtonian idea related to absolute time which is exchange with concept by relative passages of time. Moreover, theory of the special relativity principally build on two major axioms.

1. The laws of the physics are identical in all the inertial systems.
2. Speed of the light is measured as constant in all frames of references.

### 2.7.1 The Metric Tensor

In differential geometry a metric tensor is a function which takes tangent vectors  $\mu\nu$  in the form of pairs as arguments at a point in surface, and calculate a scalar number  $g_{\mu\nu}$ . A four-dimensional manifold system known as Minkowski time-space, it combine the three dimensions of space  $x^i$ ,  $i = 1, 2, 3$  and single dimension of time  $x^0 = ct$ . It has a metric template of  $(-, +, +, +)$ . Four vectors  $x^\mu$  where  $\mu = 0, \dots, 3$ , for  $x^0 = ct$ , denotes the observer's time whereas  $x^i$ , for  $i = 1, 2, 3$  denoting components of  $x^\mu$ . To avoid the complexity, let  $c = 1$  is the speed of light. Now, we can express the metric tensor  $g_{\mu\nu}$  as

$$ds^2 = g_{\mu\nu} dx^\mu dx^\nu, \quad (2.34)$$

where  $g_{\mu\nu}$  is defined by

$$g_{\mu\nu} = \begin{cases} -1, & \text{if } \nu = \mu = 1, 2, 3, \\ 0, & \text{if } \nu \neq \mu, \\ 1, & \text{if } \nu = \mu = 0. \end{cases} \quad (2.35)$$

Futhermore,  $g_{\mu\nu} = g^{\mu\nu}$ .

### 2.7.2 Lorentz Transformations

The universal Laws of the nature are consistent under special relativity for a specific group of the space and time coordinate transformation between two coordinate frames, moving at constant velocity are known as Lorentz-transformations. A system that are involve with the space and time by special coordinates  $x^\alpha$  linearly transforms to an other system having

coordinates  $x'^\alpha$  under Lorentz-transformations  $\Lambda_\beta^\alpha$ , satisfying the following relations

$$g_{\mu\nu} = \Lambda_\mu^\alpha \Lambda_\nu^\beta g_{\alpha\beta}, \quad x'^\alpha = \Lambda_\beta^\alpha x^\beta, \quad \Lambda_0^0 \geq 1, \quad \det \Lambda = +1.$$

It is noted that given below expression that produces tensor for a proper Lorentz's transformation

$$\epsilon_{\alpha\beta\omega\delta} = \begin{cases} 1, & \text{if } \alpha\beta\omega\delta \text{ even permutation for } 0123, \\ -1, & \text{if } \alpha\beta\omega\delta \text{ odd permutation for } 0123, \\ 0, & \text{otherwise,} \end{cases} \quad (2.36)$$

is the so-called Levi-Civita tensor.

### 2.7.3 Vectors and Tensors

Any object having four components, that transforms in such a specific way  $f'^\alpha = \Lambda_\beta^\alpha f^\beta$  under Lorentz transformation, is known as four-vector. The four vectors along with single lower index and obeying the property of Lorentz-transformation, is named as covariant four-vectors.

$$u^\alpha(y) \rightarrow u'_\alpha(y') = \Lambda_\beta^\alpha u^\beta(y). \quad (2.37)$$

A four-vector with the single index at upper and following the Lorentz's transformation defined property is named as contravariant four-vectors, as shown below

$$v^\alpha(y) \rightarrow v'_\alpha(y') = \Lambda_\beta^\alpha v^\beta(y). \quad (2.38)$$

Here,  $\Lambda_\beta^\alpha = g_{\beta\omega} g^{\alpha\delta} \Lambda_\delta^\omega$ . The metric tensor  $g_{\alpha\delta}$  and  $g^{\alpha\delta}$  are the same as numerically i.e.,  $g_{\alpha\delta} = g^{\alpha\delta}$ . For each covariant vector  $u_\alpha$  then there exists a corresponding contravariant four vectors

$$u_\alpha = u_\beta g_{\alpha\beta}. \quad (2.39)$$

Similarly, to each contravariant four vectors  $v_i^\alpha$  there is corresponding covariant four vectors

$$v_\beta = g_{\alpha\beta} v^\alpha. \quad (2.40)$$

A contravariant or covariant is a tensor having one index and the tensors that have no indices are generalizations of scalars. A vector can be expressed in covariant or contravariant forms. Some vectors as  $dx^\alpha$  occur naturally contravariant while the others appear more covariant. Numerous physical quantities neither vectors nor scalars but more complex quantities are called tensors. The tensor with many covariant or contravariant indices under Lorentz-transformations can be seen in

$$T_{\alpha\beta}^\omega \rightarrow T_{\alpha\beta}^{\prime\omega} \Rightarrow \Lambda_\delta^\omega \Lambda_\alpha^\epsilon \Lambda_\beta^\xi T_{\epsilon\xi}^\delta. \quad (2.41)$$

Here, it is noted that derivatives of the tensor,  $\partial/\partial x^\alpha$  is again tensor with single extra index  $\alpha$  at lower. As an example, the tensor  $T^{\alpha\beta}$  can be represented by

$$T_\alpha^{\beta\omega} = \frac{\partial T^{\beta\omega}}{\partial x^\alpha}. \quad (2.42)$$

#### 2.7.4 Four-Velocity

In the special relativity, macroscopic four-velocity is a four-vector, expressing the relativistic part of velocity in three dimensional vector space. The macroscopic four-velocity  $u^\mu$  is expressed as

$$u^\mu = N^\mu/\rho \quad \text{and} \quad \rho = \sqrt{N_\nu N^\nu}, \quad (2.43)$$

wherein,  $\rho$  represents density of rest-mass and  $N^\mu$  denotes the particle density four-vector.

Furthermore,  $u^\mu u_\mu = 1$ .

#### 2.7.5 The Tensor for Stress Energy

The fluids having continuous distribution with no shear stresses are categorized as perfect fluids. Mathematically, the stress-energy tensor of perfect fluids may be denoted as

$$T^{\mu\nu} = pg^{\nu\mu} + (p + e)u^\nu u^\mu, \quad \text{for } \nu, \mu = 0, \dots, 3. \quad (2.44)$$

Here,  $\rho$  indicates the density of mass-energy within rest-frame of fluid flow,  $e$  represents the density of fluid internal energy,  $u_\mu$  indicates the four velocity as well as  $p$  describes as the pressure within a rest-frame of fluid dynamics.

## **Chapter 3**

### **The Central Upwind Scheme for SRHD Model**



In this chapter, the numerical solutions of both the single and two dimension special relativistic hydrodynamic (SRHD) modeled equations simulating the dynamics system of perfect fluid flow in the absence of external forces, such as gravity are presented. For a strong shockwave the effect of gravity on the flow is negligible. After employing SRHD approximation, the equations of motion can be obtained that describes conservation laws for the momentum, mass and also for energy. Although, when it is needed to illustrate the motion of fluid particles, we infrequently discuss the energy and the momentum describe by the elements of the fluid, instead of velocities, pressure, and etc. Due to the fact that the highly nonlinearity is involved in the primitive and the conserved quantities of SRHD model make it complicated to write the explicit expressions for such primitive quantities since functions of the conserve variables.

Here, central upwind numerical scheme is employed to execute the concerned SRHD equations dimensionally in single and multi-dimensional (2D) space. For the validation and the comparison, the numerically approximated solutions of the central Nessyahu and Tadmor (NT), and kinetic flux (KFVS) techniques are presented [8, 22].

### 3.1 Derivation of SRHD Equations

According to theory of the special relativity, coordinate system with reference to the fixed frame is described by the four vectors as  $x^\mu$ , where  $\mu = 0, \dots, 3$  with  $x^0 = t$  represents observer time. Here, spatial coordinate of the event  $x^\mu$  can be denoted by the following three vectors

$$\mathbf{x} = \begin{pmatrix} x^1 \\ x^2 \\ x^3 \end{pmatrix}.$$

For simplicity,  $c = 1$  is taken as the light speed in vacuum. The metric  $g_{\mu\nu} = g^{\mu\nu}$  tensor

can be indicated as

$$g_{\mu\nu} = \begin{cases} 1, & \text{if } \nu = 0 = \mu, \\ -1, & \text{if } \nu = \mu = 1, 2, 3, \\ 0, & \text{if } \nu \neq \mu. \end{cases} \quad (3.1)$$

Furthermore, the metric tensor  $g_{\mu\nu}$  in matrix form is  $g_{\mu\nu} = g^{\mu\nu} = \text{diag}(+1, -1, -1, -1)$ .

The contravariant four-velocity vector components  $u^\mu$ , where  $\mu = 0, \dots, 3$  can be written as

$$u^0 = \omega \quad \text{and} \quad u^i = \omega v^i, \quad i = 1, 2, 3. \quad (3.2)$$

Here,  $v^i$  denotes the spatial velocity components, in the directions of  $x, y, z$  where these directions are coordinates of the three dimensional in a rectangular coordinate systems and  $\omega$ , the Lorentz-factor is defined as

$$\omega = \frac{1}{\sqrt{1 - \mathbf{v}^2}}, \quad (3.3)$$

and

$$\mathbf{v}^2 = \sum_{i=1}^3 (v^i)^2. \quad (3.4)$$

Eqs. (3.2) – (3.4) gives

$$u^\mu u_\mu = u^\mu (u^\nu g_{\mu\nu}) = (u^0)^2 - \sum_{i=1}^3 (u^i)^2 = \omega^2 [1 - (\mathbf{v})^2] = 1. \quad (3.5)$$

Utilizing the Einstein's summation conventions, equation describes the relativistic motion of a fluid by assuming  $\mu, \nu = 0, \dots, 3$  are given as

$$\frac{\partial N^\mu}{\partial x^\mu} = 0 \quad \text{and} \quad \frac{\partial T^{\mu\nu}}{\partial x^\mu} = 0, \quad (3.6)$$

where the particle density four vectors  $N^\mu$  and a energy-momentum  $T^{\mu\nu}$  tensor can be express as

$$N^\mu = \rho u^\mu \quad \text{and} \quad T^{\mu\nu} = (e + p)u^\mu u^\nu + pg^{\mu\nu}. \quad (3.7)$$

The flow properties such as,  $\rho$  representing for rest-mass densities,  $u^\mu$  be a four-velocity,  $p$  shows pressure of the fluid and  $e$  represents for specific (internal) energy. Here, equation (EOS) for state variable may be indicated as

$$e = [p/(\Gamma - 1)] + \rho, \quad (3.8)$$

where,  $\Gamma$ , the adiabatic index is defined in two states. In the first state,  $\Gamma = \frac{5}{3}$  is used for mildly relativistic whereas in the second state,  $\Gamma = \frac{4}{3}$  is used for ultrarelativistic.

In Minkowski spacetime, the cartesian coordinates  $x^\mu = (t = x^0, x = x^1, y = x^2, z = x^3)$  along with the conservation Eq. (3.6) describe the relativistic fluid motion that is the cast by a first-order flux of conservative system in term of

$$\frac{\partial \vec{C}}{\partial t} + \sum_{i=1}^3 \frac{\partial \vec{A}^i(\vec{C})}{\partial x^i} = 0. \quad (3.9)$$

The vectors of the conserve variables  $\vec{C}$  and their respective fluxes  $\vec{A}$  for the above equations, are given as

$$\vec{C} = \begin{pmatrix} C_1 \\ C_{j+1} \\ C_5 \end{pmatrix} = \begin{pmatrix} N^0 \\ T^{0j} \\ T^{00} \end{pmatrix} = \begin{pmatrix} \rho\omega \\ (e+p)\omega^2 v^j \\ (e+p)\omega^2 - p \end{pmatrix}, \quad j = 1, 2, 3, \quad (3.10)$$

$$\vec{A}^i = \begin{pmatrix} A_1^i \\ A_{j+1}^i \\ A_5^i \end{pmatrix} = \begin{pmatrix} N^i \\ T^{ij} \\ T^{i0} \end{pmatrix} = \begin{pmatrix} \rho\omega v^i \\ (e+p)\omega^2 v^i v^j + p\delta^{ij} \\ (e+p)\omega^2 v^i \end{pmatrix}, \quad i, j = 1, 2, 3. \quad (3.11)$$

Here, the symbol  $\delta^{ij}$  represents the Knoecker delta. The vector of primitive variables are expressed by  $\vec{c} = [\rho, v^i, p]^T$ , which contains the physical quantities in local rest frame.

### 3.1.1 Recovery of Primitive Variables

The numerical frame work is establish to recapture the primitive variable from conserved variables. Wherein the relativistic approach, the task to recover the primitive quantities

$(\rho, v^i, p)^T$  through conservative variables  $\vec{C}_N$  is much more complicated. In the conserved formulation this is unavoidable in the sense that the flux can not be write in the form of conserved variables only. The Eqs. (3.8) – (3.10) are used to get the required primitive variables. The following equation shows that every primitive variable indeed the implicit function by the  $\vec{C}_N$ , which are conserved variables.

Assume that

$$D = \vec{C}_1, \quad Q^i = \vec{C}_{i+1} \quad \text{for } i = 1, 2, 3, \quad \text{with } E = \vec{C}_5, \quad (3.12)$$

moreover

$$U = (e + p) \omega^2, \quad \Gamma = \Gamma_1(\Gamma - 1). \quad (3.13)$$

Then, with the help of Eqs. (3.4) – (3.10), we obtain

$$U = (\rho + \Gamma_1 p) \omega^2 = D\omega + \Gamma_1 \omega^2 p \quad (3.14)$$

with

$$E = \vec{C}_5 = U - p. \quad (3.15)$$

Using Eqs. (3.14) and (3.15), the parameter  $p$  can be eliminate and it gives

$$U = U(D, E, \omega) = \frac{E \Gamma_1 \omega^2 - D\omega}{\Gamma_1 \omega^2 - 1}, \quad \Gamma_1 \omega^2 \neq 1. \quad (3.16)$$

As pointed out by [50], there does not any closed form of a solution for this inversion due to the coupling caused by the Lorentz factor  $\omega$ . As a result, we must use a root-finding algorithm to find the correct  $\omega$ . Moreover, by using Eq. (3.5), we have

$$v^2 = 1 - \frac{1}{\omega^2} \quad (3.17)$$

and

$$\begin{aligned} Q^2 &= \sum_{i=1}^3 [Q^i]^2 = \sum_{i=1}^3 [\vec{C}_{i+1}]^2 = [(p + e)\omega^2]^2 \sum_{i=1}^3 [v^i]^2 \\ &= [U(D, E, \omega)]^2 [v]^2 = [U(D, E, \omega)]^2 [1 - \omega^{-2}]. \end{aligned} \quad (3.18)$$

Therefore,

$$[U(D, E, \omega)]^2 (1 - \omega^{-2}) - Q^2 = 0. \quad (3.19)$$

According to Eqs. (3.18) – (3.19) implies that  $\omega$  be the implicit function with conserved quantities such as  $D$ ,  $E$  and  $Q^2$ . Furthermore, the following relations can be obtain by utilizing the results of the Eqs. (3.8), (3.12) – (3.13) and Eq. (3.15), one can get

$$\rho = \frac{D}{\omega}, \quad p = U - E, \quad \text{and} \quad v^i = Q^i/U \quad \text{for } i = 1, 2, 3. \quad (3.20)$$

The solution is not explicit. Here, it is noted that, for the value of  $\Gamma > 1$ , the Eq. (3.13) gives  $\Gamma_1 > 1$ . Also, Eq. (3.3) and (3.4) implies that  $\omega \geq 1$ . As such  $\Gamma_1 \omega^2 - 1 > 0$ , that is, the condition  $\Gamma_1 \omega^2 - 1 \neq 0$  that appear in the Eq. (3.16) which is always valid.

## 3.2 Numerical Scheme

The application of central upwind schemes can cause a rebellion in special relativistic hydrodynamics model(SRHD). These numerical methods are conservative and serve in a very natural way that provides the characteristics essential for the effectiveness, such as higher order accuracy, efficient to capture the sharp discontinuities with stability, and converges to the exact numerical solution. Furthermore, the proposed schemes central upwind are depended on single sided local speed of waves propagation that make it universal, simple and efficient.

### 3.2.1 The One-dimensional Central Upwind Scheme

Let us considered one-dimension hyperbolic system of conservative laws of special relativistic hydrodynamics (SRHD) to derive the central upwind scheme [35] as

$$\frac{\partial \vec{C}}{\partial t} + \frac{\partial \vec{A}(\vec{C})}{\partial x} = 0, \quad (3.21)$$

where,  $\vec{C} = (\rho\omega, (p+e)\omega^2 v^1, (p+e)\omega^2 - p)^T$ ,  $\vec{A} = (\rho\omega v^1, (p+e)\omega^2 (v^1)^2 + p, (p+e)\omega^2 v^1)$ .

The required scheme is based on reconstruction, evolution and projection. In the initial step, computational numeric domain  $[0, x_{\max}]$  is discretized by  $(x_{i-\frac{1}{2}})_{i \in \{1, \dots, N+1\}}$  into  $N$  grid cell. Where,  $x_i$  represents the center of cells and  $\Delta x$  is the uniform interval of each cell. Moreover,  $x_{i \pm \frac{1}{2}}$  denote the domain of the cell.

Here,

$$2x_i = x_{i-1/2} + x_{i+1/2} \quad \text{with} \quad \Delta x = x_{i-1/2} - x_{i+1/2} \quad \Rightarrow \quad \Delta x = \frac{x_{\max}}{(N+1)}, \quad (3.22)$$

where

$$x_{1/2} = 0, \quad \text{and} \quad x_{\max} = x_{N+1/2}, \quad \text{with} \quad x_{i+1/2} = \Delta x_i, \quad \text{when} \quad i = 1, 2, 3, \dots, N. \quad (3.23)$$

Consider value of  $\zeta_i \equiv [x_{i-1/2}, x_{i+1/2}]$  for the redistricted domain  $i \geq 1$ . Average values of the conservative variable  $\vec{C}(t)$  in each interval of  $\zeta_i$  can be written as

$$\vec{C}_i \equiv \vec{C}_i(t) = \frac{1}{\Delta x} \int_{\zeta_i} \vec{C}(t, x) dx. \quad (3.24)$$

Now, integrate Eq. (3.21) over  $\zeta_i$ , implies

$$\frac{d\vec{C}_i}{dt} = \frac{1}{\Delta x} \left[ \mathbf{S}_{i+\frac{1}{2}}(t) - \mathbf{S}_{i-\frac{1}{2}}(t) \right], \quad (3.25)$$

where vector of fluxes are expressed by

$$\mathbf{S}_{i+\frac{1}{2}} = \frac{1}{2} \left( \vec{A}(\vec{C}_{i+\frac{1}{2}}^-) - \vec{A}(\vec{C}_{i+\frac{1}{2}}^+) \right) + \frac{a_{i+\frac{1}{2}}}{2} \left( \vec{C}_{i+\frac{1}{2}}^+ - \vec{C}_{i+\frac{1}{2}}^- \right). \quad (3.26)$$

Here,  $\vec{C}^+$  and  $\vec{C}^-$  represent the right and left intermediate states of piecewise linear reconstruction  $\vec{C} = (\tilde{\rho}, \tilde{\rho}u, \tilde{E}^*)$  at  $x_{i+\frac{1}{2}}$ , are written as

$$\vec{C}_{i+\frac{1}{2}}^+ = \vec{C}_{i+1} - \frac{\Delta x}{2} \vec{C}_{i+1}^x, \quad \vec{C}_{i+\frac{1}{2}}^- = \vec{C}_i + \frac{\Delta x}{2} \vec{C}_i^x. \quad (3.27)$$

The approximated derivatives of  $\vec{C}_i^x$  are at a minimum first-order approximation of  $\vec{C}_x(t, x_i)$ . These derivatives can be estimated by taking nonlinear limiter which ensure the nonoscillatory nature of piecewise reconstruction Eq. (3.27). The feasible computations of slopes, stated by family comprises of the discrete derivative is parameterized by using  $\theta \in [1, 2]$ , e.g.

$$\vec{C}_i^x = MM \left[ \theta \left\{ \Delta \vec{C}_{i+\frac{1}{2}}, \frac{1}{2} \left( \Delta \vec{C}_{i+\frac{1}{2}} + \Delta \vec{C}_{i-\frac{1}{2}} \right), \Delta \vec{C}_{i-\frac{1}{2}} \right\} \right], \quad (3.28)$$

$$\Delta \vec{C}_{i+\frac{1}{2}} = \vec{C}_{i+1} - \vec{C}_i,$$

$$MM = \begin{cases} \max\{x_i\}, & \text{when } x_i < 0 \quad \forall i, \\ \min\{x_i\}, & \text{when } x_i > 0 \quad \forall i, \\ 0, & \text{when } x_i = 0 \quad \forall i. \end{cases} \quad (3.29)$$

Where,  $\Delta$  represents central difference whereas  $MM\{x_1, x_2, \dots\}$  is a min-mod (limiter) function. Finally, one sided local speed of propagation at  $a_{i+\frac{1}{2}}(t)$ , are determined by

$$\begin{aligned} a_{i+\frac{1}{2}}^+(t) &= \max \left\{ \lambda_N \left( J(\vec{C}_{i+\frac{1}{2}}^-(t)) \right), \lambda_N \left( J(\vec{C}_{i+\frac{1}{2}}^+(t)) \right), 0 \right\} \\ a_{i+\frac{1}{2}}^-(t) &= \min \left\{ \lambda_1 \left( J(\vec{C}_{i+\frac{1}{2}}^-(t)) \right), \lambda_1 \left( J(\vec{C}_{i+\frac{1}{2}}^+(t)) \right), 0 \right\}, \end{aligned} \quad (3.30)$$

where  $\lambda_1 < \lambda_2 < \dots < \lambda_N$  are the eigen-values determined by Jacobian  $J \equiv \frac{\partial \vec{A}}{\partial \vec{C}}$ . The second ordered accuracy corresponding to time can achieved by using second-order Total Variations Diminishing(TVD) and Runge-Kutta(RK) schemes to solve Eq. (3.25). Now, denote Eq. (3.25) with  $L(\vec{C})$  and update  $\vec{C}$  by the same scheme through these steps, given

by

$$\vec{C}^{(1)} = \vec{C}^n + \Delta t L(\vec{C}^n), \quad (3.31a)$$

$$\vec{C}^{n+1} = \frac{1}{2} \left( \vec{C}^{(1)} + \vec{C}^n + (\Delta t) L(\vec{C}^{(1)}) \right), \quad (3.31b)$$

here,  $\Delta t$  is a time step.  $\vec{C}^n$  represents the approximated solution by previous time  $t_n$  level whereas  $\vec{C}^{n+1}$  expresses the updated and approximated solution at forwarding time  $t_{n+1}$  level. This approach provides the scheme to automatically detect and redirect the numerical solutions in SRHD.

### 3.2.2 The two-dimensional Central Upwind Schemes

Let us take in consideration two dimension hyperbolic system of conservative law SRHD in order to derive central upwind schemes as shown by

$$\frac{\partial \vec{C}}{\partial t} + \sum_{i=1}^2 \frac{\partial \vec{A}^i(\vec{C})}{\partial x^i} = 0, \quad (3.32)$$

where

$$\vec{C} = \begin{pmatrix} \rho\omega \\ (p+e)\omega^2 v^j \\ (p+e)\omega^2 - p \end{pmatrix}, \quad \vec{A}^i = \begin{pmatrix} \rho\omega v^i \\ (e+p)\omega^2 v^i v^j + p(\delta^{ij}) \\ (p+e)\omega^2 v^i \end{pmatrix} \quad \text{where } i, j = 1, 2. \quad (3.33)$$

Here, the rectangular computational domain  $[x_0, x'] \times [y_0, y']$  along with control interval  $C_{ij} \equiv [x_{i-\frac{1}{2}}, x_{i+\frac{1}{2}}] \times [y_{j-\frac{1}{2}}, y_{j+\frac{1}{2}}]$  is discretized by  $N_i$  and  $N_j$  uniform mesh points in both  $x$ -direction and  $y$ -direction, accordingly. The variables denoted by  $x'$ ,  $y'$  represents the maximum values of respective variables. Moreover here,  $i, j = 1, 2, 3, \dots, N$ . Rectangular coordinate of population in  $C_{ij}$  is represented as  $(x_i, y_j)$ .

Let

$$(x_{1/2}, y_{1/2}) = (0, 0) \text{ and } x_i = \frac{\Delta x_i}{2}, \quad y_j = \frac{\Delta y_j}{2}, \quad (3.34)$$



where

$$\Delta x_i = (x_{i+1/2} - x_{i-1/2}) \quad \text{and} \quad \Delta y_j = (y_{j+1/2} - y_{j-1/2}).$$

Averages of cell value of conserved variables  $\vec{C}_{i,j}(t)$  at any time  $t$  is

$$\vec{C}_{i,j} \vec{C}_{i,j}(t) = \frac{1}{\Delta y_j \Delta x_i} \int_C \vec{C}(t, x, y) dx dy, \quad (3.35)$$

and the piecewise-linear variable is

$$\vec{C}(t, x, y) = \sum_{i,j=1}^N \chi_{i,j} \left[ \vec{C}_{i,j} + (x + x_i) (\vec{C}_{i,j}^x) + (y + y_j) (\vec{C}_{i,j}^y) \right]. \quad (3.36)$$

Here,  $\chi_{i,j}$  is a characteristics function to cells  $(\vec{C}_{i,j}^x) \times (\vec{C}_{i,j}^y)$  represents the approximated results of the numerical derivatives corresponding to x and the y-direction respectively, of conserved variable  $\vec{C}$  over the cell center  $(x_i, y_j)$ . In the numerical experiment, the generalized nonlinear limiter (MM) [22, 51] is used to calculate the partial derivative for non-oscillations.

$$\begin{aligned} \vec{C}_{i,j}^x &= MM \left[ \theta \left( \frac{\vec{C}_{i-1,j} - \vec{C}_{i,j}}{\Delta x}, \frac{\vec{C}_{i+1,j} - \vec{C}_{i-1,j}}{2\theta\Delta x}, \frac{\vec{C}_{i,j} - \vec{C}_{i-1,j}}{\Delta x} \right) \right], \\ \text{similarly} \quad \vec{C}_{i,j}^y &= MM \left[ \theta \left( \frac{\vec{C}_{i,j-1} - \vec{C}_{i,j}}{\Delta y}, \frac{\vec{C}_{i,j+1} - \vec{C}_{i,j-1}}{2\theta\Delta y}, \frac{\vec{C}_{i,j} - \vec{C}_{i,j-1}}{\Delta y} \right) \right], \end{aligned} \quad (3.37)$$

here,  $\theta \in [1, 2]$ . The integral approximation of Euler equation Eq. (3.32) over the volume of special relativistic hydrodynamics (SRHD) model in two-dimension leads to extension of the scheme central upwind in two-space dimension, as expressed in

$$\frac{d\vec{C}_{i,j}}{dt} = \frac{1}{\Delta x} \left( \mathbf{S}_{i-\frac{1}{2},j}^x - \mathbf{S}_{i+\frac{1}{2},j}^x \right) - \frac{1}{\Delta y} \left( \mathbf{S}_{i,j-\frac{1}{2}}^y - \mathbf{S}_{i,j+\frac{1}{2}}^y \right). \quad (3.38)$$

Where,

$$\begin{aligned} \mathbf{S}_{i+\frac{1}{2},j}^x &= \frac{1}{2} \left[ \vec{A}^1(\vec{C}_{i+\frac{1}{2},j}^-) - \vec{A}^1(\vec{C}_{i+\frac{1}{2},j}^+) + a_{i+\frac{1}{2},j}^x \left( \vec{C}_{i+\frac{1}{2},j}^+ - \vec{C}_{i+\frac{1}{2},j}^- \right) \right], \\ \mathbf{S}_{i,j+\frac{1}{2}}^y &= \frac{1}{2} \left[ \vec{A}^2(\vec{C}_{i,j+\frac{1}{2}}^-) - \vec{A}^2(\vec{C}_{i,j+\frac{1}{2}}^+) + a_{i,j+\frac{1}{2}}^y \left( \vec{C}_{i,j+\frac{1}{2}}^+ - \vec{C}_{i,j+\frac{1}{2}}^- \right) \right], \end{aligned} \quad (3.39)$$

and, the average (intermediate) values are shown by

$$\begin{aligned}\vec{C}_{i+\frac{1}{2},j}^- &= \vec{C}_{i,j} + \frac{\Delta x}{2}(\vec{C}_{i,j}^x), \quad \vec{C}_{i+\frac{1}{2},j}^+ = \vec{C}_{i+1,j} - \frac{\Delta x}{2}(\vec{C}_{i+1,j}^x), \\ \vec{C}_{i,j+\frac{1}{2}}^- &= \vec{C}_{i,j} + \frac{\Delta y}{2}(\vec{C}_{i,j}^y), \quad \vec{C}_{i,j+\frac{1}{2}}^+ = \vec{C}_{i,j+1} - \frac{\Delta y}{2}(\vec{C}_{i,j+1}^y).\end{aligned}\quad (3.40)$$

Corresponding to single dimension case, the one sided local speed of propagating  $a_{i+\frac{1}{2},j}$  and  $b_{i,j+\frac{1}{2}}$  are calculated via

$$\begin{aligned}a_{i+\frac{1}{2},j}^+(t) &= \max \left\{ \lambda_N \left( J_1(\vec{C}_{i+1,j}^-(t)) \right), \lambda_N \left( J_1(\vec{C}_{i,j}^+(t)) \right), 0 \right\}, \\ b_{i,j+\frac{1}{2}}^+(t) &= \max \left\{ \lambda_N \left( J_2(\vec{C}_{i,j+1}^-(t)) \right), \lambda_N \left( J_2(\vec{C}_{i,j}^+(t)) \right), 0 \right\}, \\ a_{i+\frac{1}{2},j}^-(t) &= \min \left\{ \lambda_1 \left( J_1(\vec{C}_{i+1,j}^-(t)) \right), \lambda_1 \left( J_1(\vec{C}_{i,j}^+(t)) \right), 0 \right\}, \\ b_{i,j+\frac{1}{2}}^-(t) &= \min \left\{ \lambda_1 \left( J_2(\vec{C}_{i,j+1}^-(t)) \right), \lambda_1 \left( J_2(\vec{C}_{i,j}^+(t)) \right), 0 \right\},\end{aligned}$$

here  $\lambda_1$  is the smallest eigen value whereas  $\lambda_N$  is the largest eigen value of  $J_1 \equiv \frac{\partial \vec{A}^1}{\partial \vec{C}}$  and  $J_2 \equiv \frac{\partial \vec{A}^2}{\partial \vec{C}}$ , respectively. Complete derivation of the scheme introduced in [52].

### 3.3 The Numerical Tests

The current section incorporates some numerical approximations for both single and two-space dimension numerical problems. The scheme profiles of state-variables sustain the degree of accuracy, capability and authenticity of suggested numerical solver.

#### 3.3.1 The One-dimensional Problems

Here, we are considered single dimensional numerical tests. For our choice of accuracy, authenticity and comparison, the test is also apply to some additional numerical schemes. First of all we have implemented the central scheme introduced by Nessayhu-Tadmor(NT),

which is a simple as well as efficient method. In the second phase, the implementation of KFVS scheme [8, 22] is found to be very competitive. Here, the numerical methods for computing solution are demonstrating the competency as well as the authenticity of the suggested schemes in order to capture several Riemann problems discontinuities profile.

**Problem 1: The Experimental order of convergence**

Here, to achieve the validation our EOC of the central upwind, the KFVS and the central(NT) schemes. The simplest initial conditions for the test problem are shown below

$$(\rho, v, p) = (\rho, 0, 1.0) ,$$

$$\text{where } \rho = \frac{1}{\sqrt{2\pi}\sigma} e^{-[\frac{(x-\mu)^2}{2\sigma^2}]}, \text{ with } \mu = 0.5 \text{ and } \sigma = 0.13. \quad (3.41)$$

The numerical domain is computed in the  $[0, 1]$  interval which is discretized by  $N$  mesh cells whereas time step is taken by  $t = 0.5$ , moreover  $L^1$ -norm can be presented as

$$\| \vec{C}(t, \cdot) - \vec{C}_h(t, \cdot) \|_{L^1(\mathbb{R})} = ch^\alpha . \quad (3.42)$$

There,  $\vec{C}_h$  representing the approximate solution,  $\vec{C}$  represents exact solution and  $\alpha$  is its order. If  $h = \Delta x$  then  $L^1$ -error is written as

$$\| \vec{C}(t, \cdot) - \vec{C}_h(t, \cdot) \|_{L^1} = \sum_{i=1}^N | \vec{C}(t, \cdot) - \vec{C}_h(t, \cdot) | (\Delta x).$$

Therefore, Eq. (3.42) gives

$$EOC \stackrel{\text{def}}{=} \alpha = \ln \left( \frac{\| \vec{C}(t, \cdot) - \vec{C}_{\frac{h}{2}}(t, \cdot) \|_{L^1}}{\| \vec{C}(t, \cdot) - \vec{C}_h(t, \cdot) \|_{L^1}} \right) / \ln \left( \frac{1}{2} \right) . \quad (3.43)$$

Table 3.1 displays good capability to provide the  $L^1$ -errors successfully. It also focussed on EOC which is quite comparable to other schemes like the central(NT), the central upwind

and the KFVS. Figure 3.1 represents a plots for  $L^1$ -errors where the central upwind scheme ensures better accuracy in the solution profile. In addition, these techniques have second order convergence. Table 3.1 displays good capability to provide the  $L^1$ -errors successfully. It also focussed on EOC which is quite comparable to other schemes like the central(NT), the central upwind and KFVS. Figure 3.1 represents a plots for  $L^1$ -errors where the central upwind scheme ensures better accuracy in the solution profile. In addition, these techniques have second order convergence.

Table 3.1: Comparative numerical results of  $L^1$ -errors associative with EOC.

N	Central upwind		Central(NT)		KFVS	
	$L^1 - error$	$EOC$	$L^1 - error$	$EOC$	$L^1 - error$	$EOC$
60	0.00160671580	-	0.00522649282	-	0.01439462579	-
120	0.00021253982	2.9218	0.00097061566	2.42	0.00441346372	1.7049
240	0.00003073447	2.7958	0.00024655245	1.96	0.00124105908	1.8200
480	0.00000517274	2.5685	0.00006298962	1.96	0.00033419285	1.8918
960	0.00000112326	2.2037	0.00001841696	1.76	0.00009005463	1.8908
1920	0.00000030125	1.9037	0.00000378090	2.28	0.00002382608	1.9167

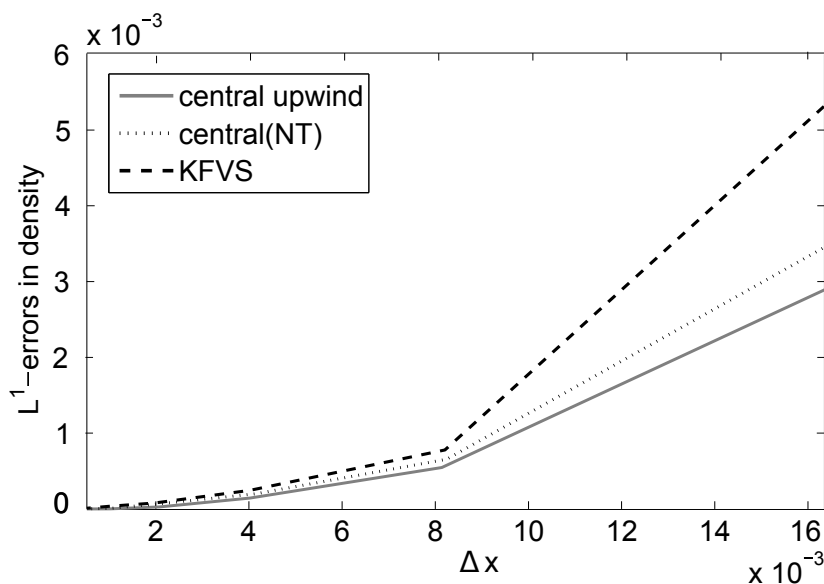


Figure 3.1: Comparison of  $L^1$ -errors.

### Shock tube numerical problems:

One-dimensional shock tube test problems are useful for discretization of central upwind scheme. The Shock tube waves are discontinuous profiles in the proposed scheme. This problem involved one-dimensional pipe having computational domain  $[0, 1]$  with  $N$  mesh points. In all shock tube cases, data is divided into two parts as  $(\rho, v, p)^L$  stand for the left ( $0 < x \leq 0.5$ ) whereas  $(\rho, v, p)^R$  stand the right ( $0.5 < x \leq 1$ ) pertaining to the diaphragm set initially in middle position of the test tube and after then pulled out. Each wave pattern is composed of shocks or rarefaction wave which is separating on the both sides left and right, and also contact discontinuity in the middle of the uniform stat solution. In relativistic procedure, these attributes are stable qualitatively, but the formation of the characteristics remains same whereas the effects of density jumps are unlimited by any adiabatic index and it is noted that due to non-linear Lorentz transformation formulae [50], the rarefaction waves do not have the straight profiles. The central upwind is able to deliver robustness and accurately which resolve the discontinuous profiles than the KFVS and central schemes (NT) [8, 22].

## Problem 2: The Shock tube problem-I

This problem initiate with the following condition for two constant states can be separated by

$$\begin{aligned}
 (\rho, v, p) &= (10, 0, 13.23) && \text{if } x \leq 0.5, \\
 (\rho, v, p) &= (1, 0, 0.67 \times 10^{-6}) && \text{if } x > 0.5.
 \end{aligned}
 \tag{3.44}$$

One-dimensional computational region  $[0, 1]$  at time level  $t = 0.4$  with 400 grid points. This problem is break into two initial states. In first state the transonic rarefaction wave propagates away from domain towards left whereas in the second state the shock wave propagates toward right. Here, the assumption is made that the motion of fluid moves with the mildly relativistic flow speed ( $v = 0.71c$ ) towards right. The shock wave accumulate the flow particles towards a dense shell that results in compressing and heating the fluid. According to the thermodynamic theoretic point of law the concerned fluid is more relativistic whereas dynamically it is only mildly relativistic.

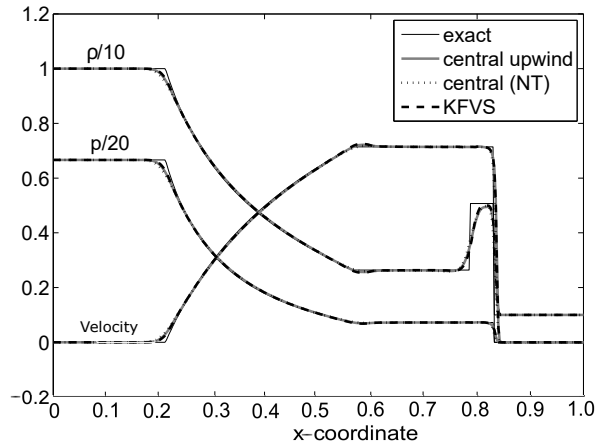


Figure 3.2: Comparison at  $t = 0.4$  for the shock problem-I.

Figure 3.2 presents these results graphically. It is seen that current scheme which is central

upwind provides the similar solutions produced by central scheme. Our proposed scheme demonstrates the discontinuity profile better than central (NT) solver.

### Problem 3: The Shock tube problem-II

The concerned shock problem in a single dimension having initialized test data is defined by

$$\begin{aligned}
 (\rho, v, p) &= (1, 0, 1000) \quad \text{when } x \leq 0.5, \\
 (\rho, v, p) &= (1, 0, 0.01) \quad \text{when } x > 0.5.
 \end{aligned}
 \tag{3.45}$$

The interval of computational numerical domain can defined by  $[0, 1]$ . The fluid under the above condition gives the extreme flow pattern as compared to the problem 2, time step  $t = 0.35$  with 500 grids elements. The post shocks, there exist an extremely very thin layer dense-shell and with width of this shell is nearly 1%. Here, the velocity for the fluid is taken as  $v = 0.95c$ . The density jump is maximum 10.6 for an exact numerical solution of Riemann test problem whereas 7.2 is approximated solution of LLF and HHF schemes of third order, [50].

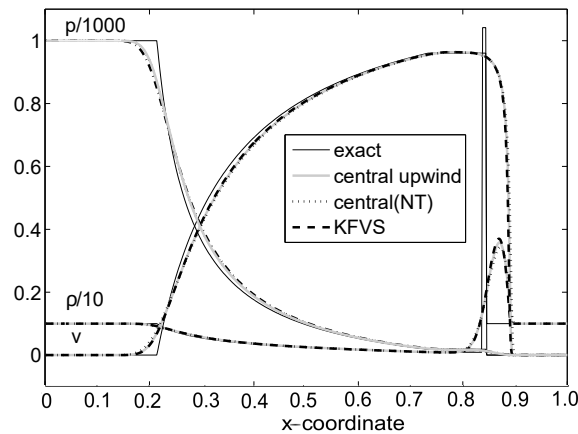


Figure 3.3: Comparison at  $t = 0.35$  for the shock test problem-II.

The simulated numerical solutions are displayed in Figure 3.3. Depicted results indicate that our suggested scheme (central upwind) provide good approximation when it is analyzed with central (NT) and KFVS techniques [50].

**Problem 4: The Perturbed relativistic shock tube flow**

Present test case had proposed by [50, 53]. Shock tube involves a discontinuity under the given initial condition by

$$\begin{aligned}
 (\rho, v, p) &= (4, 0, 40) && \text{when } x \leq 0.5, \\
 (\rho, v, p) &= (\rho_R, 0.0, 5.0) && \text{when } x > 0.5.
 \end{aligned}
 \tag{3.46}$$

Which produces a sinusoidal wave having perturbed density,  $\rho_R = 3 + 0.2 \sin(50x)$  toward right region. These tests are performed with 400 mesh points having time step  $t = 0.35$ . The numerical results for primitive variables under the above assumption are presented by Figure 3.4. It is quite clear that central upwind scheme performed much better results than the central and KFVS schemes. Furthermore, our scheme shows better sinusoidal results than those provided by [53] in literature.



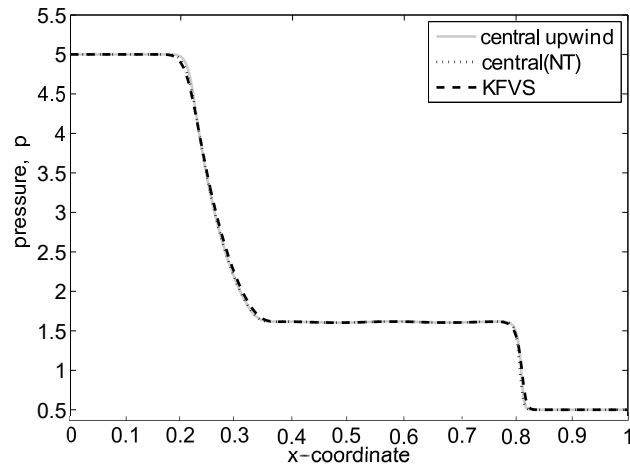
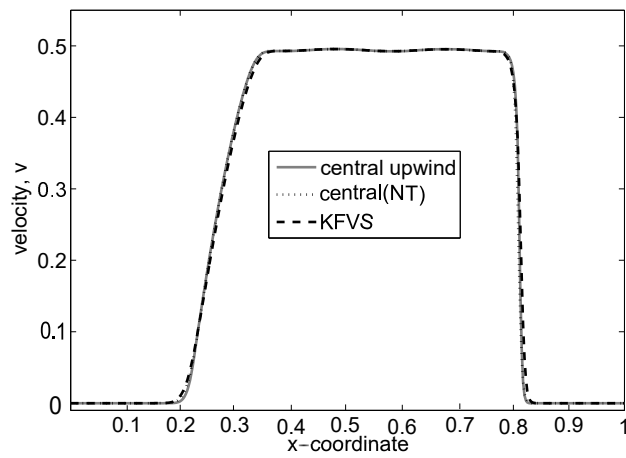
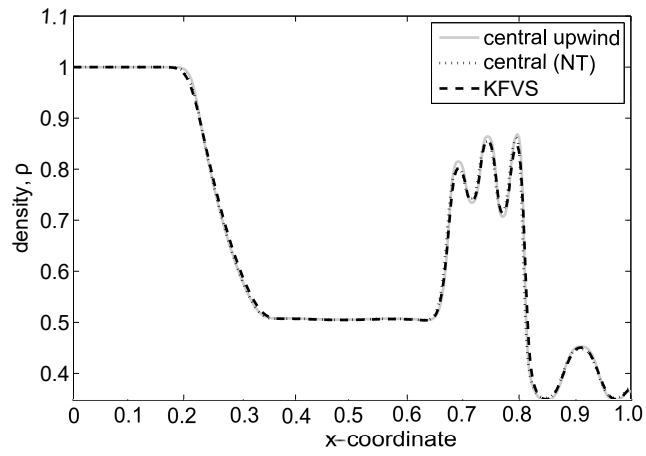


Figure 3.4: Comparison at  $t = 0.35$  for the relativistic-shock test problem .

### 3.3.2 The Two-dimensional Problems

The current section deals with the multi dimensional test problems that are much complicated when it is compared with the single dimension test problems due the the complexity in the relativistic flow. In order to validate and authenticity of the implementation of central upwind scheme, the numerical solutions of both central NT scheme and KFVS scheme is comparable to the proposed scheme.

#### Problem 5: The Experimental order of convergence

For this two-dimension test problem, in order to validate our EOC of central upwind, KFVS and central(NT) scheme. Simplest initialized conditions are shown by

$$\begin{aligned} \rho &= \frac{1}{\sqrt{2\pi\sigma}} e^{-[\frac{(x-\mu)^2}{2\sigma^2} + \frac{(y-\mu)^2}{2\sigma^2}]}, \text{ with } \mu = 0.5 \text{ and } \sigma = 0.13, \\ p &= 1.0, \quad v = 0.0. \end{aligned} \quad (3.47)$$

The numerical computational is set to be in the interval  $[0, 1] \times [0, 1]$  that is discretized by  $N$  mesh points at time  $t = 0.5$  with  $h = \Delta x$ , moreover  $L^1$ -norm can be define as

$$\| \vec{C}(t, \cdot) - \vec{C}_h(t, \cdot) \|_{L^1(\mathbb{R})} = ch^\alpha. \quad (3.48)$$

since,  $\vec{C}_h$  is a approximate solution,  $\vec{C}$  represents exact solution and  $\alpha$  is its order. If  $h = \Delta x$  then  $L^1$ -error is written as

$$\| \vec{C}(t, \cdot) - \vec{C}_h(t, \cdot) \|_{L^1} = \sum_{i=1}^N | \vec{C}(t, \cdot) - \vec{C}_h(t, \cdot) | (\Delta x).$$

Therefore, the above equation gives

$$EOC \stackrel{\text{def}}{=} \alpha = \ln \left( \frac{\| \vec{C}(t, \cdot) - \vec{C}_{\frac{h}{2}}(t, \cdot) \|_{L^1}}{\| \vec{C}(t, \cdot) - \vec{C}_h(t, \cdot) \|_{L^1}} \right) / \ln \left( \frac{1}{2} \right). \quad (3.49)$$

Table displays good capability to provide the  $L^1$ -errors successfully. It also focussed on EOC which is quite comparable to other schemes like the central(NT), central upwind and KFVS. Plots are presented in Figure 3.5 for  $L^1$ -errors. It is noted that the central upwind method is capable to reduce the errors profile. Furthermore, these numerical techniques present second-order convergence rate.

Table 3.2: Comparative numerical results of  $L^1$ -errors associative with EOC.

N	Central upwind		Central(NT)		KFVS	
	$L^1 - error$	EOC	$L^1 - error$	EOC	$L^1 - error$	EOC
30	0.000047056576445	-	0.001251733644641	-	0.000825412015137	-
60	0.000014232555355	1.7454	0.000208294899187	2.59	0.000163605138051	2.3451
120	0.000004568548676	1.6392	0.000044596868191	2.21	0.000038486608572	2.0982
240	0.000001427668873	1.6881	0.000011605147500	1.93	0.000010383948554	1.8897
480	0.000000441460058	1.6943	0.000003428395149	1.75	0.000010383858554	1.7660

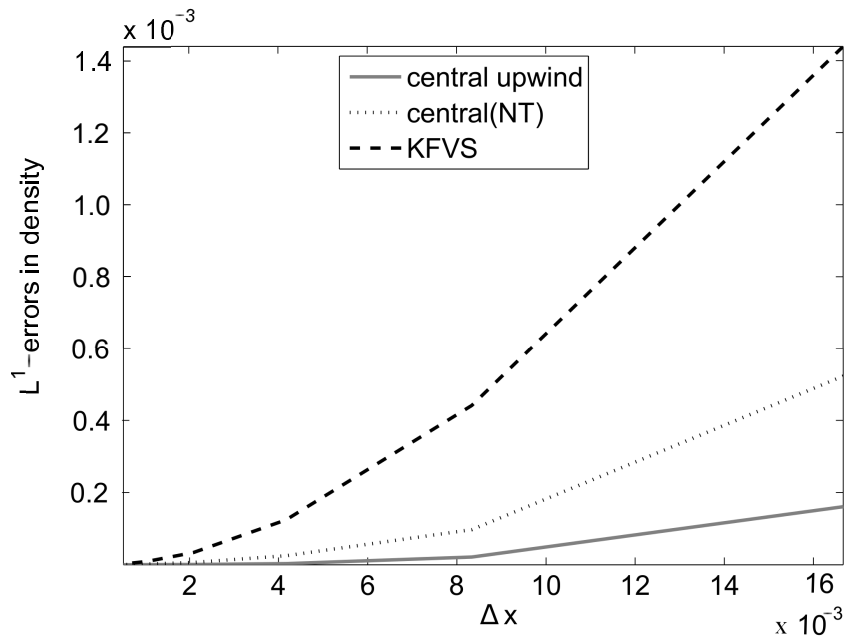


Figure 3.5: Comparison of  $L^1$ -errors.

### Problem 6: Two-dimensional shock tube problem

The two-space dimension shock test is consists of a square shock tube with side having unit length. The diaphragm is initially broken into four quadrants as shown in initial data as

$$\begin{aligned}(\rho, v^1, v^2, p)^{NE} &= (1.0, 0, 0, 0.01), \\(\rho, v^1, v^2, p)^{NW} &= (1.0, 0.98, 0, 1.0), \\(\rho, v^1, v^2, p)^{SW} &= (5.0, 0, 0.0, 1.0), \\(\rho, v^1, v^2, p)^{SE} &= (1.0, 0.0, 0.99, 1.0).\end{aligned}\tag{3.50}$$

These four quadrants are symmetrical to the main diagonal, divides two for contact discontinuities and remaining two for one-dimensional shocks. It is observed that the exact one-dimensional shock can not be propagates towards the N and E interfaces that may be observed in Figure 3.7 which displaying computational results of discontinuities traveling to the NE corner by approximate Riemann solvers. In the remaining domain the pattern consist of curved shock waves with the complex structure is presented in SW interface, implicative of an inclined impingement jets with the converging curved shocks front along with the bow shock. These lines corresponding to bow shock are infect caused by spurious waves that are produce by S and W quadrant in the SW direction with numerical propagation term involved in energy equation, (two constant states appear in the kinetic energy with jump), and can not be eliminate while by Roe-type solver [50]. As presented in Figure 3.7. Our proposed scheme are reasonably comparable with the central(NT) as well as the KFVS schemes for primitive variables as shown by Figure 3.6. The numerical approximations produced by our proposed scheme seems to be in good agreements by those presented in [50] with more accuracy.

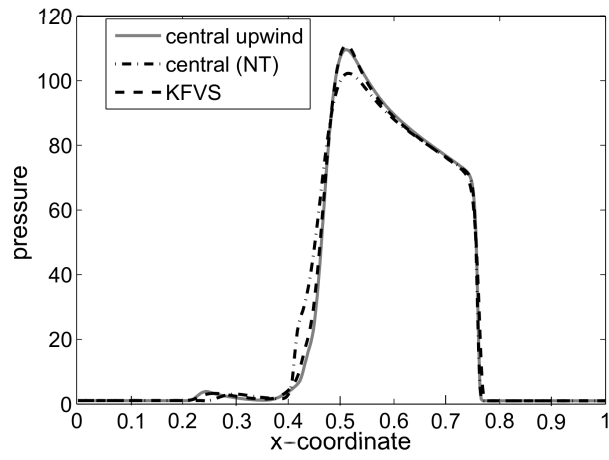
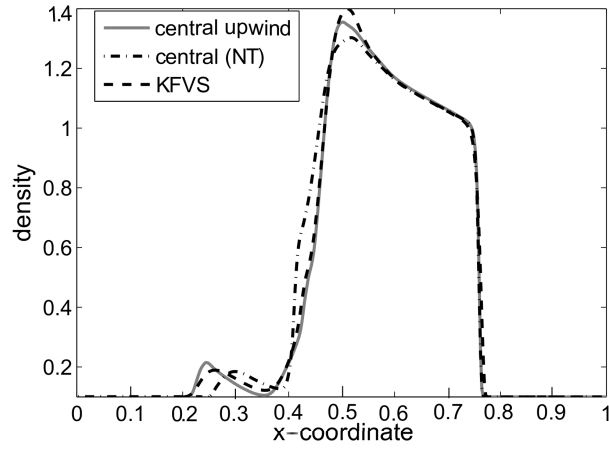


Figure 3.6: Comparison at  $t = 0.4$  for  $400 \times 400$  mesh cells.

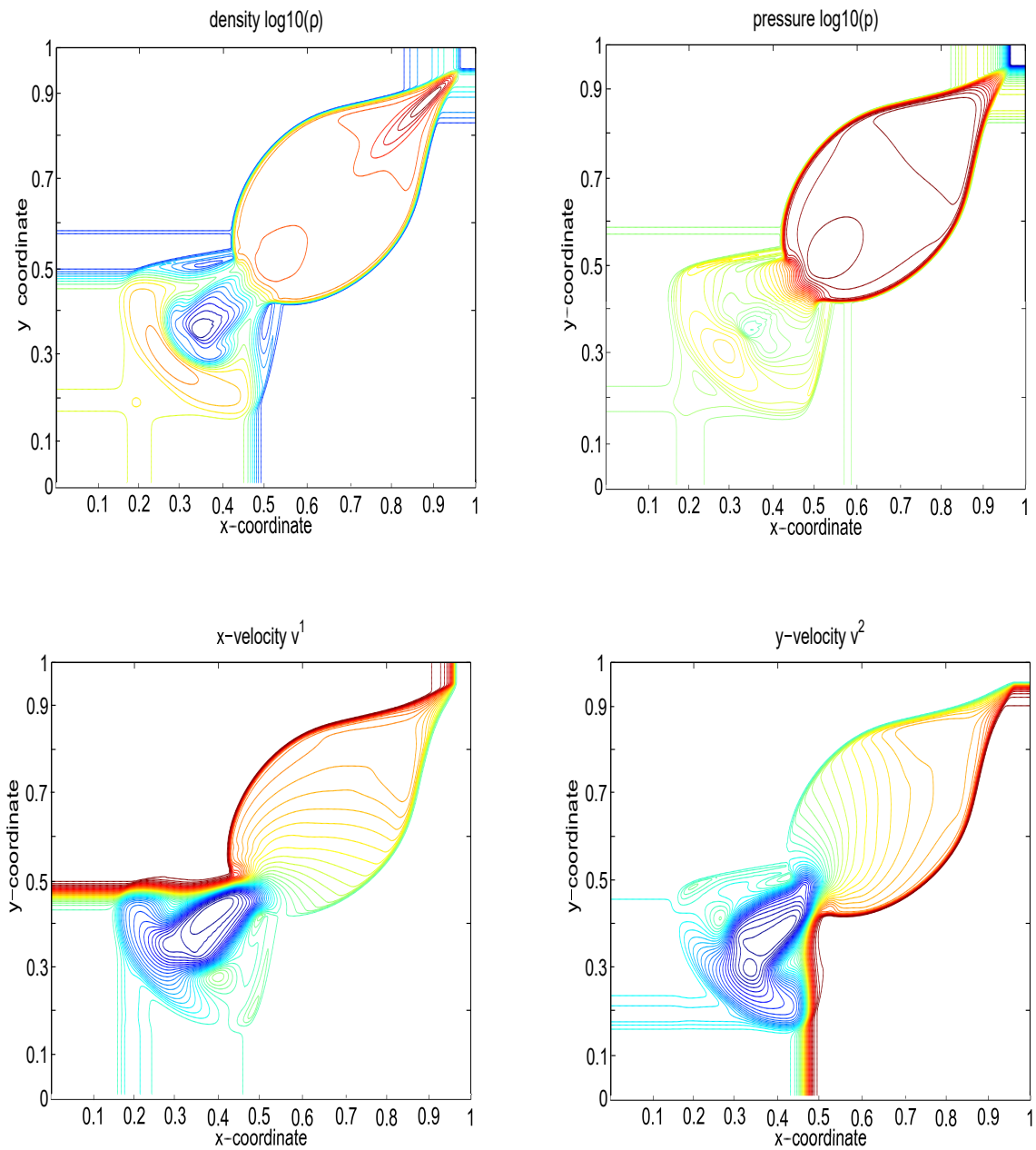


Figure 3.7: Results at  $t = 0.4$  for the shock test problem.

### Problem 7: Diffracting shock waves and forwarded face step

This test is concerned with the diffraction shock waves at a corner. Relativistic problem is investigated by Dyke [54] analog of the classical solution. In this problem, the computational dimensions for the square region are not more than those introduced by [54]. Figure 3.8 displays the initial data where  $x = 0.0$  represents the starting position of the shock wave. Figure 3.9 presents the final results. The rolled up vortex is generated at a corner. Numerical computations are carried out on a  $300 \times 300$  mesh cells with a time step sets to  $t = 1.7$ . The Figure 3.10 shows a good comparison in between the numerical central scheme and our proposed scheme. Central upwind scheme provides accuracy, efficiency and stability.

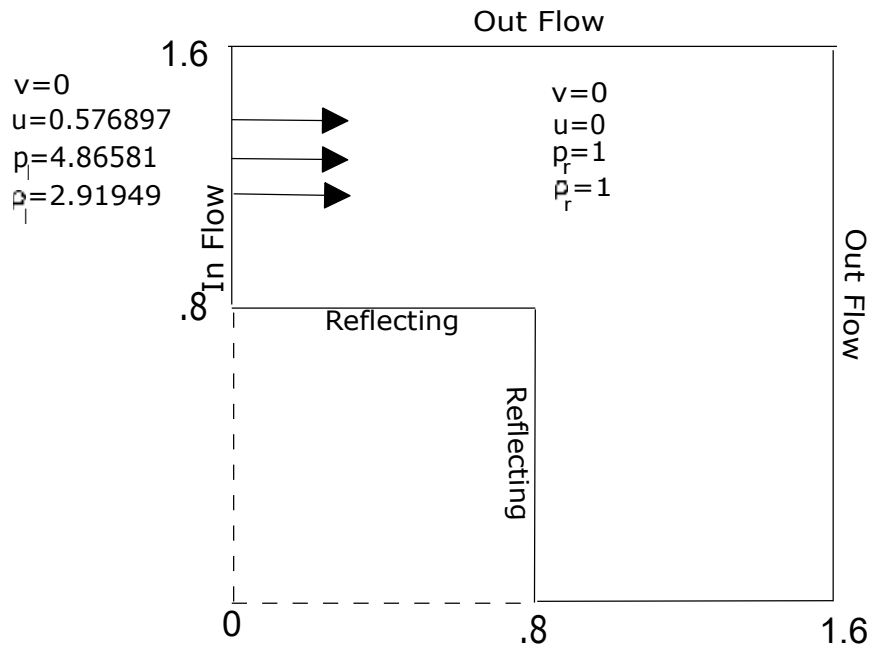


Figure 3.8: The representation for initial data.

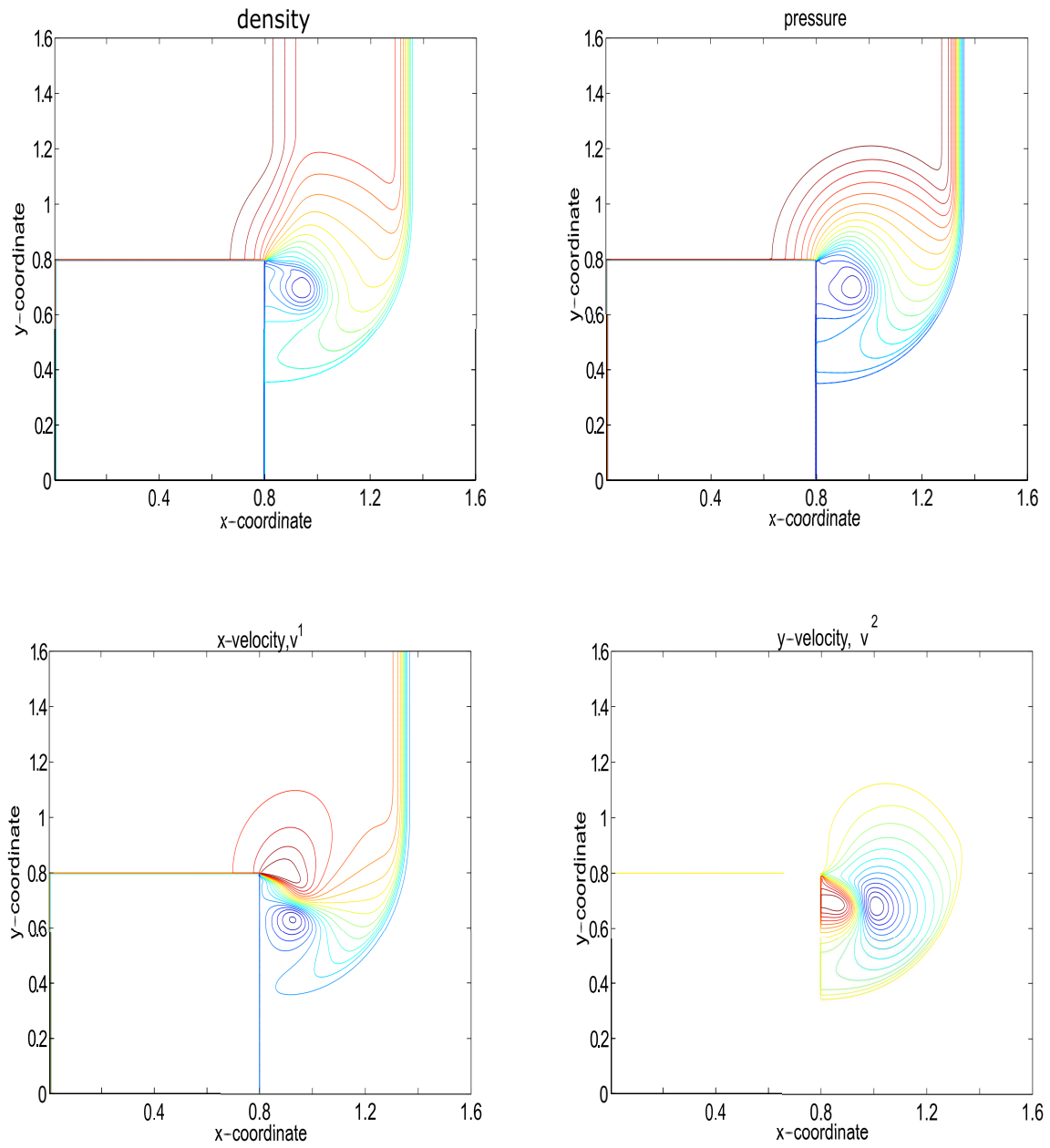


Figure 3.9: Results at  $t = 1.7$  for diffracting the shock waves test problem.



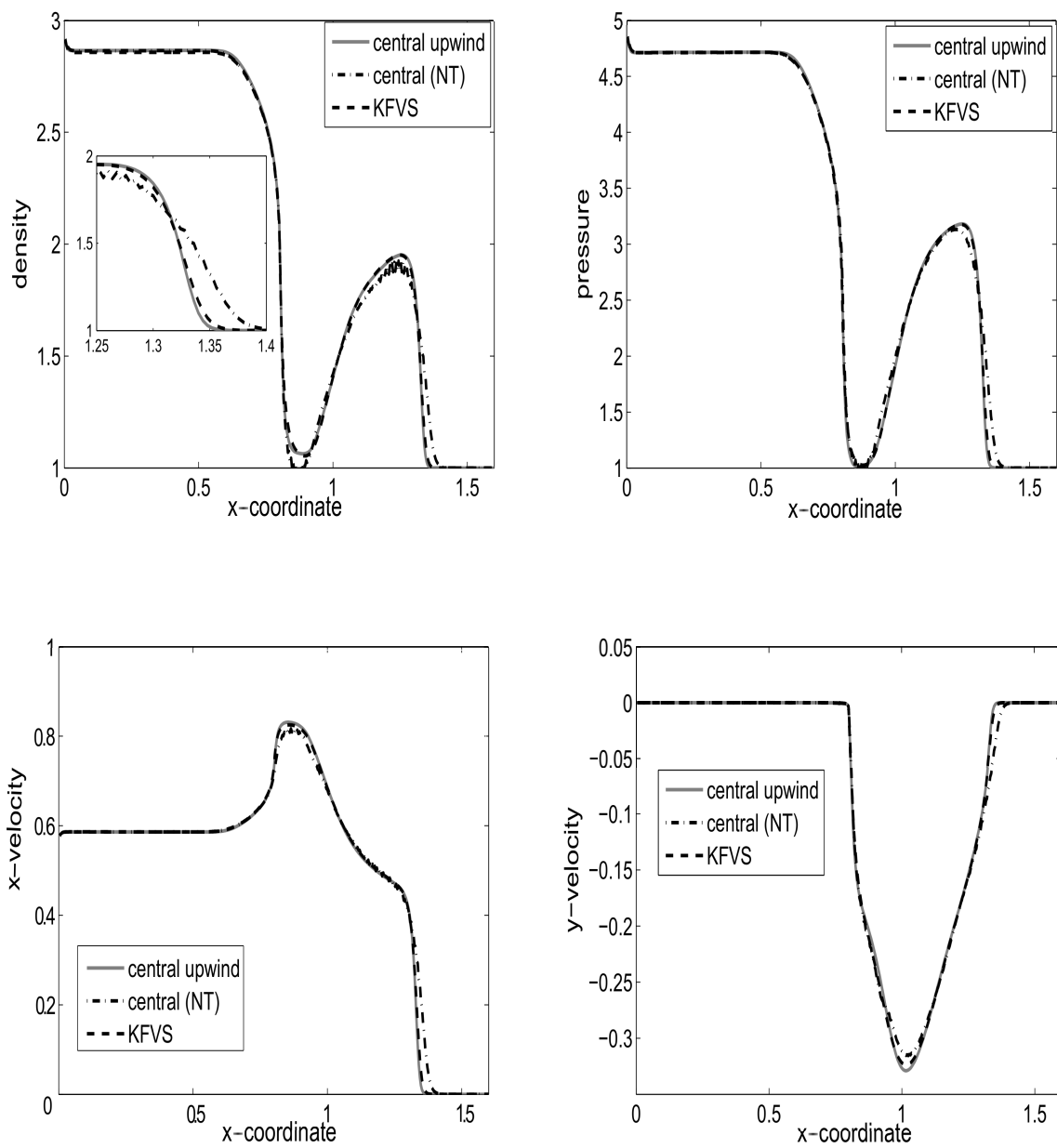


Figure 3.10: Comparison at  $t = 1.7$  for  $300 \times 300$  mesh cells.

### Problem 8: Cylindrical Explosion Problem.

We are consider here the initial data for two-dimension cylindrical explosion test problem as shown by

$$\begin{aligned}(\rho, v, p) &= (10, 0, 10) && \text{when } r \leq 0.2, \\(\rho, v, p) &= (0.1, 0, 0.01) && \text{otherwise.}\end{aligned}\tag{3.51}$$

The numerical computational is set to be in the square region  $[0, 1] \times [0, 1]$  that is discretized by  $200 \times 200$  mesh cells with time step  $t = 0.2$ . The cylindrical explosion region having center at  $(0.5, 0.5)$  and radius 0.2 is with in the domain. In this case, circular rarefaction waves travel towards the origin whereas the circular shock waves travel outward from the origin, and follow by the circular contacts discontinuity which is traveling in the similar direction. Similar behaviors of central upwind are also observed by centra(NT) and the KFVS schemes as shown in Figure 3.11. However, the numerical simulations of suggested scheme central upwind ensure the less error accuracy. Figure 3.12 displays contour plots of current scheme. Similar behaviors of central upwind are also observed with the other schemes such as central(NT) and the KFVS as shown in Figure 3.11. However, results of current scheme ensure less error accuracy. Figure 3.12 displays contour plots of current scheme.

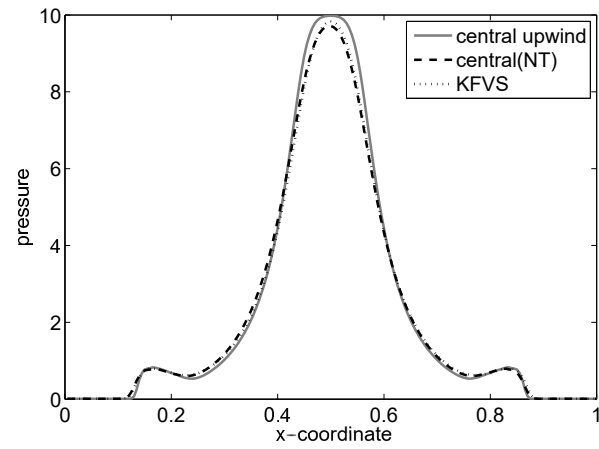
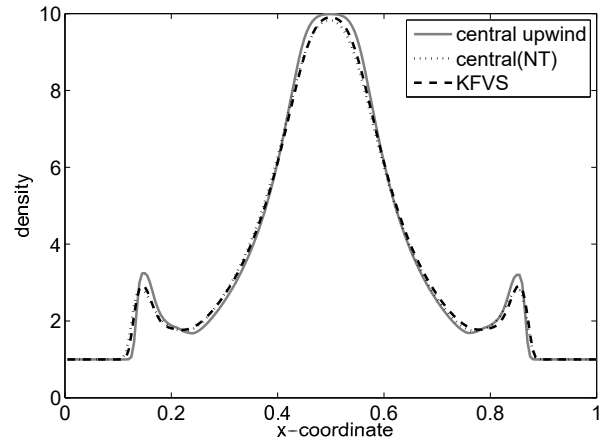


Figure 3.11: Comparison at  $t = 0.2$  at  $200 \times 200$  mesh cells.

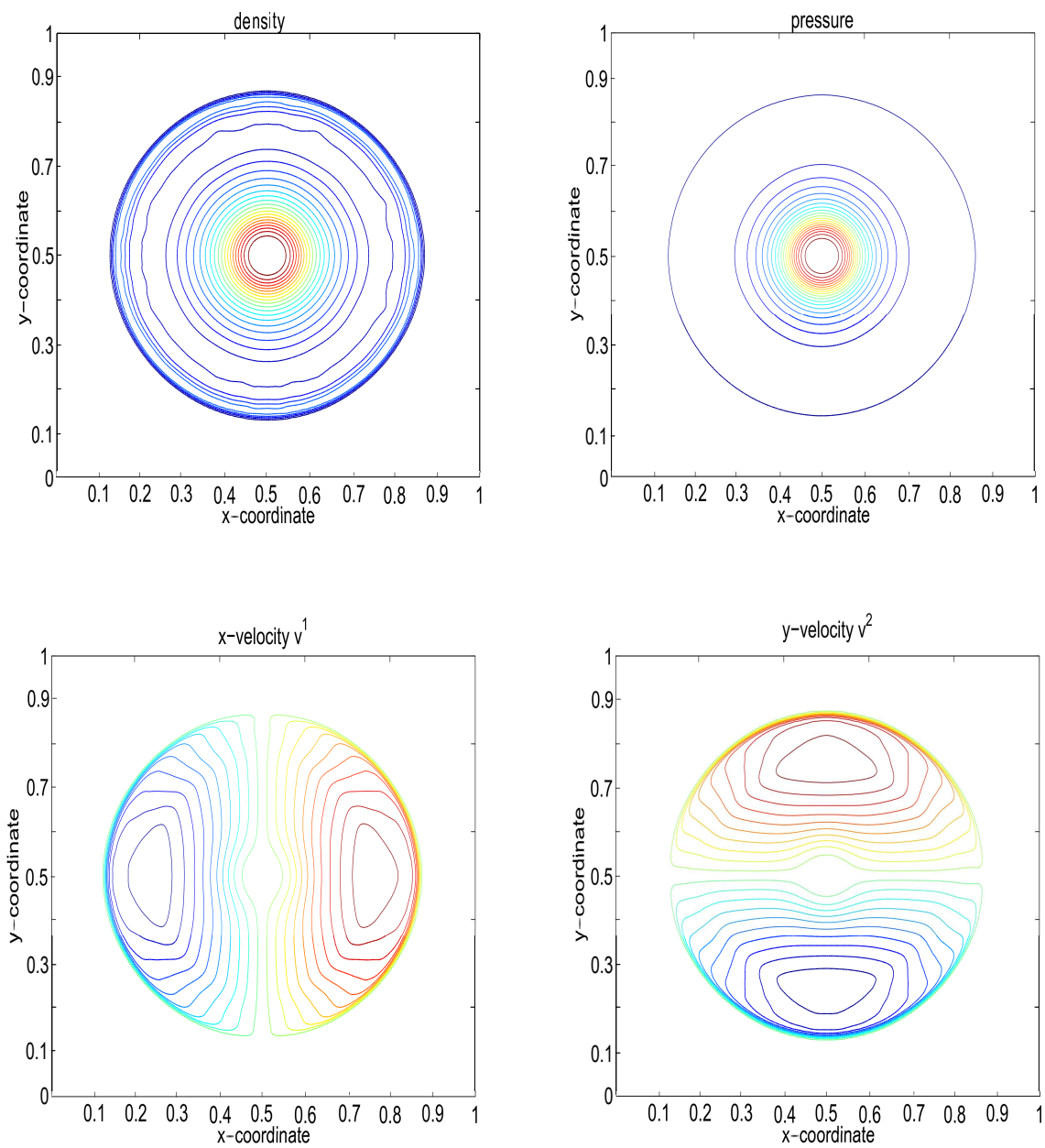


Figure 3.12: Results at  $t = 0.2$  for the cylindrical blast test problem.

### Problem 9: The box explosion

For this problem the concern data that initializing the test of primitive variables may be written as

$$\begin{aligned}(\rho, v, p) &= (1, 0, 10.0) \quad l = 0.2, \\(\rho, v, p) &= (1, 0, 0.01) \quad l = 1.0.\end{aligned}\tag{3.52}$$

Wherein,  $l$  corresponds for length of the square boxes. The numerical computational is set to be in the square region  $[0, 1] \times [0, 1]$ , is discretized by  $400 \times 400$  mesh cells with reflecting walls. In this problem the small box is placed at the middle of the large box. Figures 3.13 to 3.15, displays the final achievement at different times level such as  $t = 1.0$  is taken as the initial time step whereas  $t = 2.0$  is the second time steps accordingly. Similar behaviors of suggested scheme are also observed with the schemes that are available in the literature e.g. central(NT) and KFVS as shown in Figures 3.13 to 3.15. However, our central upwind demonstrates the good profile for the discontinuity profile as compared to NT scheme.

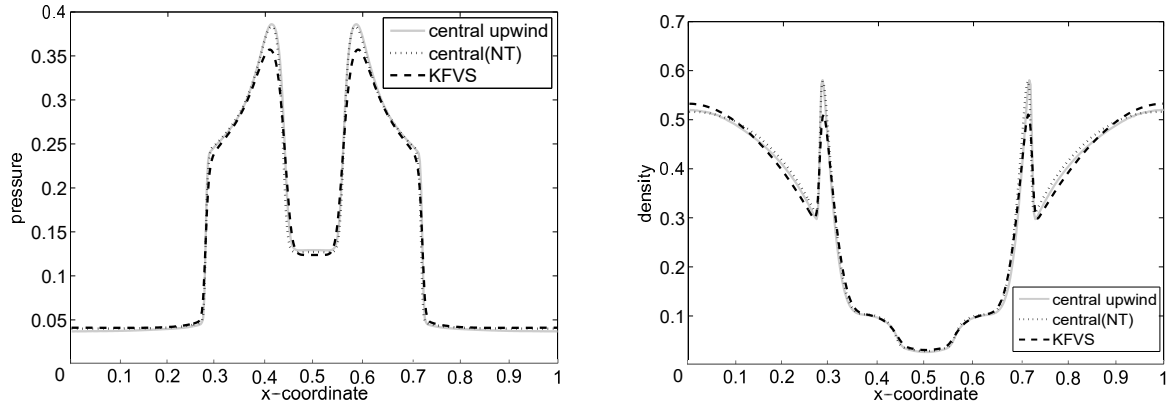


Figure 3.13: Comparison at  $t = 1.0$  for  $400 \times 400$  mesh cells.

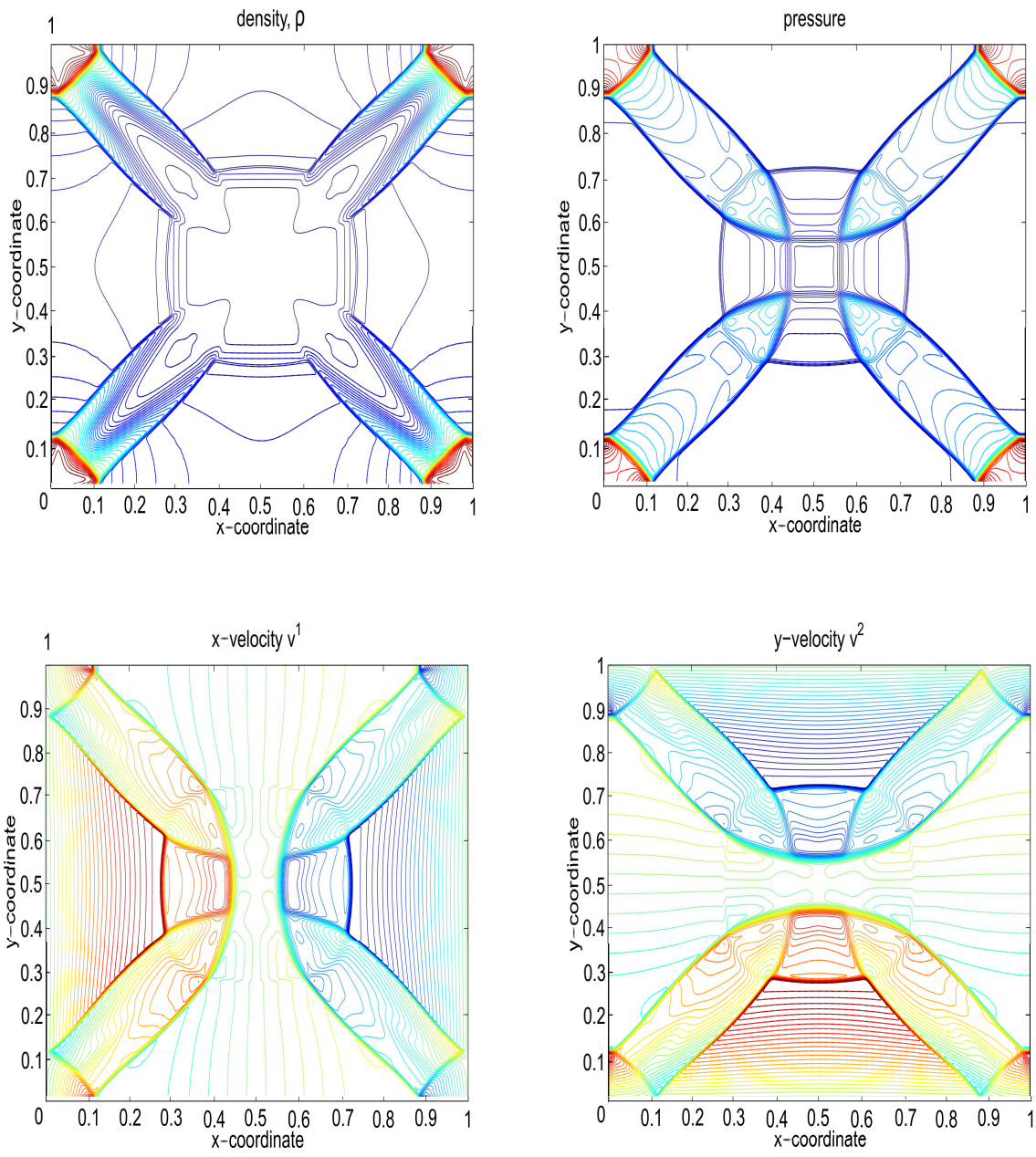


Figure 3.14: The results at  $t = 1$  for explosion in the box.

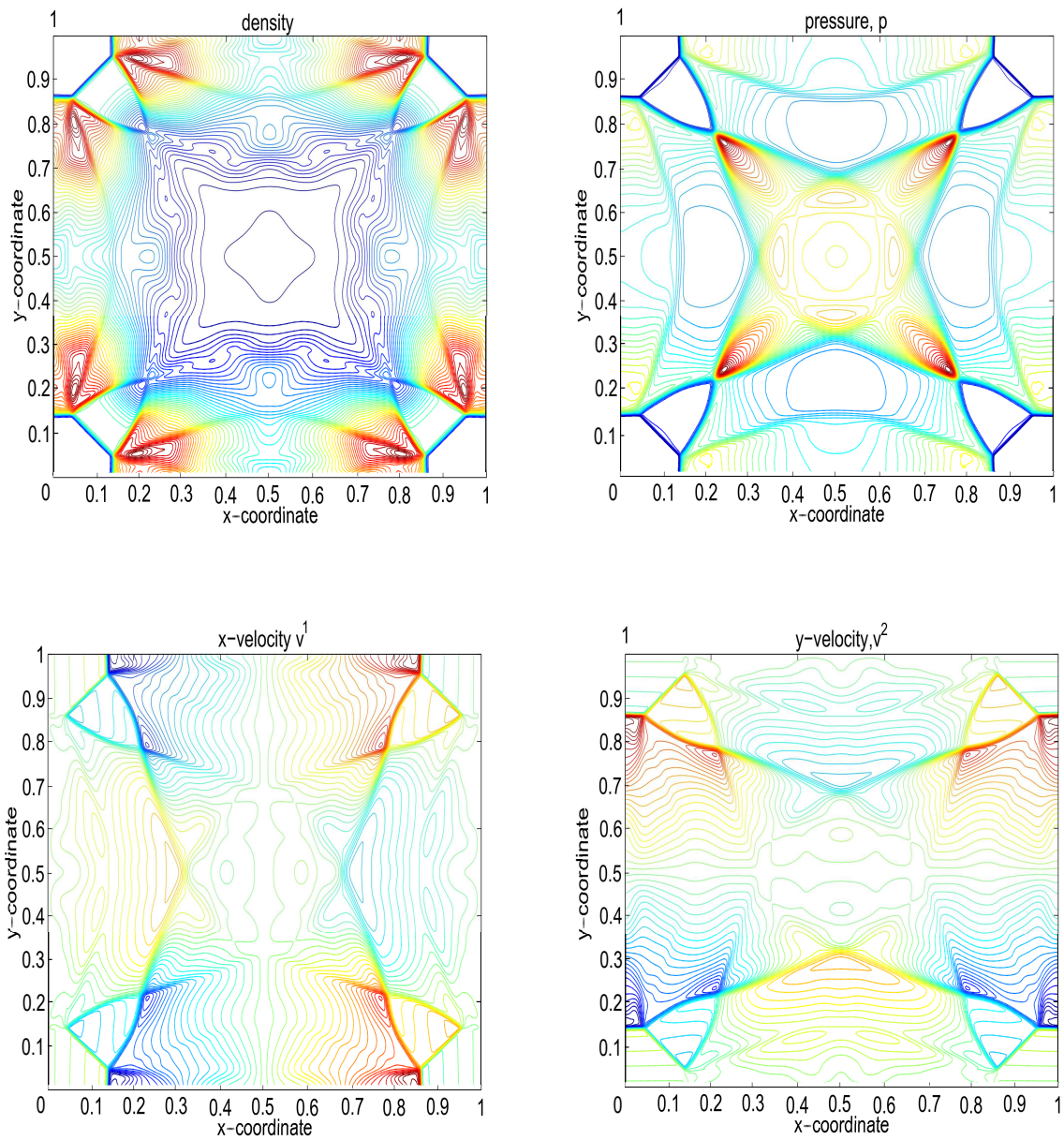


Figure 3.15: The results at  $t = 2$  for explosion in the box.

### 3.4 Summary

Here, the central upwind schemes [51] was performed and implemented to numerically solve for the single and multi-dimensional (2D) special relativistic hydrodynamics Euler equations. Our proposed scheme is simple, compact, resolve sharp and complex discontinuities. This scheme reduce the numerical dispersion in a solution profile. These future of propose technique makes it very fascinating specially in two-dimension, where computation robustness, accurately and efficiency has extremely important. Comparison of central(NT) and the KFVS schemes with the numerical evaluations of our central upwind technique, demonstrates good agreement. In addition, the final approximation agreed well with those that are present in literature [25, 55, 56].



## **Chapter 4**

### **The Central Upwind Scheme for URHD Model**

The equations that illustrate a fluid undergoing relativistic speeds are known as the relativistic hydrodynamic equations, Einstein-Euler equations, or the relativistic Euler equations. In an ultra-relativistic limit, the flow of a fluid is moving with a velocity very close to the speed of a light through vacuum  $c$  and its local internal energy density is much larger as compared to the local rest mass density of fluid. Mathematically, this limit allows to ignore the fluid's rest mass density. The execution of central upwind schemes code approximates the ultrarelativistic Euler equation for single and multi-dimensional (2D) spaces. In order to validity and comparability, the numerical solution of staggered central(NT) schemes [22, 23] and the KFVS schemes [8, 19, 20, 21] are illustrated in addition. Various numerical test problems are studies for consideration. The observation was made that the proposed schemes produces equivalent results as provided by KFVS schemes however the results of our scheme are more superior than the central(NT) schemes.

## 4.1 The Ultra-relativistic Hydrodynamics (URHD)

Flow velocities in a ultrarelativistic (UR) limit tends to speed of light. Due to this fact the internal thermal energy density of fluids dominating the rest-mass density then the UR equation of state can be written as

$$e = 3p. \quad (4.1)$$

In a previous chapter we have briefly discussed for SRHD models. Now, employing Eq. (4.1) into Eqs. (3.7)–(3.11) and considered the system in two dimensional space, we obtain

$$\frac{\partial \vec{C}}{\partial t} + \sum_{i=1}^2 \frac{\partial \vec{A}^i(\vec{C})}{\partial x^i} = 0, \quad (4.2)$$

where

$$\vec{C} = \begin{pmatrix} C_1 \\ C_{i+1} \\ C_4 \end{pmatrix} = \begin{pmatrix} N^0 \\ T^{0i} \\ T^{00} \end{pmatrix} = \begin{pmatrix} \rho\sqrt{1+\mathbf{u}^2} \\ 4pu^i\sqrt{1+\mathbf{u}^2} \\ 3p+4p\mathbf{u}^2 \end{pmatrix} \quad (4.3)$$

and

$$\vec{A}^i = \begin{pmatrix} A_1^i \\ A_{j+1}^i \\ A_4^i \end{pmatrix} = \begin{pmatrix} N^i \\ T^{ij} \\ T^{i0} \end{pmatrix} = \begin{pmatrix} \rho u^i \\ 4pu^i u^j + p\delta^{ij} \\ 4pu^i\sqrt{1+\mathbf{u}^2} \end{pmatrix}, \quad i, j = 1, 2. \quad (4.4)$$

Here,  $\mathbf{u} = \sqrt{\sum_{i=1}^2 (u^i)^2}$ ,  $\omega = \frac{1}{\sqrt{1-\mathbf{v}^2}} = \sqrt{1+\mathbf{u}^2}$ ,  $u^0 = \omega$  and  $u^i = \omega v^i$ . The symbol  $\delta^{ij}$  is for kronecker delta. The parameter vector that contains the quantities of physical interests, can be choose in the local rest-frame,  $[\rho, u^i, p]^T$ . These primitive variable can be found from Eq. (4.3)

$$p = \frac{1}{3} \left[ -\vec{C}_5 + \sqrt{4\vec{C}_5^2 - 3 \sum_{k=1}^2 \vec{C}_{k+1}^2} \right], \quad u^i = \frac{\vec{C}_{i+1}}{2\sqrt{p(p + \vec{C}_5)}} \\ \text{and } \rho = \frac{\vec{C}_1}{\sqrt{\mathbf{u}^2 + 1}} \quad \text{where } i = 1, 2, 3. \quad (4.5)$$

In the development of an upwind code to approximate the hyperbolic system of conservation equation, the eigen structure of Jacobian matrix is needed. A mathematical model, forming a system of PDEs, is hyperbolic strictly if every eigenvalues of the Jacobian matrix is distinct and real. Moreover, the corresponding values of eigenvectors form set of basis functions. In the case when some of the eigenvalues are coinciding then the system is weakly hyperbolic [57]. Since our model Eq. (4.2) is seems to be strictly hyperbolic that are dealing with the eigenvalues defined by

$$\lambda_{\pm} = \frac{1}{3+2\mathbf{u}^2} \left\{ 2u\sqrt{\mathbf{u}^2+1} \pm \sqrt{3+2\mathbf{u}^2-2u^2} \right\}, \quad \lambda = \frac{u}{\sqrt{\mathbf{u}^2+1}}. \quad (4.6)$$

The above equation in one-dimension can be written as

$$\lambda_{\pm} = \frac{2u\sqrt{u^2+1} \pm \sqrt{3}}{2u^2+3}, \quad \lambda = \frac{u}{\sqrt{u^2+1}}. \quad (4.7)$$

In all time advancing numerical schemes, the state variables  $\vec{C}$  need to be derived from the conserved variables and the state variables can be obtained from the conserved one, by using the relation defined in Eq. (4.3).

## 4.2 Central Upwind Schemes

Here, central upwind schemes defined by Tadmor and Kurganov [52] are implemented for numerically approximating the considered ultrarelativistic Euler equations in one and two dimension. In the current chapter, the model for URHD are derive by using the central upwind schemes. Here, consider single dimensional hyperbolic systems of conservative law of special relativistic hydrodynamics (URHD) to derive the central upwind scheme [35] as

$$\frac{\partial \vec{C}}{\partial t} + \frac{\partial \vec{A}(\vec{C})}{\partial x} = 0, \quad (4.8)$$

Let us considered  $\zeta_i \equiv [x_{i+1/2}, x_{i-1/2}]$  for the positive inter  $i$  where the averages of conservative variable  $\vec{C}$  in each interval of  $\zeta_i$  can be expressed as

$$\vec{C}_i \equiv \vec{C}_i(t) = \frac{1}{\Delta x} \int_{\zeta_i} \vec{C}(t, x) dx. \quad (4.9)$$

Now, integrate Eq. (4.8) over  $\zeta_i$ , implies

$$\frac{d\vec{C}_i}{dt} = \frac{1}{\Delta x} [\mathbf{S}_{i+\frac{1}{2}}(t) - \mathbf{S}_{i-\frac{1}{2}}(t)], \quad (4.10)$$

where the vector fluxes are expressed by

$$\mathbf{S}_{i+\frac{1}{2}} = \frac{1}{2} \left( \vec{A}(\vec{C}_{i+\frac{1}{2}}^-) - \vec{A}(\vec{C}_{i+\frac{1}{2}}^+) \right) + \frac{a_{i+\frac{1}{2}}}{2} \left( \vec{C}_{i+\frac{1}{2}}^+ - \vec{C}_{i+\frac{1}{2}}^- \right), \quad (4.11)$$

Here,  $\vec{C}^+$  and  $\vec{C}^-$  represent the right and left intermediate states of piecewise linear reconstruction  $\tilde{C} = (\tilde{\rho}, \tilde{\rho}u, \tilde{E}^*)$  at  $x_{i+\frac{1}{2}}$ , are written as

$$\vec{C}_{i+\frac{1}{2}}^+ = \vec{C}_{i+1} - \frac{\Delta x}{2} \vec{C}_{i+1}^x, \quad \vec{C}_{i+\frac{1}{2}}^- = \vec{C}_i + \frac{\Delta x}{2} \vec{C}_i^x. \quad (4.12)$$

The derivatives of  $\vec{C}_i^x$  are at a minimum of first order approximation by  $\vec{C}_x(x_i, t)$ . These derivatives can be estimated by taking nonlinear limiter which ensures the nonoscillatory characteristic of piecewise reconstruction Eq. (4.12). The feasible estimation of slopes, stated by family comprises of the discrete derivative is parameterized by using  $\theta \in [1, 2]$ , e.g.

$$\vec{C}_i^x = MM \left[ \theta \left\{ \Delta \vec{C}_{i+\frac{1}{2}}, \frac{1}{2} \left( \Delta \vec{C}_{i+\frac{1}{2}} + \Delta \vec{C}_{i-\frac{1}{2}} \right), \Delta \vec{C}_{i-\frac{1}{2}} \right\} \right], \quad (4.13)$$

$$\Delta \vec{C}_{i+\frac{1}{2}} = \vec{C}_{i+1} - \vec{C}_i,$$

$$MM = \begin{cases} \max\{x_j\}, & \text{when } x_j < 0 \quad \forall j, \\ \min\{x_j\}, & \text{when } x_j > 0 \quad \forall j, \\ 0, & \text{when } x_j = 0 \quad \forall j. \end{cases} \quad (4.14)$$

Where,  $\Delta$  represents the central difference whereas  $MM$  is a min-mod (limiter) function.

Finally, one sided local speed of propagation at  $a_{i+\frac{1}{2}}(t)$ , are determined by

$$\begin{aligned} a_{i+\frac{1}{2}}^+(t) &= \max \left\{ \lambda_N \left( J(\vec{C}_{i+\frac{1}{2}}^-(t)) \right), \lambda_N \left( J(\vec{C}_{i+\frac{1}{2}}^+(t)) \right), 0 \right\} \\ a_{i+\frac{1}{2}}^-(t) &= \min \left\{ \lambda_1 \left( J(\vec{C}_{i+\frac{1}{2}}^-(t)) \right), \lambda_1 \left( J(\vec{C}_{i+\frac{1}{2}}^+(t)) \right), 0 \right\}, \end{aligned} \quad (4.15)$$

where  $\lambda_1 < \lambda_2 < \dots < \lambda_N$  are the eigen-values determined by Jacobian  $J \equiv \frac{\partial \vec{A}}{\partial \vec{C}}$ . The second-order accuracy with respect to time can be achieved by employing the second-order Total Variation Diminishing(TVD) Runge-Kutta(RK) numerical schemes in order to solve Eq. (4.10). Now, denote Eq. (4.10) with  $L(\vec{C})$  and update  $\vec{C}$  by the same scheme through these steps, given by

$$\vec{C}^{(1)} = \vec{C}^n + (\Delta t) L(\vec{C}^n), \quad (4.16a)$$

$$\vec{C}^{n+1} = \frac{1}{2} \left( \vec{C}^{(1)} + \vec{C}^n + (\Delta t) L(\vec{C}^{(1)}) \right), \quad (4.16b)$$

here,  $\Delta t$  is a time step and  $\vec{C}^n$  is denotes approximated numerical solution at a previous time  $t_n$  step whereas  $\vec{C}^{n+1}$  is represents updated approximated numerical solution at a next time  $t_{n+1}$  step. This approach provides the scheme to automatically detect and redirect the numerical solutions in URHD. In contrast to the SRHD model, the primitive variables in ultra-relativistic limit are explicitly expressible in the form of conservative variable.

In the previous chapter, the methods have been derived for two-dimension SRHD models and, can easily be derive in the same manner for URHD models. The central upwind schemes performed much better results than those provided in literature.

### 4.3 Central Schemes(NT)

Here, our concern is to approximate the Euler equations of ultrarelativistic hydrodynamics (URHD) in one-dimension, it is consider

$$\frac{\partial \vec{C}}{\partial t} + \frac{\partial \vec{A}(\vec{C})}{\partial x} = 0, \quad (4.17)$$

where  $\vec{A}(\vec{C})$  is the flux function of a conserved quantity  $\vec{C}$ . Date back to 1950s, the Lax-Friedrichs(LxF) schemes of first-order was introduced and then applied to first order central scheme. This LxF scheme of first order was then extended to second order Nessyahu and Tadmor (NT) in one-dimensional central scheme [22]. Central NT schemes are usually implemented for solving the hyperbolic system of conservation law correlate the various state of physics. Such high resolution with nonoscillatory schemes have implemented for the multi-dimensional problems [22, 23].

The central (NT) schemes are developed on the well known method named predictor-corrector which depends on two basic steps. In the first step, the algorithm starts with the known values of cell averages then it is applied to the nonoscillatory piecewise (linear)

reconstruction to predict point value. Whereas in a final step named corrector, realizing the evolution of these predicted mid-values of reconstructed polynomial in term of their staggered cell averages.

$$\vec{C}_i^{n+\frac{1}{2}} = \vec{C}_i^n - \frac{\lambda}{2} \vec{A}^x(\vec{C}_i). \quad (4.18)$$

$$\vec{C}_{i+\frac{1}{2}}^{n+1} = \frac{1}{2}(\vec{C}_i^n + \vec{C}_{i+1}^n) + \frac{1}{8}(\vec{C}_i^x - \vec{C}_{i+1}^x) + \lambda \left[ \vec{A}(\vec{C}_i^{n+\frac{1}{2}}) - \vec{A}(\vec{C}_{i+1}^{n+\frac{1}{2}}) \right]. \quad (4.19)$$

Moreover,

$$\frac{1}{\Delta x} \vec{A}^x(\vec{C}_i) = \frac{\partial}{\partial x} \vec{A}(\vec{C}(t, x = x_i) + O(\Delta x), \quad (4.20)$$

where  $\frac{1}{\Delta x} \vec{A}^x(\vec{C}_i)$  indicates the discrete numerical derivative of flux variable  $\vec{A}(\vec{C}(t, x = x_i))$ . The feasible estimation of the slope, stated with the family comprises of the discrete derivative is parameterized by using  $\theta \in [1, 2]$ , e.g.

$$\vec{C}_i^x = MM \theta \left\{ \Delta \vec{C}_{i+\frac{1}{2}}, \frac{1}{2} \left( \Delta \vec{C}_{i+\frac{1}{2}} + \Delta \vec{C}_{i-\frac{1}{2}} \right), \Delta \vec{C}_{i-\frac{1}{2}} \right\}, \quad (4.21)$$

$$\Delta \vec{C}_{i+\frac{1}{2}} = \vec{C}_{i+1} - \vec{C}_i,$$

$$MM = \begin{cases} \max\{x_i\}, & \text{when } x_i < 0 \quad \forall i, \\ \min\{x_i\}, & \text{when } x_i > 0 \quad \forall i, \\ 0, & \text{otherwise .} \end{cases} \quad (4.22)$$

Where,  $\Delta$  represents the central difference whereas  $MM$  is a min-mod (limiter) function. The central (NT) schemes does not require characteristic decomposition and Riemann solver. which makes them stable, simple and efficient. The detailed numerical derivation are presented [22] for the reader. Here, the single and multi-dimensional (2D) central NT schemes have implemented for the analysis and validity of the approximated results.

## 4.4 The KFVS Method

The KFVS schemes are implemented to estimate various models in the gas dynamics. The numerical fluxes are correlated with the flow across the cell interface. Theory of KFVS for one-dimension is applied to URHD equations [58]. The scheme is depending upon the numerical approximation of macroscopic fluxes splitting vector through uniform mesh cell boundary. The vectors flux functions is determined by the motion of the fluid particles and, from the statistical mechanics, particles phase density can often utilized to express this motion as follows

$$\mathcal{A}(\rho, T, \mathbf{u}, \mathbf{q}) = \frac{\rho \lambda^3}{8\pi} \exp(-\lambda u_\mu q^\mu). \quad (4.23)$$

Here, the normalization factor  $\lambda = \frac{4\rho}{e+p}$ ,  $\omega$  representing by the Lorentz-factor,  $q^\mu = (q^0, \mathbf{q})$  with  $\mathbf{q} = (q^1, q^2, q^3)^T$  is a 4-momentum, the 4-velocity is denoted as  $u^\mu = \frac{1}{\rho} N^\mu$ , where  $\rho = \sqrt{N^\nu N_\nu}$  with  $N^\mu$  being the flux vector corresponding to mass,  $u^\mu u_\mu$  is unity, and the quantity  $\mathbf{u} = \sqrt{\sum_{i=1}^3 (u^i)^2}$ . The total refinements in  $\mathcal{A}$  is presented in Eq. (4.23) by introducing changes in the value of  $\lambda$ . As introduced in a ultrarelativistic limiting case  $e = 3p$ , so that the value of  $\lambda = \frac{1}{T}$  is obtained in ultra-relativistic model, where  $T = \frac{p}{\rho}$  represents temperature. Actually, the transportation of flow quantities is because of the movements of flow particles. Applying  $\mathcal{A}$  in Eq. (4.23) implies that the flow particles are divided in two parts: in one part the particles are moving towards right with  $\nu > 0$  whereas in the rest part, the movement of the particles are towards left as  $\nu < 0$ . By considering the one dimensional space SRHD numerical equations along with phase density for  $i, j = 1$  in Eq. (4.2), The flux of SRHD defined in Eq. (4.4) (for  $i, j = 1$ ) are split into two parts:

$$\vec{A} = \vec{A}_A^+ + \vec{A}_A^-, \quad (4.24)$$



where

$$\vec{A}_{\mathcal{A}}^{\pm} = \langle u^1 \rangle_{\pm} \begin{pmatrix} \rho\omega \\ (e+p)\omega^2 v \\ (e+p)\omega^2 \end{pmatrix} + \langle u^0 \rangle_{\pm} \begin{pmatrix} 0 \\ p \\ 0 \end{pmatrix}, \quad (4.25)$$

with

$$\langle u^0 \rangle_{\pm} = \frac{(1 \pm v)}{2}, \quad \langle u^1 \rangle_{\pm} = \pm \frac{(1 \pm v)^2}{4}. \quad (4.26)$$

The detailed derivation can be analyze in [20]. By the corresponding distributions of the flux function at the cell interface are given by

$$\vec{A}_{i+\frac{1}{2}}^{\mathcal{A}} = \vec{A}_{i,\mathcal{A}}^+ + \vec{A}_{i+1,\mathcal{A}}^-, \quad (4.27)$$

here  $A$  represents free transport flux function. This method is very robust particularly when the grid points are unrefined. In the non-relativistic magnetohydrodynamics(MHD), Xu [45] had implemented the mechanism for the flux transportation of particle-collision to overcome dissipation numerically. By the interpretation of Eqs. (4.3) and (4.24), an equilibrium flux  $\vec{A}^e(\vec{C}_{i+\frac{1}{2}})$  is obtained as

$$\vec{C}_{i+\frac{1}{2}} = \vec{C}_i^+ + \vec{C}_{i+1}^-, \quad (4.28)$$

where

$$\vec{C}_i^{\pm} = \begin{pmatrix} \rho\omega \langle u^0 \rangle_{\pm} \\ (e+p)\omega^2 \langle u^1 \rangle_{\pm} \\ [(e+p)\omega^2 - p] \langle u^0 \rangle_{\pm} \end{pmatrix}. \quad (4.29)$$

Corresponding vector fluxes are shown by

$$\vec{A}_{i+\frac{1}{2}}^e = \vec{A}^e(\vec{C}_{i+\frac{1}{2}}), \quad (4.30)$$

where  $\vec{C}_{i+\frac{1}{2}}$  is defined in Eq. (4.28). Then the final vector fluxes is written as

$$\vec{A}_{i+\frac{1}{2}} = (1 - \chi)\vec{A}_{i+\frac{1}{2}}^e + \chi\vec{A}_{i+\frac{1}{2}}^{\mathcal{A}}, \quad (4.31)$$

where  $\chi \in [0, 1]$  is the adaptive parameter. The further detail is available in Xu [45]. By integrating (4.2) within the cell  $I_i = [x_{i-\frac{1}{2}}, x_{i+\frac{1}{2}}]$ , kinetic upwind method that is a semi-discrete can be achieved as

$$\frac{d\vec{C}_i}{dt} = \frac{1}{\Delta x} \left[ \vec{A}_{i-\frac{1}{2}} - \vec{A}_{i+\frac{1}{2}} \right], \quad (4.32)$$

where  $\vec{A}_{i+\frac{1}{2}}$  are the corresponding fluxes at the boundary  $x_{i+\frac{1}{2}}$  and defined in Eq. (4.31).

Here,  $\Delta x$  is the numerical cell width and the averaged value of the cell  $\vec{C}_i$  is expressed by

$$\vec{C}_i = \vec{C}_i(t) = \frac{1}{\Delta x} \int_{x_{i-\frac{1}{2}}}^{x_{i+\frac{1}{2}}} \vec{C}(x, t) dx. \quad (4.33)$$

## 4.5 MUSCL-Type Reconstruction Method

These schemes have accuracy of first-order only whereas the higher-order of accuracy can also be achieved by using initial reconstructions method for cell average variables  $\vec{C}_i$ . The second order piecewise linear MUSCL type numerical approximations can be constructed by utilizing discrete slope vector differences  $\vec{C}^x$  in order to achieve the piecewise constant approximated solution,  $\vec{C}_{i,j}$ . The approaching values at the boundaries can be written as

$$\vec{C}_i^{LX} = \vec{C}_i - \frac{1}{2}\vec{C}_i^x, \quad \vec{C}_i^{RX} = \vec{C}_i + \frac{1}{2}\vec{C}_i^x. \quad (4.34)$$

These boundary values are approximated with the defined min-mod (MM) limiter along with the initial reconstruction method that can be seen as

$$\vec{C}_i^x = MM \left[ \theta \left\{ \Delta \vec{C}_{i+\frac{1}{2}}, \frac{1}{2} \left( \Delta \vec{C}_{i+\frac{1}{2}} + \Delta \vec{C}_{i-\frac{1}{2}} \right), \Delta \vec{C}_{i-\frac{1}{2}} \right\} \right], \quad (4.35)$$

here  $\theta \in [1, 2]$  is representing the parameter and  $\Delta$  is denoting the central differencing,

$$\Delta \vec{C}_{i+\frac{1}{2}} = \vec{C}_{i+1} - \vec{C}_i. \quad (4.36)$$

Where,  $MM$  has already defined in Eq. (4.22). At the final stage, the expression for the semi-discrete higher resolution kinetic flux scheme presented as

$$\frac{d\vec{C}_i}{dt} = -\frac{\vec{A}_{i+\frac{1}{2}} \left( \vec{C}_{i+1}^{LX}, \vec{C}_i^{RX} \right) - \vec{A}_{i-\frac{1}{2}} \left( \vec{C}_i^{LX}, \vec{C}_{i-1}^{RX} \right)}{\Delta x}. \quad (4.37)$$

The second-order numerical accuracy with time function can be achieved to solve Eq. (4.37) by using the TVD RK-scheme of second-order. Now, denote Eq. (4.37) with  $L(\vec{C})$  and update  $\vec{C}$  by the same scheme through these steps [36], given by TVD RK-method of second order

$$\vec{C}^{(1)} = \vec{C}^n + \Delta t L(\vec{C}^n), \quad (4.38)$$

$$\vec{C}^{n+1} = \frac{1}{2} \left( \vec{C}^{(1)} + \vec{C}^n + \Delta t L \left( \vec{C}^{(1)} \right) \right), \quad (4.39)$$

here  $\Delta t$  is a time step.  $\vec{C}^n$  is approximated numerical solutions at the previous time level  $t_n$  whereas  $\vec{C}^{n+1}$  is the updated approximated result at the next time level  $t_{n+1}$ .

Here, the KFVS schemes for both single and multi-dimensional (2D) are applied to compare and validate the results.

## 4.6 Numerical Tests

We consider nonlinear systems of conservations laws for URHD to describe the central upwind scheme. The current scheme is suitable for single as well as for two-dimensional (2D) tests problems. Furthermore, the proposed scheme is compared with exact Riemann solver [59], the central (NT) [22, 60] and KFVS schemes [8, 19, 20]. All these schemes are already explained above.

### 4.6.1 One-dimensional Problems

The single-dimensional flow discontinuities tests that provide a good test for the numerical

codes efficiency to capturing the shocks and contact discontinuities with the small number of grid points. First of all, the current scheme is implemented to reproduce smooth and simple profile in the first test Problem to validate its order accuracy. After that, we consider the shock tube Problems (2) – (4) to validate the central upwind scheme. The numerical treatment of discontinuity can accurately be captured by using central up wind scheme. The value of Courant Friedrichs Lewy (CFL) in the current simulations is 0.5 and CPU times other all available numerical schemes are representing almost the same.

### Problem 1: Experimental order of convergence

In order to validate our EOC for the central upwind, kinetic flux vectors splitting technique and central(NT). Simplest initial conditions for the test problem are shown below

$$(\rho, v, p) = (\rho, 0.0, 1.0),$$

$$\text{where } \rho = \frac{1}{\sqrt{2\pi}\sigma} e^{-[\frac{(x-\mu)^2}{2\sigma^2}]}, \quad \mu = 0.5 \quad \text{and} \quad \sigma = 0.13. \quad (4.40)$$

The numerical computational domain in the interval  $[0, 1]$  discretized by  $N$  grid points whereas  $t = 0.5$  is taken as time step subsequently  $L^1$ -norm can be presented by the following

$$\| \vec{C}(t, \cdot) - \vec{C}_h(t, \cdot) \|_{L^1(\mathbb{R})} = ch^\alpha. \quad (4.41)$$

Here,  $\vec{C}_h$  denotes the approximate solution,  $\vec{C}$  represents exact solution and  $\alpha$  is its order.

If  $h = \Delta x$  then  $L^1$ -error is given below

$$\| \vec{C}(t, \cdot) - \vec{C}_h(t, \cdot) \|_{L^1} = \sum_{i=1}^N | \vec{C}(t, \cdot) - \vec{C}_h(t, \cdot) | (\Delta x).$$

Therefore, Eq. (4.41) gives

$$EOC \stackrel{\text{def}}{=} \alpha = \ln \left( \frac{\| \vec{C}(t, \cdot) - \vec{C}_{\frac{h}{2}}(t, \cdot) \|_{L^1}}{\| \vec{C}(t, \cdot) - \vec{C}_h(t, \cdot) \|_{L^1}} \right) / \ln \left( \frac{1}{2} \right). \quad (4.42)$$

Table 4.1 displays good capability to provide the  $L^1$ -errors successfully. It also focussed on EOC which is quite comparable to other schemes like the KFVS, central upwind as well as with the staggered central (NT) techniques. Here, it is noted that central upwind schemes ensures better accuracy in the solution profile. In addition, these techniques have second order convergence.

Table 4.1: Comparative numerical results of  $L^1$ -errors associative with EOC.

N	KFVS		Central (NT)		Central upwind	
	$L^1$ -error	EOC	$L^1$ -error	EOC	$L^1$ -error	EOC
60	0.001439462580	-	0.00522649392	-	0.00160781580	-
120	0.000441246472	1.71	0.00097061666	2.43	0.00021363982	2.91
240	0.000124106908	1.83	0.00024756245	1.97	0.00003074447	2.78
480	0.000033419385	1.90	0.00006299962	1.97	0.00000518274	2.57
960	0.000009005563	1.90	0.00001851696	1.77	0.00000112426	2.20
1920	0.000002383608	1.92	0.00000378190	2.29	0.00000030025	1.90

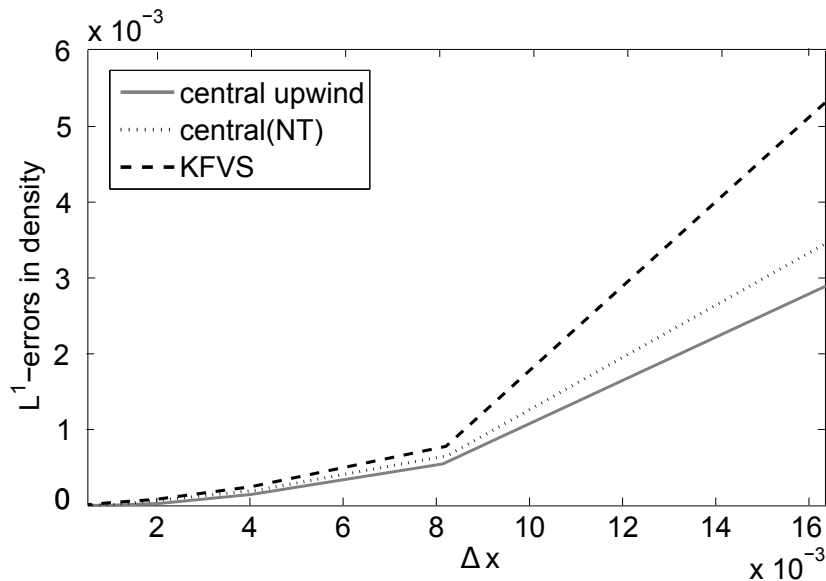


Figure 4.1: Comparison of  $L^1$ -errors.

### Shock tube problems:

For the simulation of discontinuous profiles in shock test tube problems, the scheme central upwind is implemented. Here, a numerical one-dimension pipe with unitary length consisting of  $N$  mesh elements, the state is divided into two parts as  $(\rho, v, p)^L$  stand for the left ( $0 \leq x \leq 0.5$ ) whereas  $(\rho, v, p)^R$  stand for the right side ( $0.5 < x \leq 1$ ). These physical states are actually reference to the diaphragm that is taken placed preliminarily at the center of a pipe then the diaphragm is pulled out. Each wave pattern is composed of shocks or rarefaction wave which is separating on the both left and right sides and also contact discontinuity in the middle of the uniform stat solution [50]. In all cases, the numerically approximated results of our proposed scheme are comparable with the results of KFVS method [20] and NT scheme [22] as well as with exact solution by Riemann [18].

### Problem 2: The relativistic flow

Here, the single-dimensional relativistic shock tube test initially consists of two constant states of fluid at rest under the relevant conditions given by

$$\begin{aligned}(\rho, v, p)^L &= (2.0, 0.0, 10.0) && \text{when } x \leq 0.5, \\(\rho, v, p)^R &= (1.0, 0.0, 0.5) && \text{when } x > 0.5.\end{aligned}\tag{4.43}$$

Here, uniform domain is defined by  $[0, 1]$  divided into 400 mesh cell at the time  $t = 0.45$ . Moreover, current problem is break into two initial states. In first state the transonic rarefaction wave propagates away from domain towards left whereas in the second state the shock wave propagates toward right. Assume that the motion of fluid to the right moves with the mildly relativistic speed ( $v = 0.72c$ ). By a thermodynamic view point, the fluid is intensively relativistic but dynamically mild relativistic. The Figure 4.2 depicts the validation of central upwind scheme with NT and KFVS schemes.

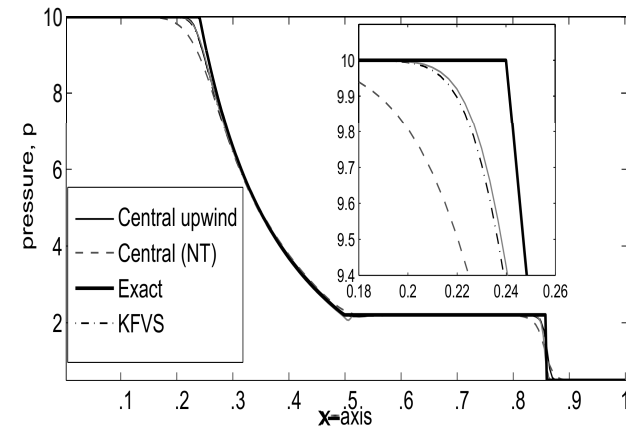
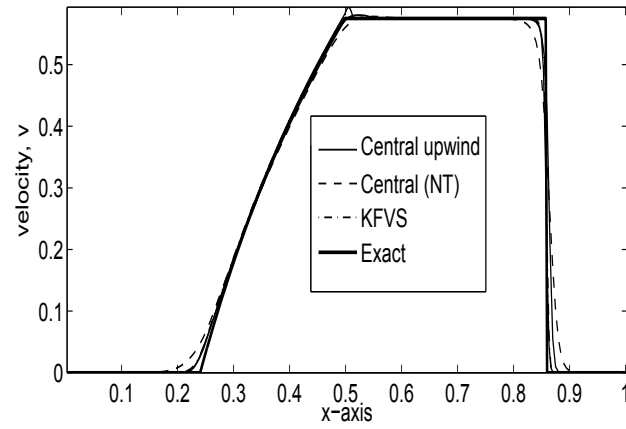
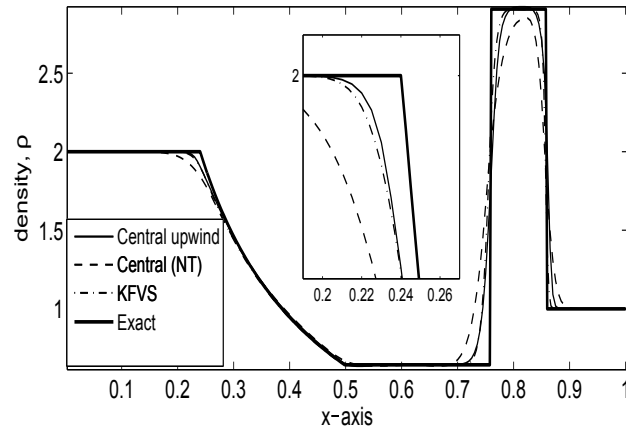


Figure 4.2: Comparison at  $t = 0.45$  for the shock test problem-I.

### Problem 3: The perturbed relativistic flow

The concern shock test involves a discontinuity under the given initial conditions as follow

$$\begin{aligned}(\rho, v, p) &= (1, 0, 1) && \text{when } x \leq 0.5, \\(\rho, v, p) &= (\rho_r, 0, 0.04) && \text{when } x > 0.5.\end{aligned}\tag{4.44}$$

Where, the computed region  $[0, 1]$  is splitting into 300 grid points. Which produces a sinusoidal wave having perturbed density,  $\rho_r = 0.1250 - 0.08750 \sin(40.0(x - 0.50))$  towards right region. The results are performed with final simulated time step  $t = 0.50$ . Our scheme shows better sinusoidal results than those provided by [53] in literature. Furthermore, it has cleared that the current scheme performed much better results than the central(NT) and the KFVS schemes. Numerical achieve results under the above assumption are presented by Figure 4.3.



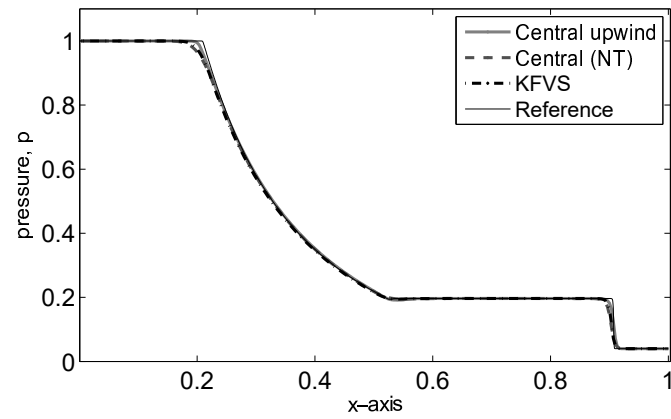
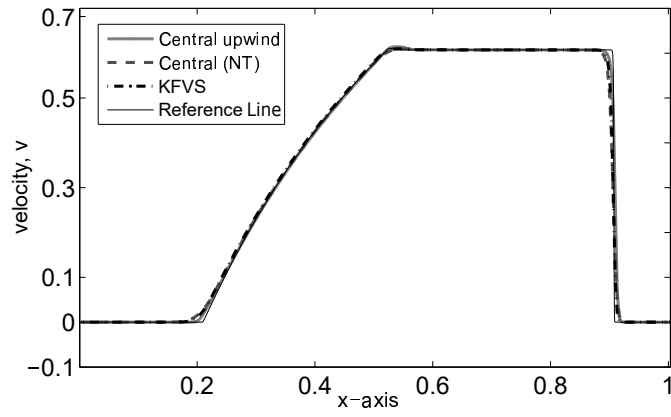
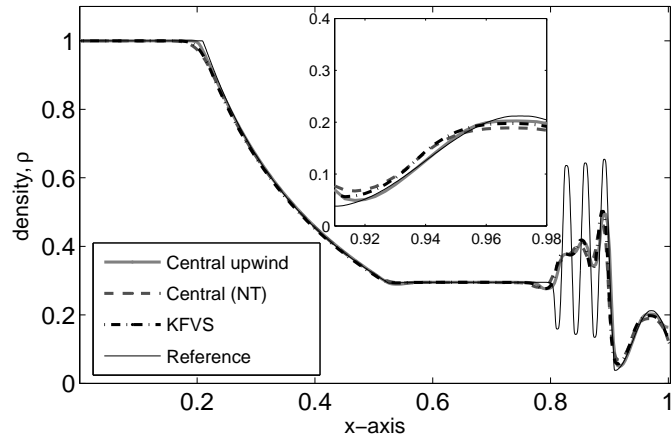


Figure 4.3: Comparison at  $t = 0.5$  for the shock test problem-II.

#### Problem 4

The initial test data of one-dimensional problem are shown below

$$\begin{aligned}(\rho, v, p) &= (1, -0.5, 2) \quad \text{when } x \leq 0.5, \\(\rho, v, p) &= (1, 0.5, 2) \quad \text{when } x > 0.5.\end{aligned}\tag{4.45}$$

This problem has a profile which consists of a trivial contact discontinuity and two strong rarefaction waves. Computational domain is defined by  $[0, 1]$  that is discretized into 400 grids at time defined by  $t = 0.5$ . Robustness of present results can be obtain from the central upwind techniques which are comparable to the central(NT) and the KFVS schemes. Furthermore, our proposed scheme has a good agreement with exact solution as shown by Figure 4.4.

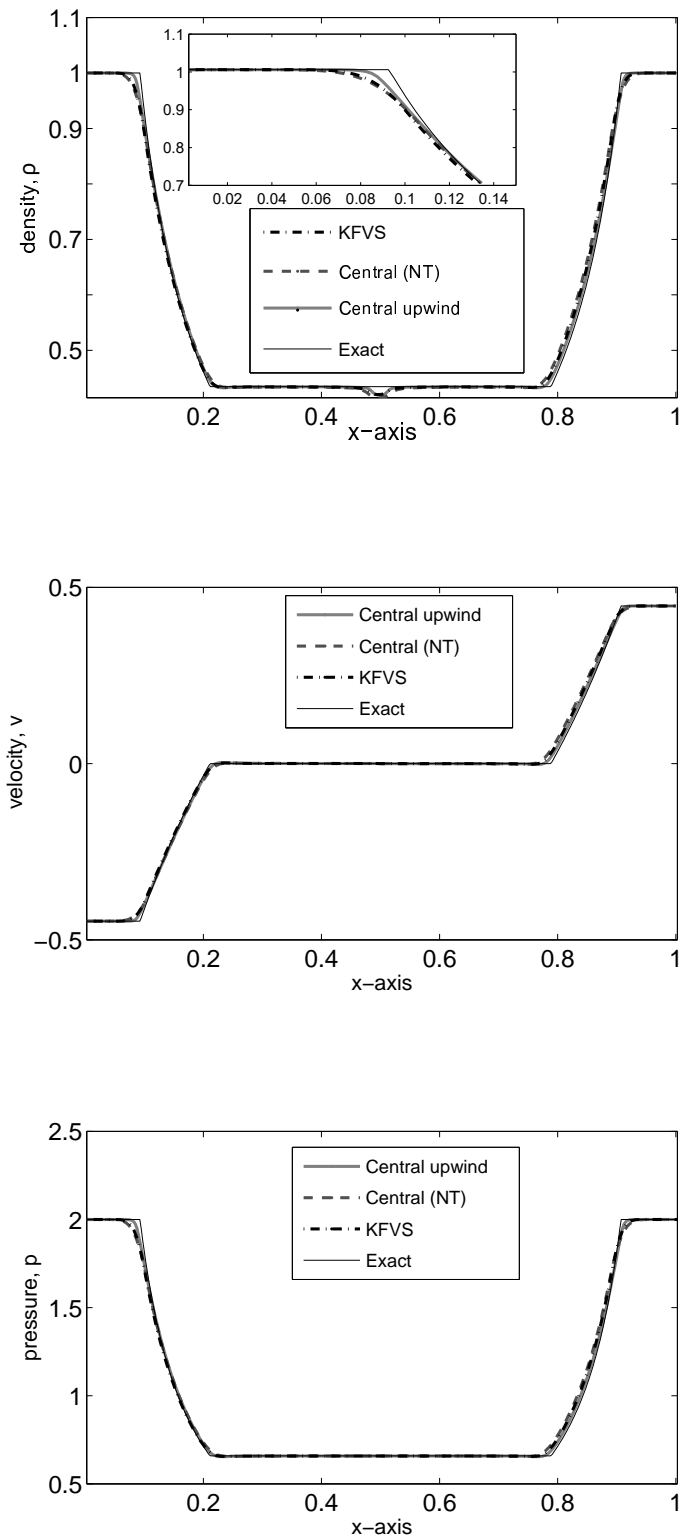


Figure 4.4: Comparison at  $t = 0.5$  for the perturbed relativistic shock test problem.

## 4.6.2 Two-dimensional Problems

Proposed numerical scheme is used for reproducing smooth profile in experimental order of convergence to validate the order of the accuracy. Then, the central upwind suggested scheme is implemented for discontinuity involved in the Problems (6) – (8). The multi-dimensional numerical simulation is much more complex with respect to one-dimensional problems.

### Problem 5: The EOC in two-dimension space

Here, we have given the comparison for EOCs of suggested schemes in two-dimensional space. The conditions that are set initial can be expressed by

$$\begin{aligned} \rho &= \frac{1}{\sqrt{2\pi}\sigma} e^{-\left[\frac{(x-\mu)^2}{2\sigma^2} + \frac{(y-\mu)^2}{2\sigma^2}\right]}, \text{ with } \mu = 0.5 \text{ and } \sigma = 0.13, \\ p &= 1.0, \quad v = 0.0. \end{aligned} \tag{4.46}$$

We have chosen the computational domain to be  $[0, 1] \times [0, 1]$  at time step  $t = 0.5$ . Table 4.2 displays  $L^1$ -norm errors and EOCs for the considered schemes. We analyze, the suggested scheme provide smaller errors with respect to central (NT) scheme and the KFVS scheme.

Table 4.2: Comparative numerical results of  $L^1$ -errors associative with EOC.

N	Central upwind		Central (NT)		KFVS	
	$L^1$ -error	EOC	$L^1$ -error	EOC	$L^1$ -error	EOC
30	0.002429	-	0.004288	-	0.018214	-
60	0.000770	1.6574	0.001309	1.7118	0.005879	1.6314
120	0.000242	1.6699	0.000410	1.6748	0.002071	1.5052
240	0.000075	1.6900	0.000123	1.7370	0.000740	1.4847
480	0.000023	1.7053	0.000036	1.7726	0.000255	1.5370

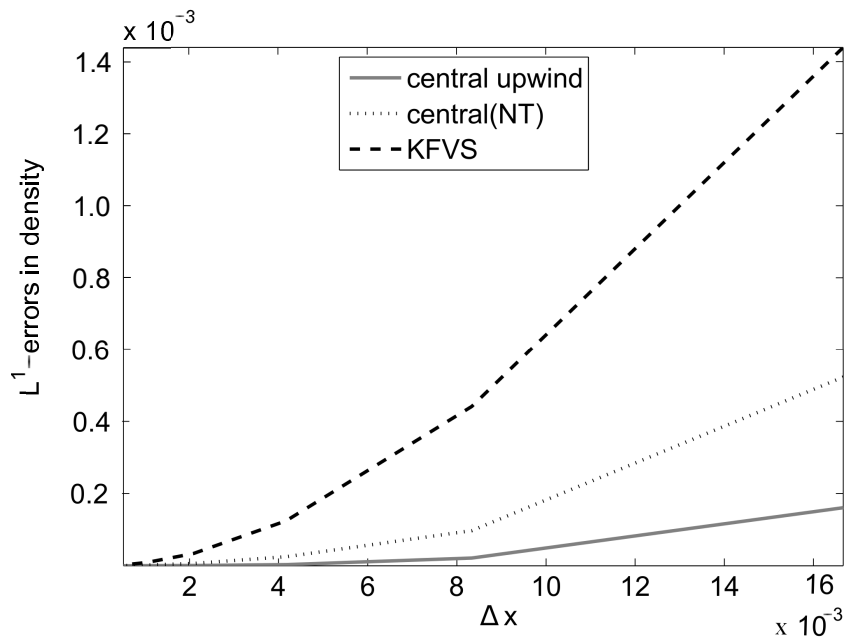


Figure 4.5: Comparison of  $L^1$ -errors.

### Problem 6: Cylindrical explosion problem

To test the proposed scheme, let us consider the initial data for two-dimensional test problem as defined as

$$\begin{aligned}(\rho, v, p) &= (10, 0, 10) && \text{if } r \leq 0.2, \\(\rho, v, p) &= (1, 0, 0.30) && \text{otherwise.}\end{aligned}\tag{4.47}$$

where the numerical domain  $[0, 1] \times [0, 1]$  is discretized into  $200 \times 200$  grid elements. The cylindrical explosion region having center at  $(0.5, 0.5)$  and radius 0.2 is within the domain. Figure 4.6 displays contour plots for current scheme at the final simulation time  $t = 0.20$ . Here, the Figure 4.7 shows comparison of of all the schemes under consideration. It is noted that the graphical results of the schemes agreed well with each other. However, the solution of the proposed scheme ensure the less error accuracy.

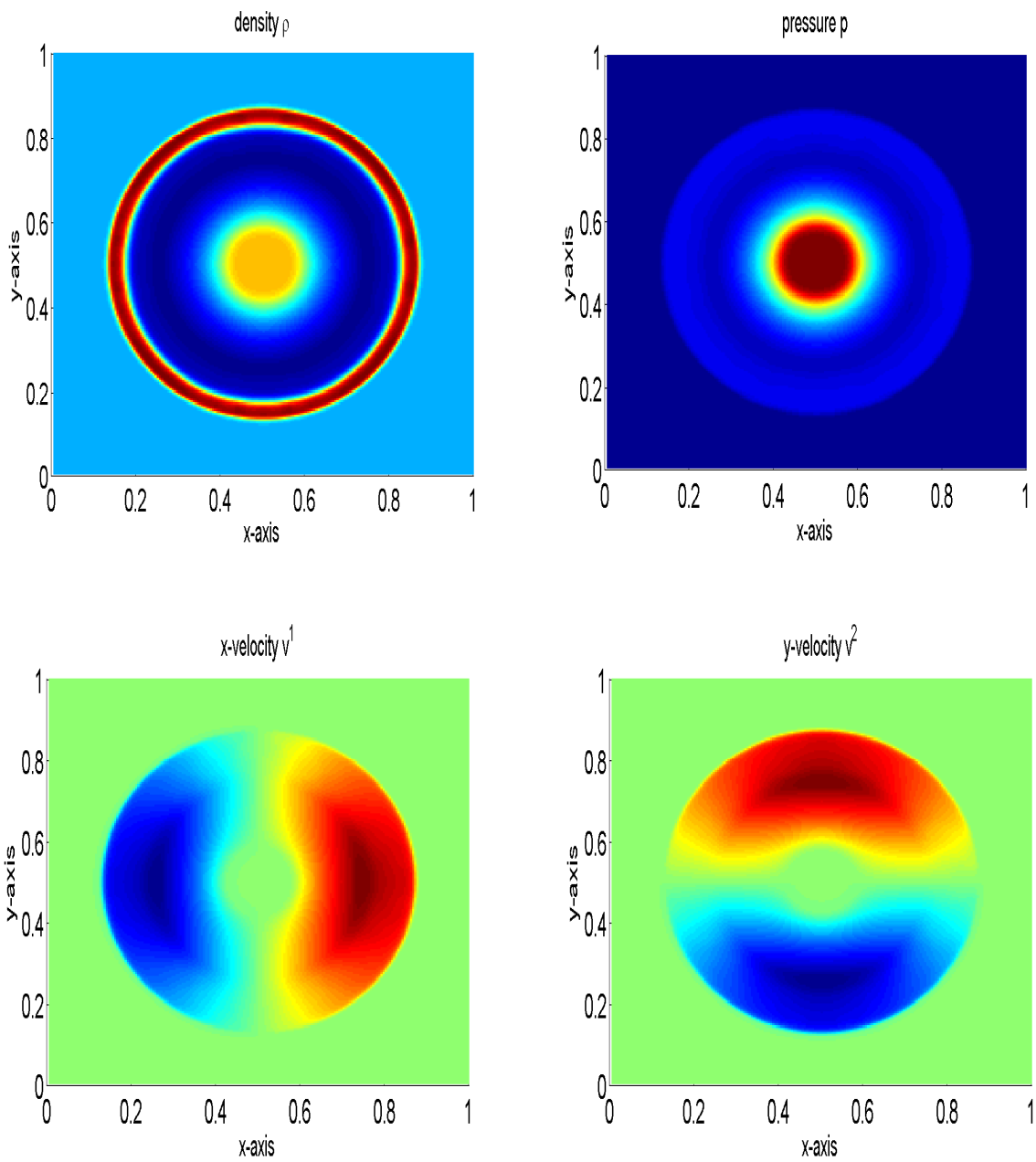


Figure 4.6: Results at  $t = 0.20$  for the cylindrical blast problem.

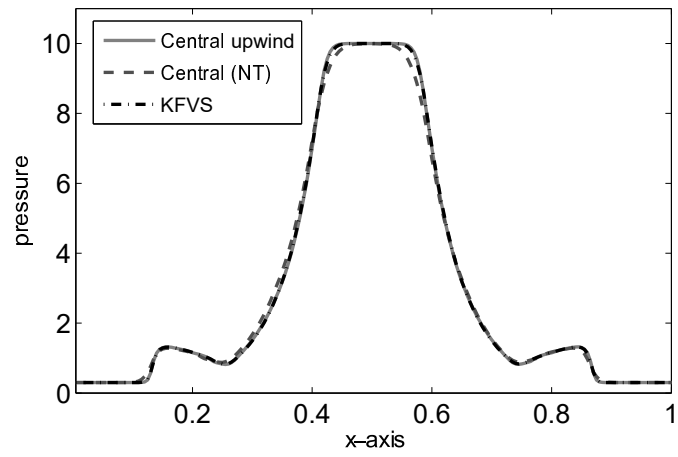
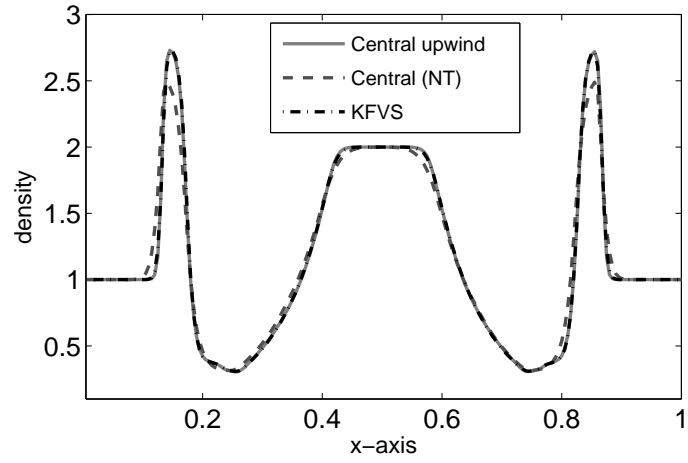


Figure 4.7: Comparison at  $t = 0.2$  for  $200 \times 200$  mesh cells.



### Problem 7: Explosion in the box

Here, multi-dimensional (2D) Riemann test is considered with available initial data followed by

$$\begin{aligned}(\rho, v, p) &= (4, 0, 10) & l = 0.5, \\(\rho, v, p) &= (1, 0, 1) & l = 2.0.\end{aligned}\tag{4.48}$$

The length of the square boxes are represented by  $l$ . The numerical computational is set to be in the square region  $[0, 2] \times [0, 2]$ , is discretized into  $300 \times 300$  grid points with reflecting walls. Where, the small box is placed at the middle of the large box which subdivides the considered problem in two distinct regions, the inside and the out side of a small box. Figure 4.8, depicts the final results at time  $t = 3.0$ . Similar behaviors of proposed scheme are also observed with central NT and the KFVS schemes as shown in Figure 4.9. However, the current central upwind schemes demonstrates discontinuity profile is best than these scheme.

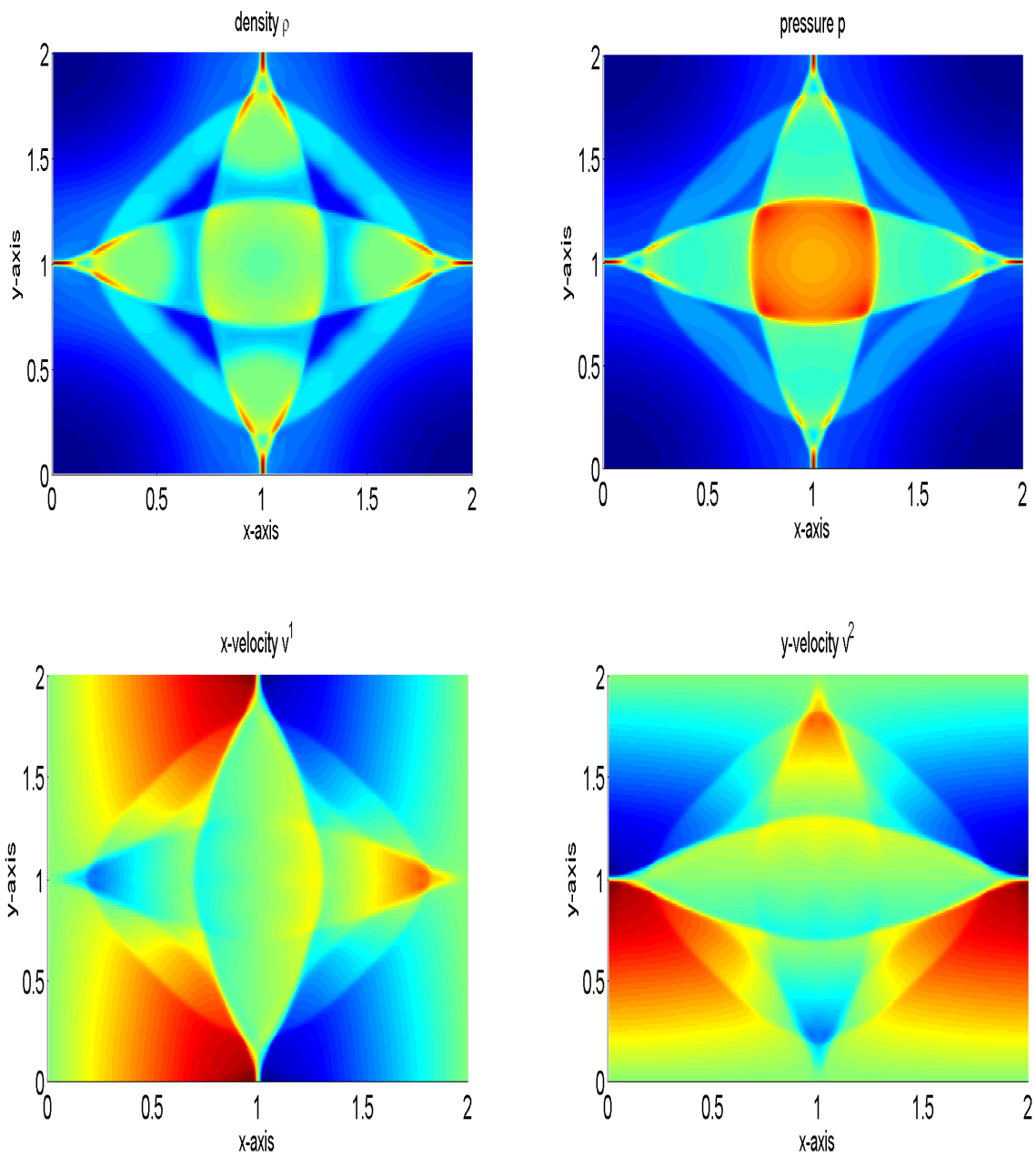


Figure 4.8: Results at  $t = 3.0$  for explosion in the box.

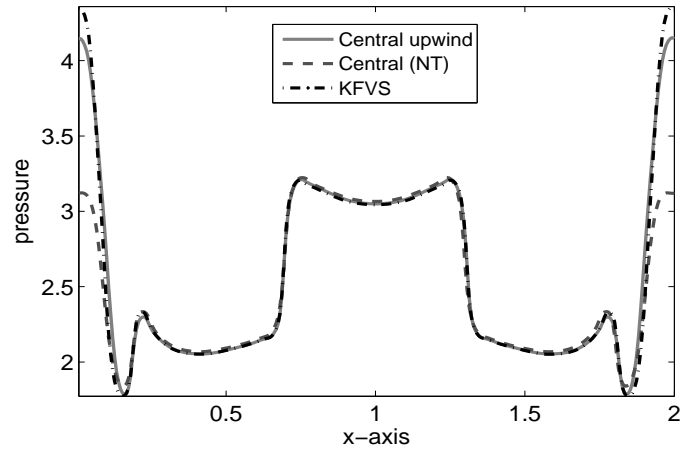
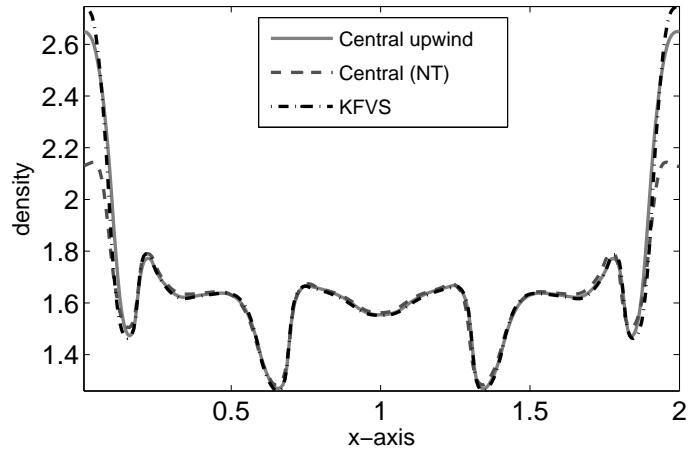


Figure 4.9: Comparison at  $t = 3.0$  for  $300 \times 300$  mesh cells.

### Problem 8: Bubble interaction

We consider the shock bubble interaction. The initial data are

$$(\rho, v^1, v^2, p) = \begin{cases} (2.9, 0, 0, 2), & \text{when } (y - 0.5)^2 + (x - 0.7)^2 < 0.04, \\ (2.725, 0.6495, 0, 4), & \text{when } 0 \leq x \leq 1 \text{ and } 0 \leq y \leq 1, \\ (1, 0.6495, 0, 1), & \text{otherwise.} \end{cases} \quad (4.49)$$

The computational region is defined by  $[0, 1] \times [0, 1]$ , and under different simulation times  $t = 0.5, 1.0, 2.0$  are taken for the problem. Figure 4.10 displays the numerical results for the density and the pressure using the proposed central upwind scheme. Moreover, Figure 4.11 shows the detail comparisons of result obtained from central upwind, central (NT) and KFVS schemes.

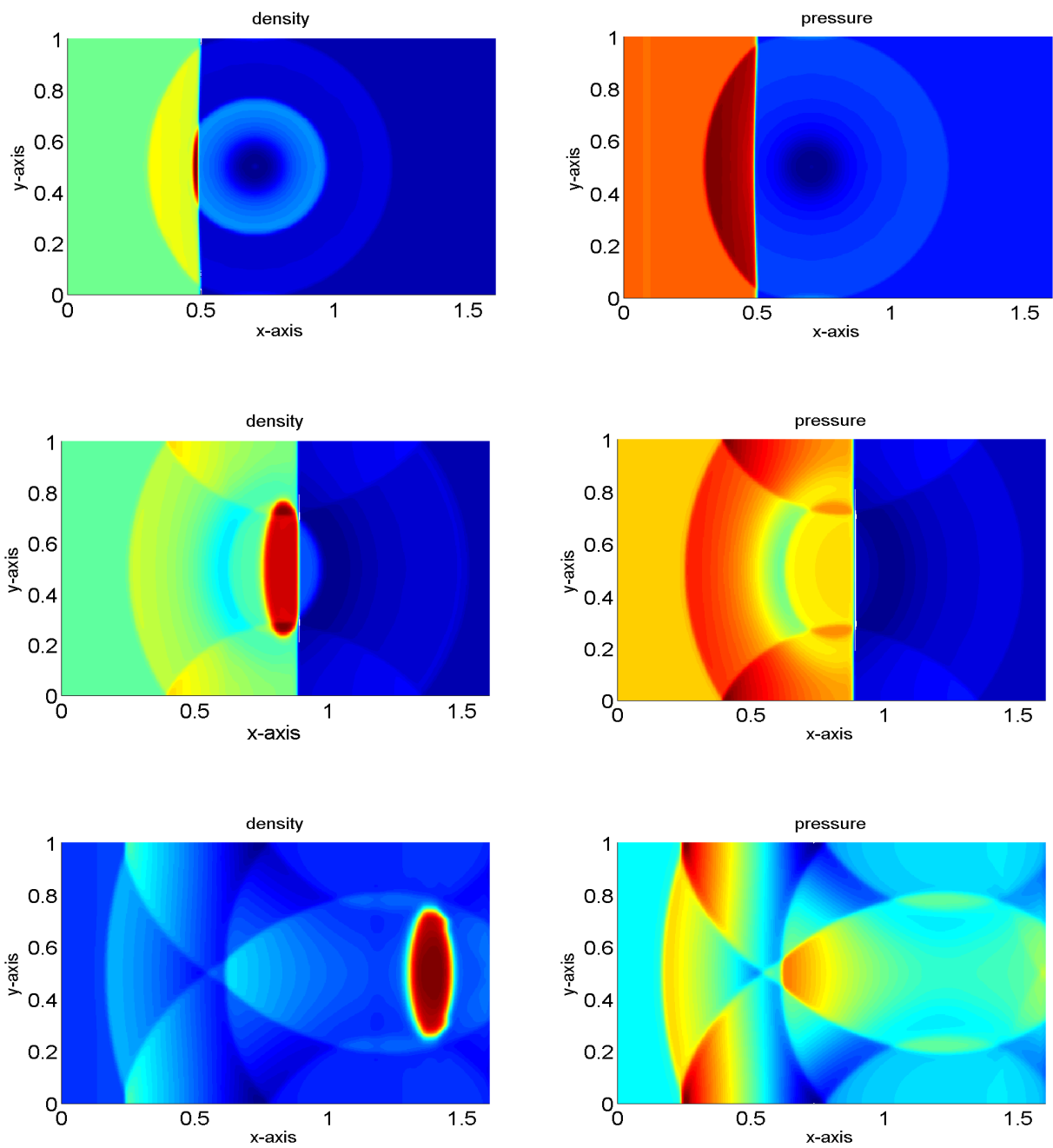


Figure 4.10: Results at  $t = 0.5, 1.0, 2.0$  (from top to bottom) for the shock bubble interaction.

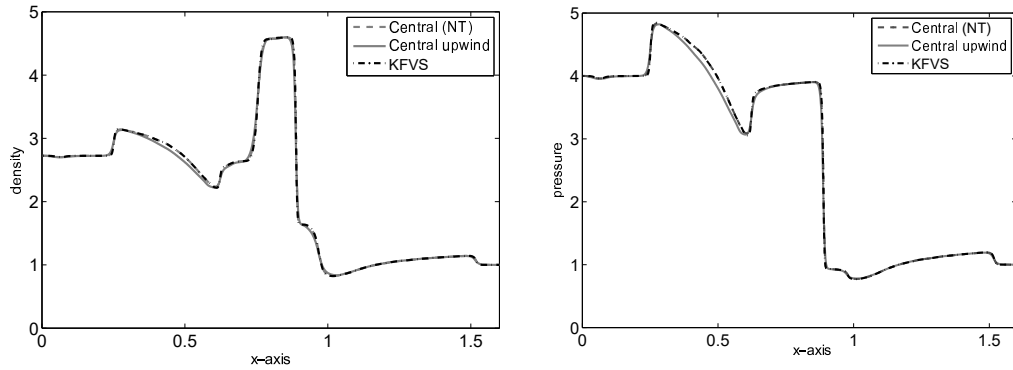


Figure 4.11: Comparison at  $t = 1.0$  for  $300 \times 300$  mesh cells.

## 4.7 Summary

The central upwind scheme was executed in order to solve both single and multi-dimensional (2D) URHD system of equations. Here, we have observed that current scheme has ability to captured the accurate sharp discontinuities and wavefronts of the ultra-relativistic fluid free of spurious oscillations or excessive numerical dissipation near the critical regions. The error analysis showed that central upwind scheme is second order accurate and produces less errors as compared to both staggered central(NT) and KFVS schemes. Furthermore, It was inaugurate that these numerical schemes have analogous results for discontinuous solutions. In some cases, the performance of the proposed scheme was found better than other techniques. The present investigations on central upwind scheme are made by using URHD model. However, many other models of relativistic hydrodynamics are available in literature [25, 49, 55, 61] that may be useful to find the better solution profile in the future.

## Chapter 5

### The Central Scheme (NT) for Relativistic Flow Model

Here, the current chapter is deliberated in order to formulate and implement the higher-order central schemes to solve the single and multi-dimensional relativistic multi-component flow models. Evolution of the RHD models are based on primitive variables and conserved quantities. The components in equilibrium state are associated with space-time possessing the common velocities and the same temperature. These proposed schemes ensure the exact conservation of mass for every component along with exact conservation for total energy and momentum in entire system of particle. Moreover, these schemes have stable profiles of all variables which can efficiently resolves the strong shocks removing spurious oscillation near the interface in the relativistic flows. The numerical approximation of central schemes for non-linear equations will provide the smooth waves solution.

The first order LxF scheme was introduce in 1950s and then extended to a second order Nessyahu and Tadmor (NT) central scheme [22]. Further, derive two-dimensional non-oscillatory central scheme with the help of one-dimensional setup [22, 23]. The central (NT) schemes are developed on the methods of predictor corrector which based on two main steps. In the initial step, the algorithm starts with the known values of cell averages then it is applied to the nonoscillatory piece-wise (linear) reconstructions to the predict point values. In final (corrector) step, realizing the evolution of these predicted mid-values of reconstructed polynomial in term of their staggered cell averages. The central (NT) schemes does not require characteristic decomposition and Riemann solver.

In this chapter, these schemes were efficiently implement on the variety of problems, for instance, the compressible and incompressible Euler equations [22, 23, 62], nonlinear optics [63], hyperbolic relaxation systems [64] and multicomponent flow presented by Qamar and Warnecke [9]. Several numerical problems in both one and two-dimensional are in-



incorporated, which validates the applications of the proposed schemes by relativistic multi-component flow and makes them stable, simple and efficient.

## 5.1 Mathematical Formulation

Consider a simple model that contains the combination of two different gases. The analysis for the multi-components is analogous. Here, it is assumed that the mixture total density is  $\rho = \rho_1 + \rho_2$ , where  $\rho_1$  and  $\rho_2$  represent the densities of first and second component, respectively. Further assume that these are the ideal gases in the state of thermal equilibrium with  $\omega$  is the ratio of their specific heats, as shown below

$$\omega = \frac{\mathbb{C}_p}{\mathbb{C}_v} = \frac{Y_1 \mathbb{C}_{p1} + Y_2 \mathbb{C}_{p2}}{Y_1 \mathbb{C}_{v1} + Y_2 \mathbb{C}_{v2}}. \quad (5.1)$$

Where  $\mathbb{C}_{v1}$ ,  $\mathbb{C}_{v2}$  denote the specific heats of gases at constant volume and  $\mathbb{C}_{p1}$ ,  $\mathbb{C}_{p2}$  denote the specific heats of gasses at constant pressure. Assume that  $Y_1$  and  $Y_2$  are the mass fractions of each first and second components. The equation of state for perfect gas in functional form represents as

$$p = (\Gamma - 1) \rho \epsilon \quad \text{and} \quad p = p(\rho, \epsilon) \quad (5.2)$$

here  $\Gamma$  represents the adiabatic index. Dynamics of the mixture under consideration, can be model by using the compressible Euler equation. The conservation form of RHD is express in the vector notation by

$$\frac{\partial \vec{C}}{\partial t} + \frac{\partial \vec{A}(\vec{C})}{\partial x} = 0, \quad (5.3)$$

here the conserved variables  $\vec{C}$  and fluxes  $\vec{A}$  are presented below

$$\vec{C} = \begin{pmatrix} \rho_1 \\ \rho_2 \\ \rho u \\ E \end{pmatrix}, \quad \vec{A}(\vec{C}) = \begin{pmatrix} \rho_1 u \\ \rho_2 u \\ \rho u^2 + p \\ u(E + p) \end{pmatrix}. \quad (5.4)$$

Here, the average flow velocity are  $u$  and total energy is  $E = \frac{1}{2}\rho u^2 + \frac{p}{\omega-1}$ . The physical quantities namely the mass density, momentum and the energy expressed in local frame work. The primitive variables such as  $u$  and  $p$  of conserved quantities are expressed by

$$u = \frac{\sum_{i=1}^2 \rho_i}{\rho}, \quad p = \left( \sum_{i=1}^2 E_i - \frac{1}{2}\rho u^2 \right) (\omega - 1) \quad \text{for } i = 1, 2, \quad (5.5)$$

where  $\rho = \rho_1 + \rho_2$ , and  $\omega$  is given by Eq. (5.1). The further detail is available in the non-relativistic one and two-dimensional homogeneous multi-component flow models of Qamar and Warnecke [9]. This chapter deals with the relativistic multi-component flows model. Now, utilizing the Einstein's summation convention over repeated index and units, the equations that describe the relativistic fluid motion by assuming  $\mu, \nu = 0, 1, 2, 3$  are give by

$$\frac{\partial N_1^\mu}{\partial x^\mu} = 0, \quad \frac{\partial N_2^\mu}{\partial x^\mu} = 0 \quad \text{and} \quad \frac{\partial T^{\mu\nu}}{\partial x^\mu} = 0, \quad (5.6)$$

where  $N_1^\mu, N_2^\mu$  are the matter density four-vectors and,  $T^{\mu\nu}$  denotes the energy and momentum tensor. They can be written as

$$N_1^\mu = \rho_1 u^\mu, \quad N_2^\mu = \rho_2 u^\mu, \quad T^{\mu\nu} = p g^{\mu\nu} + (p + e) u^\nu u^\mu. \quad (5.7)$$

Here,  $\rho$  be the density for rest-mass whereas  $p$  shows pressure,  $e$  represents the internal specific energy, and  $u^\mu$  is the contravariant four-velocity components for the values of  $\mu$  as 0, 1, 2, 3, is given by

$$u^0 = \omega \quad \text{and} \quad u^i = \omega v^i, \quad (5.8)$$

where  $v^i$  denotes the spatial velocity components of perfect fluid for  $i = 1, 2, 3$  and  $\omega$  represents the Lorentz factor, can be defined as

$$\omega = \frac{1}{\sqrt{1 - \mathbf{v}^2}} \quad \text{with} \quad \mathbf{v}^2 = \sum_{i=1}^3 (v^i)^2. \quad (5.9)$$

Eqs. (5.8) and (5.9) imply that

$$u^\mu u_\mu = u^\mu g_{\mu\nu} u^\nu = (u^0)^2 - \sum_{i=1}^3 (u^i)^2 = \omega^2 [1 - (\vec{A}v)^2] = 1, \quad (5.10)$$

where  $g^{\mu\nu}$  is the metric tensor defined as

$$g_{\mu\nu} = g^{\mu\nu} = \begin{cases} -1, & \text{if } \nu = 0 = \mu \\ 1, & \text{if } \nu = \mu = 1, 2, 3 \\ 0, & \text{if } \nu \neq \mu \end{cases} .$$

The specific enthalpy of fluid mixture represents as

$$h = 1 + \epsilon + \frac{p}{\rho}, \quad (5.11)$$

here  $\epsilon$  represents specific internal energy. For simplicity,  $c = 1$  is taken as speed of light.

In Minkowski space time in cartesian coordinate  $(t, x^1, x^2, x^3)$ , the hyperbolic system of conservation equations defined in Eq. (5.6) is expressed by

$$\frac{\partial \vec{C}}{\partial t} + \sum_{i=1}^3 \frac{\partial \vec{A}^i(\vec{C})}{\partial x^i} = 0, \quad (5.12)$$

along with conserved quantities define in  $\vec{C}$  and the fluxes  $\vec{A}^i(\vec{C})$  are shown by

$$\vec{C} = \begin{pmatrix} D_1 \\ D_2 \\ S^1 \\ S^2 \\ S^3 \\ \tau \end{pmatrix}, \quad \vec{A}^i(\vec{C}) = \begin{pmatrix} D_1 v^i \\ D_2 v^i \\ S^1 v^i + p \delta^{1i} \\ S^2 v^i + p \delta^{2i} \\ S^3 v^i + p \delta^{3i} \\ S^i - D v^i \end{pmatrix}. \quad (5.13)$$

The conserved quantities, such as  $D_1, D_2$  shows the rest mass densities of two components whereas  $S^1, S^2, S^3$  represents momentum densities and  $\tau$  denotes energy density. These are calculated in the laboratory frame and the physical quantities which are expressed in term of primitive variables, as shown by

$$D_1 = \rho_1 \omega, \quad D_2 = \rho_2 \omega, \quad S^i = \rho h \omega^2 v^i, \quad \tau = \rho h \omega^2 - p - D. \quad (5.14)$$

The system of Eqs. (5.12)–(5.14) are closed with respect to the EOS for the perfect gas, represents as

$$p = (\Gamma - 1)\rho\epsilon, \quad (5.15)$$

here  $c_s$  denotes the speed of sound whereas  $s$  be the specific entropy, formulated as

$$hc_s^2 = \left. \frac{\partial p}{\partial \rho} \right|_s, \quad \text{and} \quad c_s = \left( \frac{\omega p}{\rho h} \right)^{\frac{1}{2}}, \quad (5.16)$$

which is conserved along fluid lines. The Mach number by Königl [65]

$$M_a = \frac{v \omega}{c_s \omega_s}.$$

The initial conserved variable (macroscopic) with respect to space and time are,

$$\vec{C}_1 = (\rho_1, v_1^i, p_1), \quad \vec{C}_2 = (\rho_2, v_2^i, p_2), \quad \text{for } i = 1, 2, 3, \quad (5.17)$$

the primitive variables in the term of  $\rho$ ,  $v^i$ , and  $p$  can be determined in implicit function from the conserved quantities [1, 66],

$$\begin{aligned} D &= (\rho_1 \omega) + (\rho_2 \omega), \\ S^i &= (\rho_1 h_1 \omega^2 v_1^i) + (\rho_2 h_2 \omega^2 v_2^i), \quad \text{for } i = 1, 2, 3, \\ \tau &= (\rho_1 h_1 \omega^2 - p_1 - \rho_1 \omega) + (\rho_2 h_2 \omega^2 - p_2 - \rho_2 \omega). \end{aligned} \quad (5.18)$$

To solve the implicit function of pressure the roots of the equation can be determined by

$$\eta(p) = (\Gamma - 1) \rho_* \epsilon_* - p, \quad (5.19)$$

with  $\rho_*$  and  $\epsilon_*$  given by

$$\rho_* = \frac{D}{\omega_*}, \quad \epsilon_* = \frac{\tau + p(1 - \omega_*^2) + D(1 - \omega_*)}{D\omega_*}, \quad (5.20)$$

where

$$\omega_* = \frac{1}{\sqrt{1 - v_*^2}}, \quad v_* = \frac{S}{\tau + D + p}.$$

The monotonicity of  $\eta(p) \in [p_{min}, \infty]$  authenticates uniqueness of a numerical solution and a lower bound of given domain,  $p_{min}$ , presented as

$$p_{min} = |\mathbf{S}| - \tau - D, \quad (5.21)$$

is determined by Eq. (5.14) along with the condition  $|\mathbf{v}| \leq 1$ . By knowing  $p$ , Eq. (5.20) then provides directly  $v$  and the density. comparative to the Aloy *et al.* [1], the required solution  $\eta(p) = 0$ , is obtained by adopting Newton-Rahphson iterative method where the derivative of  $\eta$ , is evaluated as

$$\eta' = |\mathbf{v}_*|^2 c_{s*}^2 - 1, \quad (5.22)$$

here  $c_{s*}$  denotes the sound speed and can be defined as

$$c_{s*} = \sqrt{\frac{(\Gamma - 1)\Gamma\epsilon_*}{1 + \Gamma\epsilon_*}}. \quad (5.23)$$

This approximation leads toward exact derivative. In addition, it allows to develop and extend the current algorithm for general equations of state (EOS) [1].

## 5.2 Numerical Scheme

These numerical schemes are serve in a very natural way that provides the characteristics essential for the effectiveness, such as higher order accuracy, capture the sharp discontinuities with stability, and converges to the exact numerical solution. The computer execution of central schemes are very simple and compact. However, the second-order central scheme is accomplished to determined contact discontinuity in well manner. The central (NT) schemes does not require characteristic decomposition and Riemann solver.

### 5.2.1 One-dimensional Central Schemes

In order to solve the Euler equations of relativistic hydrodynamics in one-dimensional case, we consider

$$\frac{\partial \vec{C}}{\partial t} + \frac{\partial \vec{A}(\vec{C})}{\partial x} = 0, \quad (5.24)$$

where  $\vec{A}(\vec{C})$  is a flux function of a conserved vector  $\vec{C}$ ,

$$\vec{C} = \begin{pmatrix} D_1 \\ D_2 \\ S \\ \tau \end{pmatrix}, \quad \vec{A}(\vec{C}) = \begin{pmatrix} D_1 v \\ D_2 v \\ Sv + p \\ S - Dv \end{pmatrix}. \quad (5.25)$$

Here,

$$D_1 = \rho_1 \omega, \quad D_2 = \rho_1 \omega, \quad S = \rho h \omega^2 v, \quad \tau = \rho h \omega^2 - p - D, \quad (5.26)$$

and

$$v = \frac{u}{u^0}, \quad \omega = \frac{1}{\sqrt{1 - \mathbf{v}^2}}, \quad p = (\Gamma - 1)\rho\epsilon. \quad (5.27)$$

These eminent schemes in 1950s, At that time Lax-Friedrichs(LxF) schemes of first order was introduced and then applied to first order central scheme. This first-order LxF scheme was then further extended to the second-order Nessyahu and Tadmor (NT) in one-dimensional central scheme [22]. To take into consideration a piecewise-constant reconstruction,  $\sum \chi_i(x)\vec{C}_i^n$ . The computed cells interface  $\vec{C}_i^n$  averages at the final time step  $t = t_n$  and  $\chi_i(x)$  is a characteristics function for the cell  $I_i$  such that  $\chi_i(x) = 1$  or  $\chi_i(x) = 0$  for all  $x \in I_i$  and also  $x \in \mathbb{R} \setminus I_i$ , respectively. Here,  $I_i = \{\xi \mid |\xi - x_i| \leq \frac{\Delta x}{2}\}$ , middle cell  $x_i = (\Delta x)i$ . Now, Integrating Eq. (5.24) over to the uniform rectangle  $[x_i, x_{i+1}] \times [t_n, t_{n+1}]$ ,

we have

$$\oint_{\partial\Omega} \vec{C} dx - \vec{A}(\vec{C}) dt = 0 \Leftrightarrow$$

$$- \int_{t_n}^{t_{n+1}} \vec{A} [\vec{C}(x_i, t)] dt - \int_{x_i}^{x_{i+1}} \vec{C}(\xi, t_n) d\xi + \int_{x_i}^{x_{i+1}} \vec{C}(\xi, t_{n+1}) d\xi + \int_{t_n}^{t_{n+1}} \vec{A} [\vec{C}(x_{i+1}, t)] dt = 0.$$

here it is notable that the staggered cell interfaces  $I_i$  are corresponding to the interval  $[x_i, x_{i+1}]$  of integration. That tends to Lax-Friedrichs (LxF) schemes, shown by

$$\vec{C}_{i+\frac{1}{2}}^{n+1} = \frac{1}{2}(\vec{C}_{i+1}^n + \vec{C}_i^n) + \lambda \left[ -\vec{A}(\vec{C}_{i+1}^n) + \vec{A}(\vec{C}_i^n) \right], \quad \text{where } \vec{C}_i^n := \vec{C}(x_i, t_n) = \vec{C}_i^n, \quad (5.28)$$

where  $\lambda = \frac{\Delta t}{\Delta x}$ . The piecewise-constant function of cell average in every step is stagger to the corresponding preceding steps.

## Extension to The Higher Order:

Consider a piecewise-constant approximation in space-time,  $\sum \vec{C}_i^n \chi_i(x)$ , we rebuild a piecewise (linear) MUSCL-type interpolation, defined by

$$\vec{C}(t_n, x) = \sum \left( \vec{C}_i^n + \vec{C}_i^x \frac{(x - x_i)}{\Delta x} \right) \chi_i(x), \quad (5.29)$$

here  $\vec{C}_i^x$  represents discrete slopes can be solve by nonlinear limiter, see Figure 5.1. The feasible evolution of the slope, which estimate result of non-oscillatory methods (consult [22]), The possible computations of these steps, which provides solution in the overall non-oscillatory schemes (consult [22]), presented by class of the *discrete derivative* free parameter  $\theta \in [1, 2]$ , that is for each grid element  $\{\vec{C}_i\}$  represented as

$$\vec{C}_i^x = MM \left[ \theta \left( \Delta \vec{C}_{i+\frac{1}{2}}, \frac{1}{2}(\Delta \vec{C}_{i-\frac{1}{2}} + \Delta \vec{C}_{i+\frac{1}{2}}), \Delta \vec{C}_{i-\frac{1}{2}} \right) \right]. \quad (5.30)$$

Here,  $\Delta$  indicates the centered differencing,  $\Delta \vec{C}_{i+\frac{1}{2}} = \vec{C}_{i+1} - \vec{C}_i$ . The min-mod nonlinear

function denoted by  $MM\{x_1, x_2, \dots\}$  is defined as

$$MM = \begin{cases} \max\{x_i\}, & \text{when } x_i < 0 \quad \forall i, \\ \min\{x_i\}, & \text{when } x_i > 0 \quad \forall i, \\ 0, & \text{otherwise.} \end{cases} \quad (5.31)$$

Here, according to the conservation law, the interpolate Eq. (5.29), is developed in simulation time exactly and projected by staggered cell interpolate at next step  $t_{n+1}$ , time level. Further, we consider the system within the control volume by  $[x_i, x_{i+1}] \times [t_n, t_{n+1}]$ , we have

$$\oint_{\partial\Omega} \vec{C} dx - \vec{A}(\vec{C}) dt = 0 \Leftrightarrow$$

$$- \int_{t_n}^{t_{n+1}} \vec{A}(\vec{C}(x_i, t)) dt - \int_{x_i}^{x_{i+1}} \vec{C}(\xi, t_n) d\xi + \int_{x_i}^{x_{i+1}} \vec{C}(\xi, t_{n+1}) d\xi + \int_{t_n}^{t_{n+1}} \vec{A}(\vec{C}(x_{i+1}, t)) dt = 0.$$

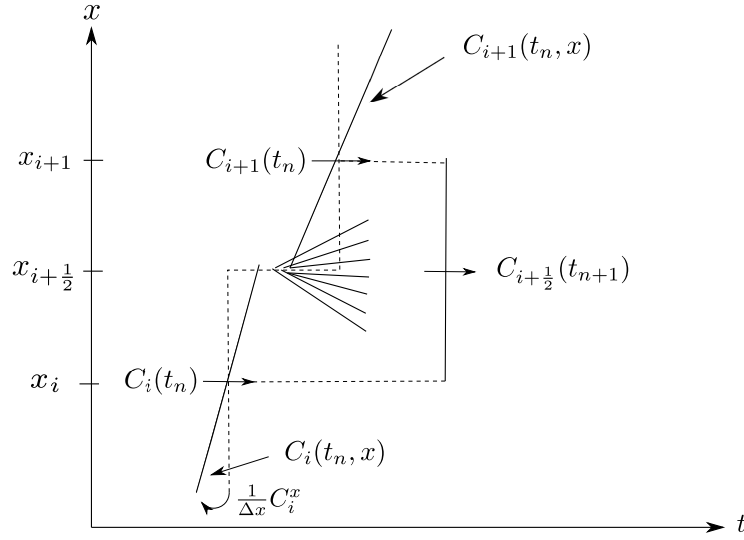


Figure 5.1: Second-order reconstruction

It yields

$$\vec{C}_{i+\frac{1}{2}}^{n+1} = \vec{C}_{i+\frac{1}{2}}(t_n) + \frac{\lambda}{\Delta t} \left( \int_{t_n}^{t_{n+1}} \vec{A}(\vec{C}(x_i, t)) dt - \int_{t_n}^{t_{n+1}} \vec{A}(\vec{C}(x_{i+1}, t)) dt \right). \quad (5.32)$$



Where  $\lambda = \frac{\Delta t}{\Delta x}$ . Average value of the linear system defined in Eq. (5.29) at  $t = t_n$ , provides

$$\begin{aligned}
\vec{C}_{i+\frac{1}{2}}^n &= \frac{1}{\Delta x} \int_{x_i}^{x_{i+1}} \vec{C}(\xi, t_n) d\xi \\
&= \frac{1}{\Delta x} \left( \int_{x_i}^{x_{i+\frac{1}{2}}} \vec{C}_i(\xi, t_n) d\xi + \int_{x_{i+\frac{1}{2}}}^{x_{i+1}} \vec{C}_{i+1}(\xi, t_n) d\xi \right), \\
&= \frac{1}{2}(\vec{C}_i^n + \vec{C}_{i+1}^n) + \frac{1}{8}(\vec{C}_i^x - \vec{C}_{i+1}^x). \tag{5.33}
\end{aligned}$$

Numerical flux on the right of the Eq. (5.33) provides the *exact* solution. Furthermore, accordingly by the Courant-Friedrichs-Levy(CFL) condition,  $\vec{A}(\vec{C}_i(t))$  and  $\vec{A}(\vec{C}_{i+1}(t))$  are smooth integral over the time  $t$  can be calculated through mid-point approximation method at the cost of  $O(\Delta t^3)$ , the local truncation error(LTE).

$$\frac{1}{\Delta t} \int_{t_n}^{t_{n+1}} \vec{A}(\vec{C}_{i+1}(t)) dt \sim \vec{A}(\vec{C}_i(t_{n+\frac{1}{2}})) + O(\Delta t^3). \tag{5.34}$$

Putting the values of Eqs. (5.33) and (5.34) in Eq. (5.32), we get

$$\vec{C}_{i+\frac{1}{2}}^{n+1} = \frac{1}{2}(\vec{C}_i^n + \vec{C}_{i+1}^n) + \frac{1}{8}(\vec{C}_i^x + \vec{C}_{i+1}^x) + \lambda \left[ \vec{A}(\vec{C}_i^{n+\frac{1}{2}}) - \vec{A}(\vec{C}_{i+1}^{n+\frac{1}{2}}) \right]. \tag{5.35}$$

Taylor's expansion is applied for prediction of mid-value of conservative variable Eq. (5.24), we get

$$\vec{C}_i^{n+\frac{1}{2}} = \vec{C}_i(t_{n+\frac{1}{2}}) = \vec{C}_i^n + \frac{\Delta t}{2}(\vec{C}_i)_t(t_n) + O(\Delta t^2) = \vec{C}_i^n - \frac{\lambda}{2} \vec{A}^x(\vec{C}_i) + O(\Delta t^2). \tag{5.36}$$

Where,  $\frac{1}{\Delta x} \vec{A}^x(\vec{C}_i)$  indicates the discrete numerical derivative of flux variable

$$\vec{A}(\vec{C}(x = x_i, t)), \quad \frac{1}{\Delta x} \vec{A}^x(\vec{C}_i) = \frac{\partial}{\partial x} \vec{A}(\vec{C}(x = x_i, t)) + O(\Delta x)$$

Moreover, the required fluxes of  $\vec{A}^x(\vec{C}_i)$  are calculated by using the MM (min-mod) approximation to each element of the conserved variable  $\vec{A}$ , i.e.,

$$\begin{aligned}\vec{A}^x(\vec{C}_i) &= MM \left[ \theta \left( \vec{A}(\vec{C}_{i-1}), \vec{A}(\vec{C}_i), \vec{A}(\vec{C}_{i+1}) \right) \right] \\ &= MM \left( \theta \Delta \vec{A}(\vec{C}_{i+\frac{1}{2}}), \frac{\theta}{2} \left( \Delta \vec{A}(\vec{C}_{i+\frac{1}{2}}) + \Delta \vec{A}(\vec{C}_{i-\frac{1}{2}}) \right), \theta \Delta \vec{A}(\vec{C}_{i-\frac{1}{2}}) \right).\end{aligned}$$

Furthermore,  $\Delta$  stands for central difference,  $\Delta \vec{A}(\vec{C}_{i+\frac{1}{2}}) = \vec{A}(\vec{C}_{i+1}) - \vec{A}(\vec{C}_i)$ , and  $MM$  function has defined in Eq. (5.31). We summarize the central scheme that the Eq. (5.35) represents the second-order corrector step whereas Eq. (5.36) represents the first order predictor.

## 5.2.2 Two-dimensional Central Schemes

Consider nonlinear Euler equation of two-dimension

$$\frac{\partial \vec{C}}{\partial t} + \sum_{i=1}^2 \frac{\partial \vec{A}^i(\vec{C})}{\partial x^i} = 0, \quad (5.37)$$

here  $\vec{C}$  denotes the conserved quantity. The vectors  $\vec{A}^1$  and  $\vec{A}^2$  are the convective fluxes, given by

$$\vec{C} = \begin{pmatrix} D_1 \\ D_2 \\ S^1 \\ S^2 \\ \tau \end{pmatrix}, \quad \vec{A}^1 = \begin{pmatrix} D_1 v^1 \\ D_2 v^1 \\ S^1 v^1 + p \\ S^2 v^1 \\ S^1 - D v^1 \end{pmatrix}, \quad \vec{A}^2 = \begin{pmatrix} D_1 v^2 \\ D_2 v^2 \\ S^1 v^2 \\ S^2 v^2 + p \\ S^2 - D v^2 \end{pmatrix}, \quad (5.38)$$

where

$$D_1 = \rho_1 \omega, \quad D_2 = \rho_2 \omega, \quad S^1 = \rho h \omega^2 v^1, \quad S^2 = \rho h \omega^2 v^2, \quad \tau = \rho h \omega^2 - p - D. \quad (5.39)$$

We can derive two-dimensional non-oscillatory central scheme with the help of one-dimensional setup [22, 23]. To approximate Eq. (5.37), the process start with piecewise-constant solutions in form of  $\sum \chi_{i,j} \vec{C}_{i,j}^n$ . where,  $\vec{C}_{i,j}^n$  is approximated by the cell averages at the final time

step,  $t = t_n$ , correlated by  $\chi_{i,j}(x, y)$ , named as characteristic function and  $C_{i,j} = I_i \times J_j$  is centered around with  $(x_i = (\Delta x)i, y_j = (\Delta y)j)$ , that is,

$$C_{i,j} = \left\{ (\xi, \eta) \left| 2|\xi - x_i| \leq \Delta x, |\xi - y_j| \leq \frac{\Delta y}{2} \right. \right\}. \quad (5.40)$$

In single dimensional system (1D), framework of the central scheme proceed by the second step of the exact solution following with the staggered averages. The second step is realize this to exact evolution at next time level step  $t = t^n$ , and staggered  $C_{i+\frac{1}{2},j+\frac{1}{2}} = I_{i+\frac{1}{2}} \times J_{j+\frac{1}{2}}$  centered around  $(x_{i+\frac{1}{2}}, y_{j+\frac{1}{2}})$ . Here, the normalized integral over its area, length etc is representing as  $\int_B = \frac{1}{|B|} \int_B$ . Assume that  $\lambda = \frac{\Delta t}{\Delta x}$  and  $\mu = \frac{\Delta t}{\Delta y}$  express the constant mesh ratio in both directions, accordingly. Consider the staggered cells averages

$$\vec{C}_{i+\frac{1}{2},j+\frac{1}{2}} = \int_{C_{i+\frac{1}{2},j+\frac{1}{2}}} \vec{C}(t, x, y) dx dy.$$

Integrating Eq. (5.37) over the volume  $C_{i+\frac{1}{2},j+\frac{1}{2}} \times [t_n, t_{n+1}]$ , we get,

$$\begin{aligned} \vec{C}_{i+\frac{1}{2},j+\frac{1}{2}}^{n+1}(t_{n+1}) &= \int_{C_{i+\frac{1}{2},j+\frac{1}{2}}} \vec{C}(x, y, t_n) dx dy \\ &\quad - \lambda \left\{ \int_{t_n}^{t_{n+1}} \int_{y_j}^{y_{j+1}} \left[ \vec{A}^1(\vec{C}(x_{i+1}, y, t)) - \vec{A}^1(\vec{C}(x_i, y, t)) \right] dy dt \right\} \\ &\quad - \mu \left\{ \int_{t_n}^{t_{n+1}} \int_{x_i}^{x_{i+1}} \left[ \vec{A}^2(\vec{C}(x, y_{j+1}, t)) - \vec{A}^2(\vec{C}(x, y_j, t)) \right] dx dt \right\}. \end{aligned} \quad (5.41)$$

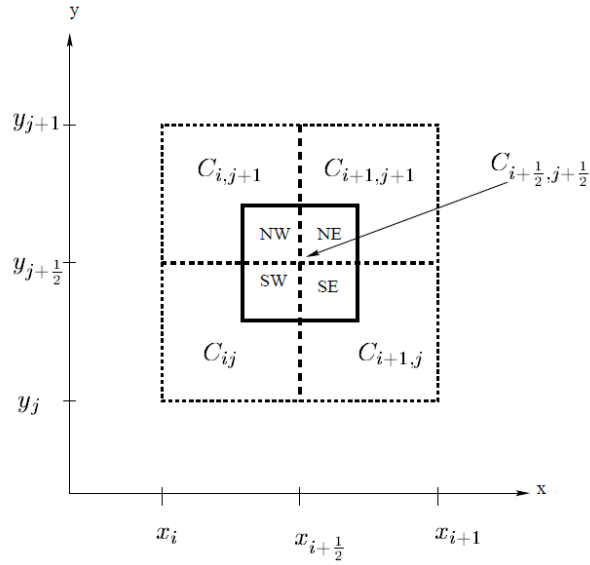


Figure 5.2: Floor plane of staggered grid.

To find cell averages,  $\int_{C_{i+\frac{1}{2},j+\frac{1}{2}}} \vec{C}(t_n, x, y) dy dx$  which approximate with the four  $C_{i,j}$ ,  $C_{i+1,j}$ ,  $C_{i+1,j+1}$  and  $C_{i,j+1}$  cells. Finally, we get exact staggered averages with the help of Figures 5.2 and 5.3

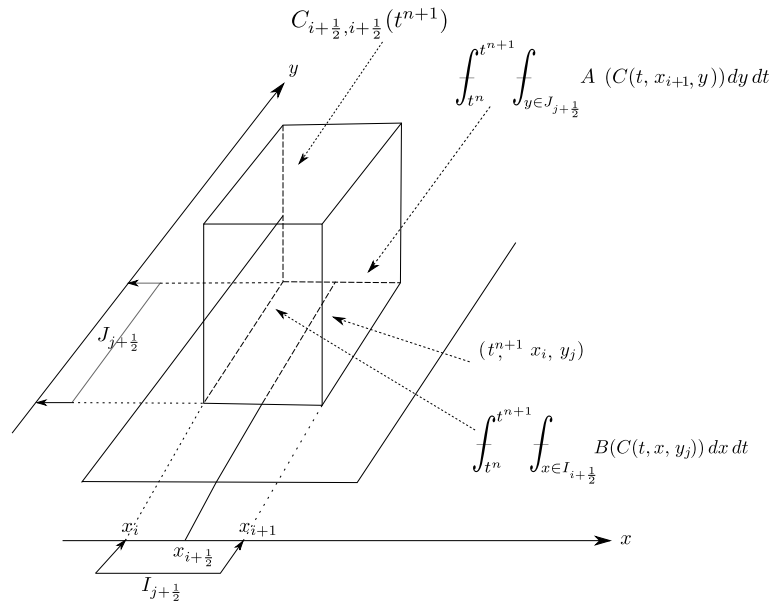


Figure 5.3: The stencil of staggered central scheme.

$$\begin{aligned}
\vec{C}_{i+\frac{1}{2},j+\frac{1}{2}}^{n+1}(t_{n+1}) &= \frac{1}{4}(\vec{C}_{i,j}^n + \vec{C}_{i+1,j}^n + \vec{C}_{i+1,j+1}^n + \vec{C}_{i,j+1}^n) \\
&\quad - \frac{\lambda}{2} \left( \vec{A}^1(\vec{C}_{i+1,j}^n) - \vec{A}^1(\vec{C}_{i,j}^n) + \vec{A}^1(\vec{C}_{i+1,j+1}^n) - \vec{A}^1(\vec{C}_{i,j+1}^n) \right) \\
&\quad - \frac{\mu}{2} \left( \vec{A}^2(\vec{C}_{i,j+1}^n) - \vec{A}^2(\vec{C}_{i,j}^n) + \vec{A}^2(\vec{C}_{i+1,j+1}^n) - \vec{A}^2(\vec{C}_{i+1,j}^n) \right). \quad (5.42)
\end{aligned}$$

## Second-Order Scheme (NT):

This section presents the second order numerical scheme [23] for nonlinear hyperbolic conservation laws. Similar to the case presented for the one-dimension, the first order Laxfriedrich (LxF) scheme is extended for the second order central scheme. It construct a piecewise polynomial (linear) interpolant depending on at each time step  $t_n$  for the cell average then interpolant yield the time and extended on the cell average at time level step  $t_{n+1}$  corresponding to Eq. (5.32), as result

$$\vec{C}(t_n, x, y) = \sum \left( \vec{C}_{i,j}^n + \vec{C}_{i,j}^x \left( \frac{x - x_i}{\Delta x} \right) + \vec{C}_{i,j}^y \left( \frac{y - y_j}{\Delta y} \right) \right) \chi_{i,j}(x, y). \quad (5.43)$$

Where,  $\vec{C}_{i,j}^x$  and  $\vec{C}_{i,j}^y$  representing the discrete slope of cell averages in the direction of  $x$  and  $y$ -coordinate, respectively. Discreet derivatives of conserved quantity are computed by second order accuracy,

$$\vec{C}_{i,j}^x \sim \Delta x \frac{\partial}{\partial x} \vec{C}(t_n, x_i, y) + O(\Delta x^2), \quad \vec{C}_{i,j}^y \sim \Delta y \frac{\partial}{\partial y} \vec{C}(t_n, x, y_j) + O(\Delta y^2). \quad (5.44)$$

These slopes are approximated by the non-oscillatory schemes for the family of discretized derivatives which is parameterized by  $\theta \in [1, 2]$ , e.g.

$$\vec{C}_{i,j}^x = MM \left[ \theta \left\{ (\vec{C}_{i+1,j}^n - \vec{C}_{i,j}^n), \frac{1}{2}(\vec{C}_{i+1,j}^n - \vec{C}_{i-1,j}^n), (\vec{C}_{i,j}^n - \vec{C}_{i-1,j}^n) \right\} \right], \quad (5.45)$$

$$\vec{C}_{i,j}^y = MM \left[ \theta \left\{ (\vec{C}_{i,j+1}^n - \vec{C}_{i,j}^n), \frac{1}{2}(\vec{C}_{i,j+1}^n - \vec{C}_{i,j-1}^n), (\vec{C}_{i,j}^n - \vec{C}_{i,j-1}^n) \right\} \right]. \quad (5.46)$$

Where,  $MM$  indicates the nonlinear min-mod limiter as defined earlier in Eq. (5.31). The piecewise (linear) reconstruction defined in (5.43) for  $\vec{C}(t_n, x, y)$  guarantees  $\sum \vec{C}_{i,j}^n \chi_{i,j}(x, y)$ , a piecewise linear constant approximations.

As for single dimensional state, the framework of the central scheme yield a second order step of exact reconstruction. By integrating Eq. (5.37) over the control volume representing by  $[i, i + 1] \times [j, j + 1] \times [t_n, t_{n+1}]$ , yields

$$\begin{aligned} \vec{C}_{i,j+\frac{1}{2}}^{n+1} &= \int_{C_{i+\frac{1}{2},j+\frac{1}{2}}} \vec{C}(t_n, x, y) dx dy \\ &\quad - \lambda \left\{ \int_{t_n}^{t_{n+1}} \int_{y_j}^{y_{j+1}} \left[ \bar{A}^1(\vec{C}(t, x_{i+1}, y)) - \bar{A}^1(\vec{C}(t, x_i, y)) \right] dy dt \right\} \\ &\quad - \mu \left\{ \int_{t_n}^{t_{n+1}} \int_{x_i}^{x_{i+1}} \left[ \bar{A}^2(\vec{C}(t, x, y_{j+1})) - \bar{A}^2(\vec{C}(t, x, y_j)) \right] dx dt \right\}. \end{aligned} \quad (5.47)$$

Here, cells averages  $\int_{C_{i+\frac{1}{2},j}} \vec{C}(t_n, x, y) dx dy$  are approximate in the first step by the  $C_{i,j}$ ,  $C_{i+1,j}$ ,  $C_{i+1,j+1}$  and  $C_{i,j+1}$  cells. Then initialized at corner by the intersecting of  $C_{i,j}$  as shown in Figure 5.2,  $C_{i+\frac{1}{2},j+\frac{1}{2}}^{SW} = C_{i+\frac{1}{2},j+\frac{1}{2}} \cap C_{i,j}$ , finally we get the exact staggered averages by Eq. (5.43),

$$\begin{aligned} \int_{C_{i+\frac{1}{2},j+\frac{1}{2}}^{SW}} \vec{C}(t_n, x, y) dx dy &= \int_{x_i}^{x_{i+\frac{1}{2}}} \int_{y_j}^{y_{j+\frac{1}{2}}} \left( \vec{C}_{i,j}^n + \vec{C}_{i,j}^x \left( \frac{x - x_i}{\Delta x} \right) + \vec{C}_{i,j}^y \left( \frac{y - y_i}{\Delta y} \right) \right) dx dy \\ &= \frac{1}{4} \left[ \vec{C}_{i,j}^n + \frac{1}{4}(\vec{C}_{i,j}^x + \vec{C}_{i,j}^y) \right]. \end{aligned} \quad (5.48)$$

Now, calculating in reverse (anticlockwise) direction, one can get

$$\int_{C_{i+\frac{1}{2},j+\frac{1}{2}}^{SE}} \vec{C}(t_n, x, y) dx dy = \frac{1}{4} \left[ \vec{C}_{i+1,j}^n + \frac{1}{4}(-\vec{C}_{i+1,j}^x + \vec{C}_{i+1,j}^y) \right], \quad (5.49)$$

$$\int_{C_{i+\frac{1}{2},j+\frac{1}{2}}^{NE}} \vec{C}(t_n, x, y) dx dy = \frac{1}{4} \left[ \vec{C}_{i+1,j+1}^n - \frac{1}{4}(\vec{C}_{i+1,j+1}^x + \vec{C}_{i+1,j+1}^y) \right], \quad (5.50)$$

$$\int_{C_{i+\frac{1}{2},j+\frac{1}{2}}^{NW}} \vec{C}(t_n, x, y) dx dy = \frac{1}{4} \left[ \vec{C}_{i,j+1}^n + \frac{1}{4}(\vec{C}_{i,j+1}^x - \vec{C}_{i,j+1}^y) \right]. \quad (5.51)$$

Here, the exact staggered cell averages for the piecewise linear reconstructions can be estimated at time  $t = t_n$ , by adding Eqs. (5.48)–(5.51)

$$\begin{aligned}
\bar{C}_{i+\frac{1}{2},j+\frac{1}{2}}^n &= \int_{C_{i+\frac{1}{2},j+\frac{1}{2}}} \vec{C}(t_n, x, y) dx dy \\
&= \frac{1}{4} \left( \bar{C}_{i+1,j}^n + \bar{C}_{i,j}^n + \bar{C}_{i,j+1}^n + \bar{C}_{i+1,j+1}^n \right) \\
&\quad + \frac{1}{16} \{ (\bar{C}_{i,j}^x - \bar{C}_{i+1,j}^x) + (\bar{C}_{i,j}^y - \bar{C}_{i,j+1}^y) + (\bar{C}_{i+1,j}^y \\
&\quad + (\bar{C}_{i,j+1}^x - \bar{C}_{i+1,j+1}^x) - \bar{C}_{i+1,j+1}^y) \}. \tag{5.52}
\end{aligned}$$

Therefore, exact evaluation of conserved quantities is depending on the integration of four fluxes Eq. (5.47) over staggered cell average. On the other hand, fluxes on right are approximated by middle-point rule and start from east face, see in Figure 5.3, we have

$$\int_{t_n}^{t_{n+1}} \int_{y \in J_{j+\frac{1}{2}}} \vec{A}(\vec{C}(t, x_{i+1}, y)) dy dt.$$

By the midpoint rules evaluation of the flux integral ,

$$\int_{y \in J_{j+\frac{1}{2}}} \vec{A}^1 \left( \vec{C}(t_{n+\frac{1}{2}}, x_{i+1}, y) \right) dy,$$

the rectangular quadratures rule of second order is applied on the spatial integrations in the  $y$ -direction, gives

$$\int_{t_n}^{t_{n+1}} \int_{y \in J_{j+\frac{1}{2}}} \vec{A}^1 \left( \vec{C}(t, x_{i+1}, y) \right) dy dt \sim \frac{1}{2} \left( \vec{A}^1(\bar{C}_{i+1,j}^{n+\frac{1}{2}}) + \vec{A}^1(\bar{C}_{i+1,j+1}^{n+\frac{1}{2}}) \right). \tag{5.53}$$

By taking the similar approach, all the other fluxes can be approximated,

$$\int_{t_n}^{t_{n+1}} \int_{x \in I_{i+\frac{1}{2}}} \vec{A}^2 \left( \vec{C}(x, y_{j+1}, t) \right) dx dt \sim \frac{1}{2} \left( \vec{A}^2(\bar{C}_{i,j+1}^{n+\frac{1}{2}}) + \vec{A}^2(\bar{C}_{i+1,j+1}^{n+\frac{1}{2}}) \right), \tag{5.54}$$

$$\int_{t_n}^{t_{n+1}} \int_{y \in J_{j+\frac{1}{2}}} \vec{A}^1 \left( \vec{C}(x_i, t, y) \right) dy dt \sim \frac{1}{2} \left( \vec{A}^1(\bar{C}_{i,j}^{n+\frac{1}{2}}) + \vec{A}^1(\bar{C}_{i,j+1}^{n+\frac{1}{2}}) \right), \tag{5.55}$$

$$\int_{t_n}^{t_{n+1}} \int_{x \in I_{i+\frac{1}{2}}} \vec{A}^2 \left( \vec{C}(x, y_j, t) \right) dx dt \sim \frac{1}{2} \left( \vec{A}^2(\bar{C}_{i,j}^{n+\frac{1}{2}}) + \vec{A}^2(\bar{C}_{i+1,j}^{n+\frac{1}{2}}) \right). \tag{5.56}$$

The fluxes in Eqs. (5.53)–(5.56) use the midpoint values,  $\vec{C}_{i,j}^{n+\frac{1}{2}} = \vec{C}(t_{n+\frac{1}{2}}, x_i, y_j)$ , here for turn to advantages of using these mid point values for the spatial integration by applying the rectangular method. In other words, these mid point values are barred at center of the cells,  $C_{i,j}$ , these approximated values are capture by using the Taylor expansion, as

$$\vec{C}(t_{n+\frac{1}{2}}, x, y) = \vec{C}_{i,j}^n + \left(\frac{\Delta t}{2}\right) \vec{C}_t(t_n, x, y) + O(\Delta t^2).$$

At the final step, using the system of conservation law Eq. (5.37) to intimate time derivative  $\vec{C}_t$ , in the spatial discrete slope derivatives expression, given by  $\vec{A}_1(\vec{C})_x$  and  $A_2(\vec{C})_x$ ,

$$\begin{aligned} \vec{C}_{i,j}^{n+\frac{1}{2}} &= \vec{C}_{i,j}^n - \left(\frac{\Delta t}{2}\right) \frac{\partial}{\partial x} \vec{A}^1(\vec{C}_{i,j}) - \left(\frac{\Delta t}{2}\right) \frac{\partial}{\partial y} \vec{A}^2(\vec{C}_{i,j}) + O(\Delta t)^2 \\ &= \vec{C}_{i,j}^n - \frac{\lambda}{2} \left(\vec{A}^{(1)x}\right) (\vec{C}_{i,j}) - \frac{\mu}{2} \left(\vec{C}^{(2)y}\right) (\vec{C}_{i,j}) + O(\Delta t^2). \end{aligned} \quad (5.57)$$

Here,

$$\begin{aligned} \vec{A}^{(1)x}(\vec{C}_{i,j}) &\sim \Delta x \frac{\partial}{\partial x} \vec{A}^1(\vec{C}(x_i, y_j, t_n)) + O(\Delta x^2), \\ \vec{A}^{(2)y}(\vec{C}_{i,j}) &\sim \Delta y \frac{\partial}{\partial y} \vec{A}^2(\vec{C}(x_i, y_j, t_n)) + O(\Delta y^2), \end{aligned}$$

are represented the two-dimensional approximated slopes of fluxes across  $x$  and  $y$ –direction, of the form reconstruct in Eq. (5.44). At the final step, these discrete slopes in the similar manner can be constructed for conservative system of vectors by using nonlinear limiter (MM) procedure. The staggered cell average in Eq. (5.52), together with discrete slopes are inserted into Eq. (5.47).



By computing the staggered cell averages at the next time level step  $t_{n+1}$ , we have

$$\begin{aligned}
\vec{C}_{i+\frac{1}{2},j+\frac{1}{2}}^{n+1} &= \frac{1}{4}(\vec{C}_{i,j}^n + \vec{C}_{i,j+1}^n + \vec{C}_{i+1,j}^n + \vec{C}_{i+1,j+1}^n) \\
&+ \frac{1}{16}(\vec{C}_{i,j}^x - \vec{C}_{i+1,j}^x) - \frac{\lambda}{2} \left( -\vec{A}^1(\vec{C}_{i,j}^{n+\frac{1}{2}}) + \vec{A}^1(\vec{C}_{i+1,j}^{n+\frac{1}{2}}) \right) \\
&+ \frac{1}{16}(\vec{C}_{i,j+1}^x - \vec{C}_{i+1,j+1}^x) - \frac{\lambda}{2} \left( -\vec{A}^1(\vec{C}_{i,j+1}^{n+\frac{1}{2}}) + \vec{A}^1(\vec{C}_{i+1,j+1}^{n+\frac{1}{2}}) \right) \\
&+ \frac{1}{16}(\vec{C}_{i,j}^y - \vec{C}_{i,j+1}^y) - \frac{\sigma}{2} \left( \vec{A}^2(\vec{C}_{i,j+1}^{n+\frac{1}{2}}) - \vec{A}^2(\vec{C}_{i,j}^{n+\frac{1}{2}}) \right) \\
&+ \frac{1}{16}(\vec{C}_{i+1,j}^y - \vec{C}_{i+1,j+1}^y) - \frac{\sigma}{2} \left( \vec{A}^2(\vec{C}_{i+1,j+1}^{n+\frac{1}{2}}) - \vec{A}^2(\vec{C}_{i+1,j}^{n+\frac{1}{2}}) \right). \tag{5.58}
\end{aligned}$$

The central scheme is summarized by the following procedure. It is based on predictor-corrector technique which involves two steps Eqs. (5.57)–(5.58). In the first predictor step Nessyahu1 Eq. (5.57), the cell averages  $\vec{C}_{i,j}^n$  are approximate by mid points values denoted by  $\vec{C}_{i,j}^{n+\frac{1}{2}}$ . In the final corrector step Eq. (5.58). The final result in the second order accuracy nonoscillatory scheme. This scheme has not involved exact Riemann solver. The discrete slops  $\vec{C}^x$ ,  $\vec{C}^y$ ,  $\vec{A}^{(1)x}(\vec{C})$  and  $\vec{A}^{(2)y}(\vec{C})$  have nonoscillatory nature of current scheme under reconstructed behaviour which is followed the corrector of second order defined in Eq. (5.58), is used to compute the new cell average by  $\vec{C}_{i,j}^{n+1}$ . Central (NT) schemes are developed on predictor-corrector rule which based on two basic steps. At the initial step, the algorithm starts with the known values of cell averages then it is applied to the non-oscillatory (linear) piecewise reconstruction to predict point values. At the final corrector step, realizing the evolution of these first step predicted mid point value of reconstructed polynomial in term of their staggered cell averages. The central (NT) schemes does not require characteristic decomposition and Riemann solver which makes them stable, simple and efficient. The proposed schemes of the second order accuracy are depend on the MUSCL-type reconstructions. The numerical results of the second order and the (non-oscillatory) central schemes are presented by [22, 23].

## 5.3 Numerical Tests

Here, the different numerical schemes are presented to provide computational accuracy and efficiency of the relativistic hydrodynamics (RHD) flow model and this section also focus on complex flow structure of our model. Let us consider single and multi-dimensional (2D) benchmarks test problem of the numeric code for non-linear Euler system. Furthermore, the proposed scheme is implemented to solve the shock tube Riemann problems to demonstrate the higher accuracy. Some of these problems of SRHD schemes available in the literature [18, 67].

### 5.3.1 One-dimensional Problems

Numerical tests and their simulations for one-dimensional problems are presented to validate the performance.

#### **Problem 1: Relativistic blast wave-I**

The present problem is presented by different authors [12, 18, 66, 68]. The initial data of one-dimensional problem are shown below

$$\begin{aligned}(\rho, v, p, \omega, c) &= (10.0, 0.0, 13.33, 1.4, 1.0) && \text{if } x \leq 0.5, \\(\rho, v, p, \omega, c) &= (1.0, 0.0, 0.66 \times 10^{-6}, 1.67, 1.0) && \text{if } x > 0.5.\end{aligned}\tag{5.59}$$

Where,  $[0, 1]$  is the domain that discretized by 400 mesh points and the ideal gas is taken as fluid with adiabatic index. This problem is break into two initial states. In first state the transonic rarefaction wave propagates away from domain towards left whereas in the second state the shock wave propagates toward right. Here, it is assumed that the motion of fluid to the right moves with the mildly relativistic speeds ( $v = 0.70980c$ ). The blast wave accumulates the flow particles towards a dense shell that results in compressing by a factor and heating the fluid. According to the thermodynamic point of view it is seen that fluid is more relativistic but dynamically it is only mildly relativistic. Figure 5.4 presents these results graphically. The robustness of present numerical results are comparable with [18, 66, 68].

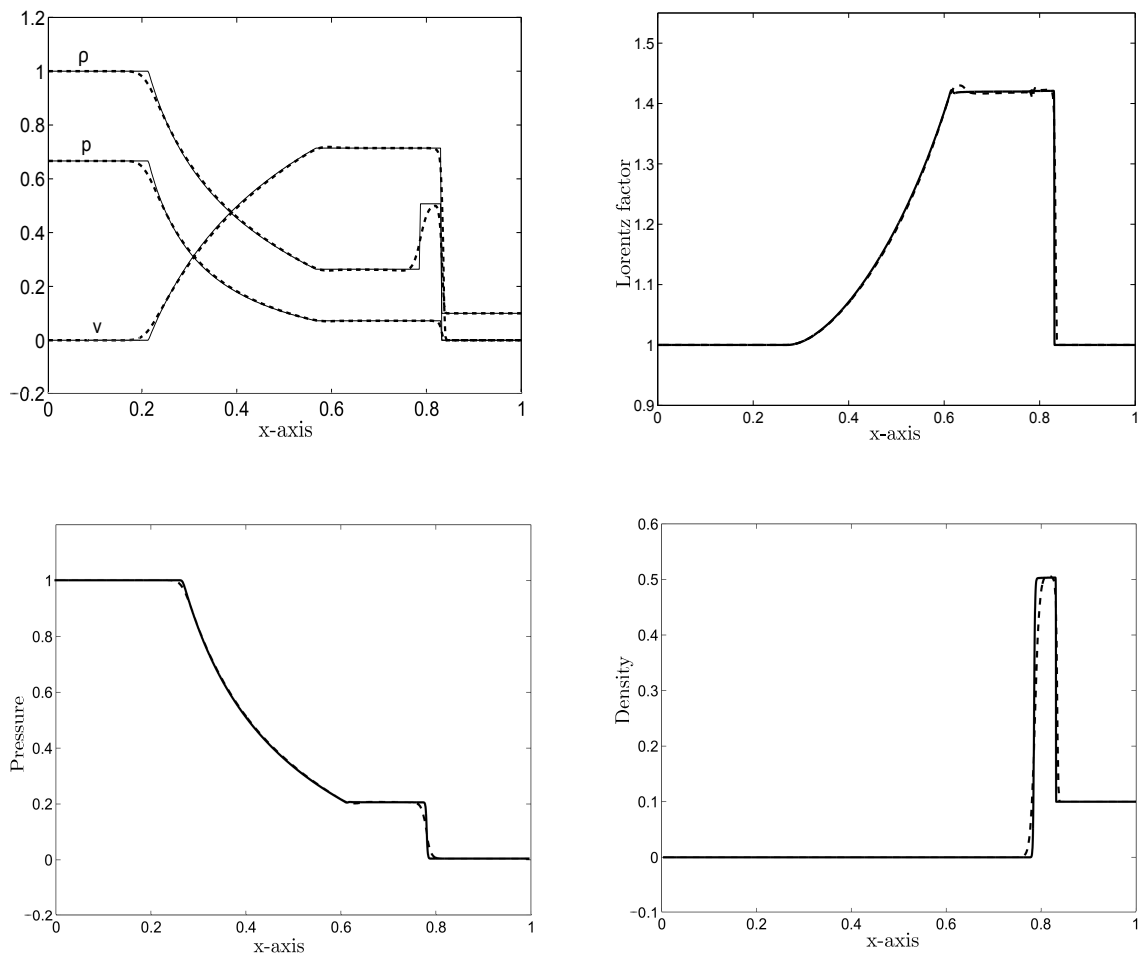


Figure 5.4: Comparison results at 400. mesh cells (dash line) versus 4000. mesh cells (solid line) when  $t = 0.40$ .

## Problem 2: Relativistic blast wave-II

This problem interaction between two blast waves proposed by Norman and Winkler [16], the initial test conditions can be defined by

$$\begin{aligned}(\rho, v, p, \omega, c) &= (1.0, 0.0, 1000.0, 1.4, 1.0) && \text{if } x < 0.5, \\(\rho, v, p, \omega, c) &= (1.0, 0.0, 0.01, 1.67, 1.0) && \text{if } x \geq 0.5.\end{aligned}$$

Computational domain is defined by  $[0, 1]$ . The fluid under the above conditions are more relativistic as compared to the problem 1 at the time  $t = 0.350$  with 4000 mesh cells. The solution of this test give rises the shock wave to the right, left travelling rarefaction waves and stationary contact discontinuity between them. Here, post shock wave is producing extremely thin layer dense shell of having width is only 2% of grid length. Relativistic shells that involve large density in contrasts is challenging for any type of numerical code. The movement of fluid in the dense shell is  $v_{\text{shell}} = 0.957$  (i.e.,  $\omega_{\text{shell}} = 3.35$  where the density takes jump to the value of 8.17 in the shell. The simulation solutions for the density along with velocity and pressure is presented by Figure 5.7.

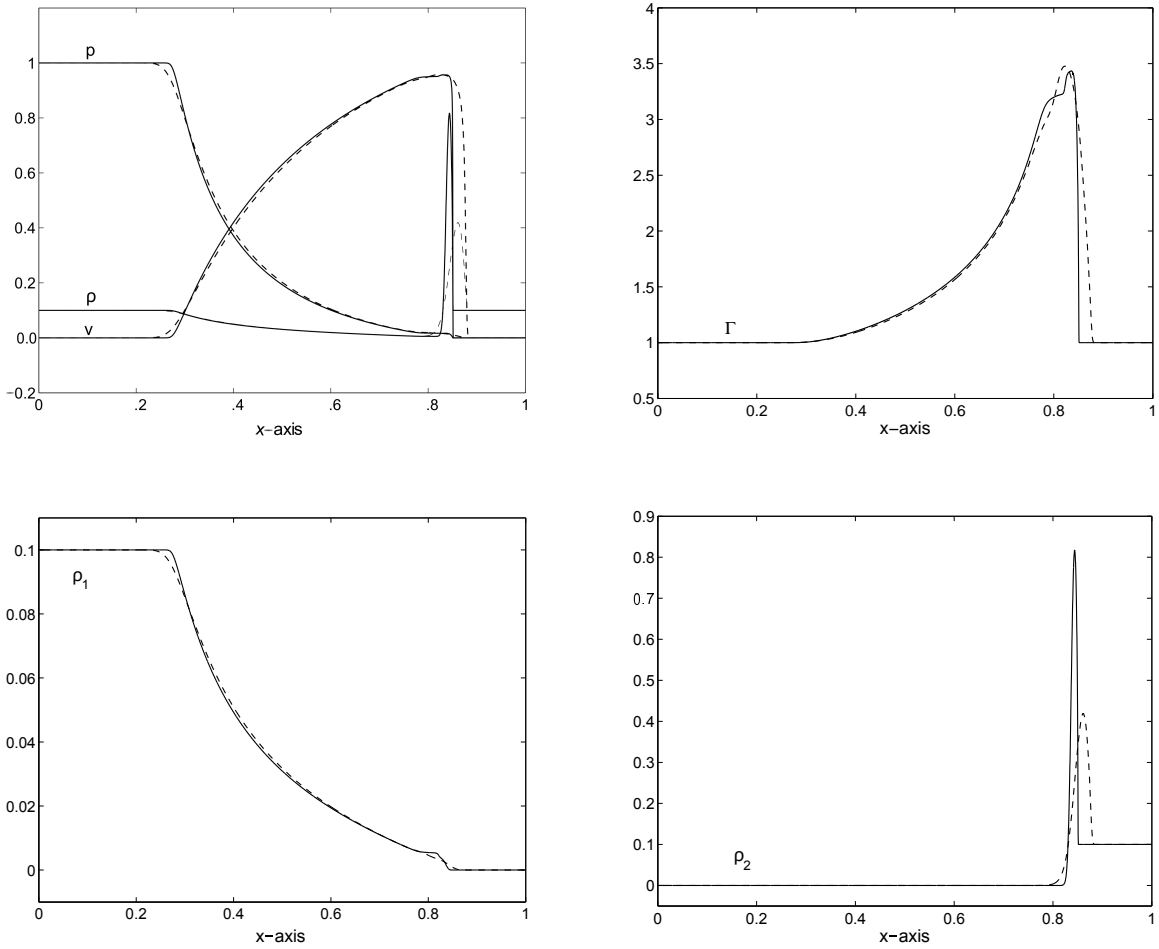


Figure 5.5: Comparison result on 400. mesh cells (dashed line) versus 4000. mesh cells (solid line) at  $t = 0.350$ .

### 5.3.2 Two-dimensional Problems

A relativistic hydrodynamics code incorporates the proposed non linear Euler equation for multi-relativistic flow, based on the center scheme. The ability of the code is test in order to handle the strong shocks in two-dimension. Here, we have executed through some standard tests that have published in literature.

#### Problem 3: Cylindrical blast problem

We consider the initial data for two-dimensional cylindrical explosion test problem as shown by

$$\begin{aligned}(\rho, v, p) &= (10.0, 0.0, 13.33) && \text{if } r \leq 0.2, \\(\rho, v, p) &= (1.0, 0.0, 0.066 \times 10^{-6}) && \text{otherwise.}\end{aligned}\tag{5.60}$$

The numerical computational is set to be in the square domain denoted by  $[0, 1] \times [0, 1]$ , that discretized by  $400 \times 400$  mesh cells with time step set to  $t = 0.15$ . The cylindrical explosion region having center at  $(0.5, 0.5)$  with radius 0.2 in the domain. In this case, the specific heat of the air and helium at constant volume is 1.0 whereas their specific heats ratios are 1.4 and 1.67, respectively. Here, consider the wave with circular rarefaction travels towards the origin whereas the circular shock waves travels outward from the origin, and followed by the circular contact discontinuity travels with similar directions. Figure 5.6 displays contour plots of the proposed scheme.

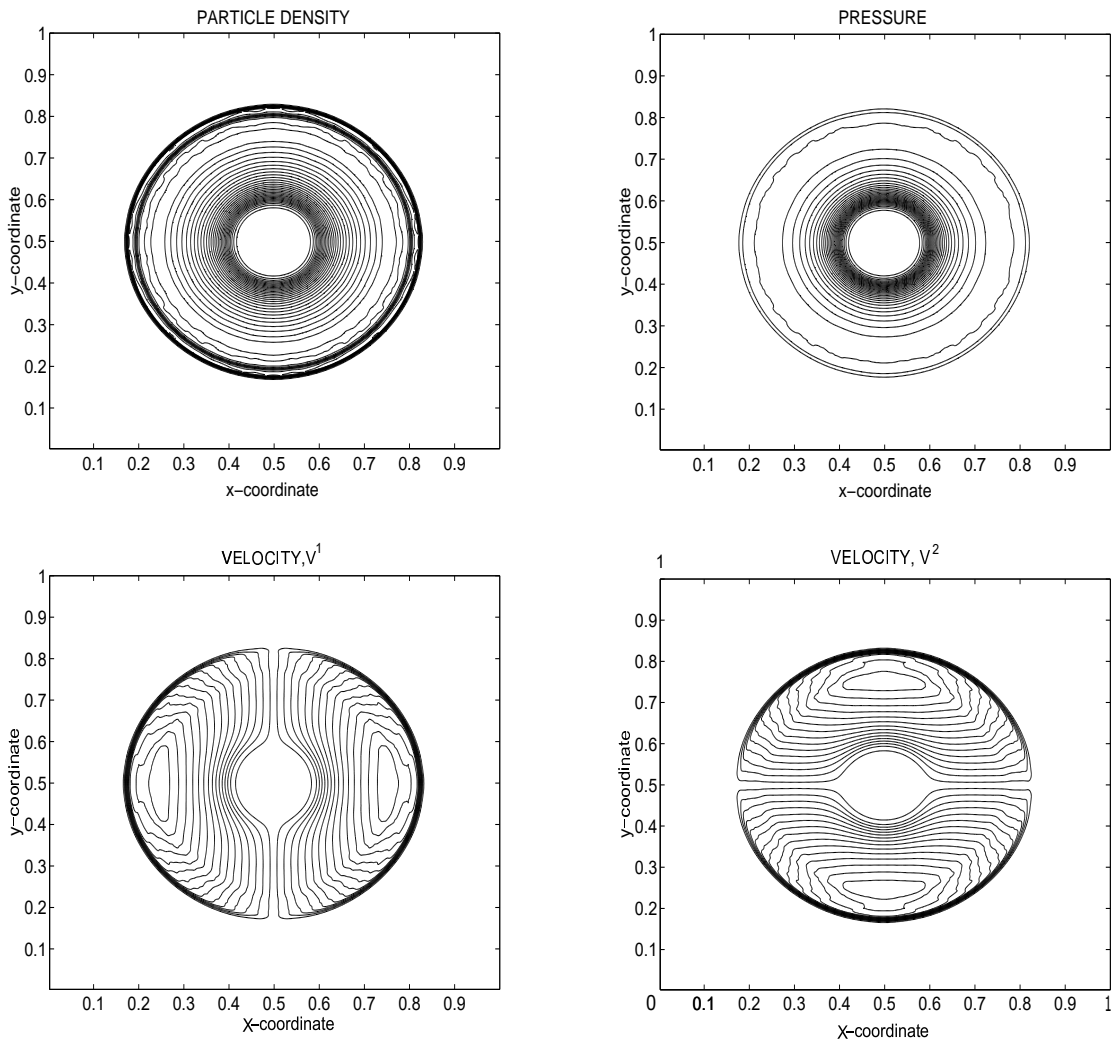


Figure 5.6: Result at  $t = 0.15$  for the cylindrical blast problem.



#### Problem 4: Cylindrical helium bubble

The analysis over the dynamics of shock-bubble interaction are investigated. A similar work on Cylindrical helium bubble problem has been investigated by Haas and Sturtevant [69] to estimate their code performance of the relativistic hydrodynamics. The interaction of the  $Ms = 1.16$  single planar shock interaction wave that is moving through the air along with the helium cylindrical bubble whereas, the surrounding air is heavier than the helium bubble. Computational setup more describe in Figure 5.9 will plot symmetrically in all four quadrants where the left and right boundaries are out flow quantities while upper and lower boundaries are both reflecting. It is noted the upstream and the the downstream boundaries treatment are not critical because there is no physical wave reach at these boundaries which are generated when its natural profile of shocks smear provide the exact discontinuity on the initial conditions. In front shock each grid points are initialized simply by one of the two states that are relay on its center lay inside or out side of the bubble. The very initial data in non-dimensionalized form can be written as

$$\begin{aligned}(\rho, v, p, \omega, c)^L &= (1.0, 0.0, 1.0, 1.4, 0.72) && \text{for the air pre-shock ,} \\(\rho, v, p, \omega, c)^M &= (1.36931, -0.178598, 1.55603, 1.4, 0.72) && \text{for the air post-shock ,} \\(\rho, v, p, \omega, c)^R &= (0.1368, 0.0, 1, 1.67, 2.42) && \text{for helium .}\end{aligned}$$

Additionally, the bubble region remains stable at low density. The results are shown in Figure 5.7. This is to notable that the inviscid simulation provides much qualitatively better agreement with the experiment depicts in the Figure 5.8.

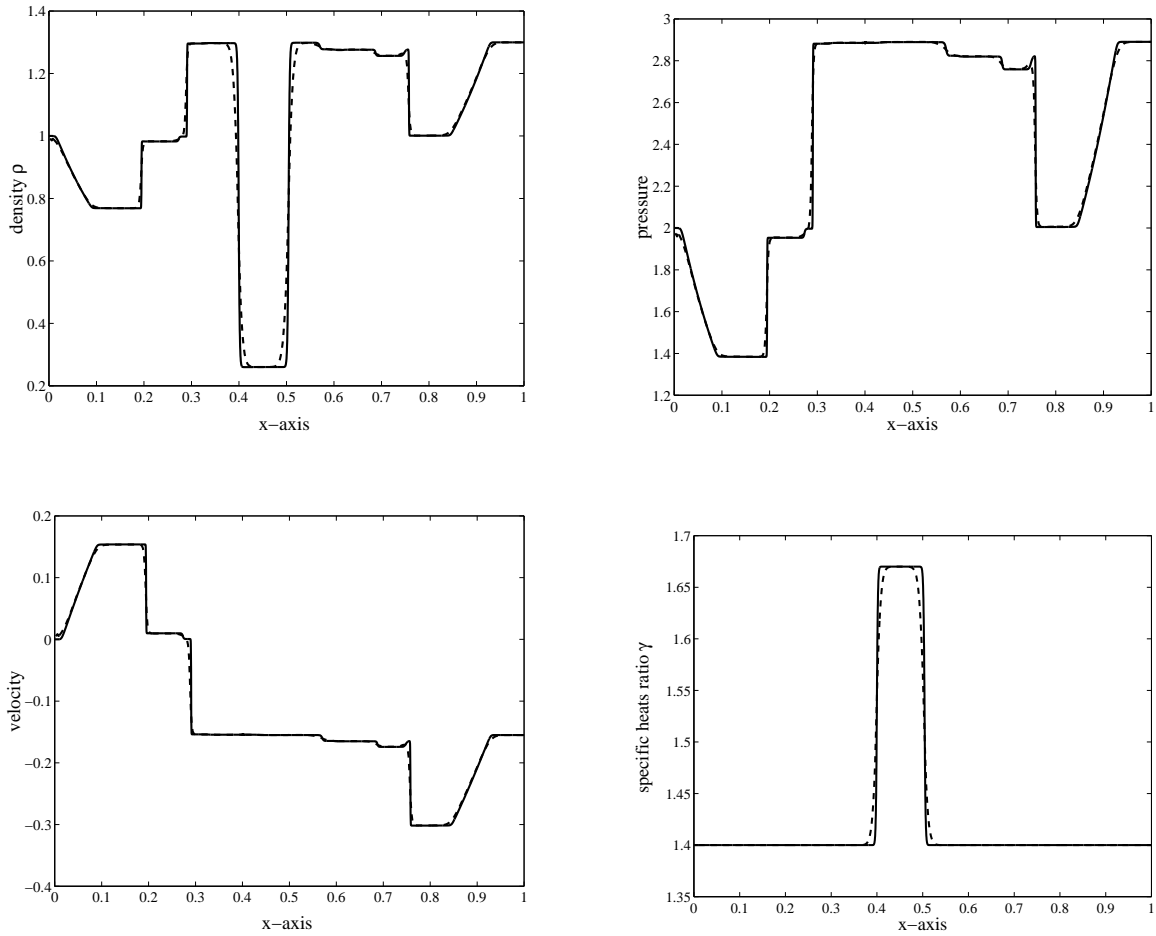


Figure 5.7: Comparison results on 400. mesh cells (dashed line) versus 4000. mesh cells (solid line) at the time  $t = 0.7$ .

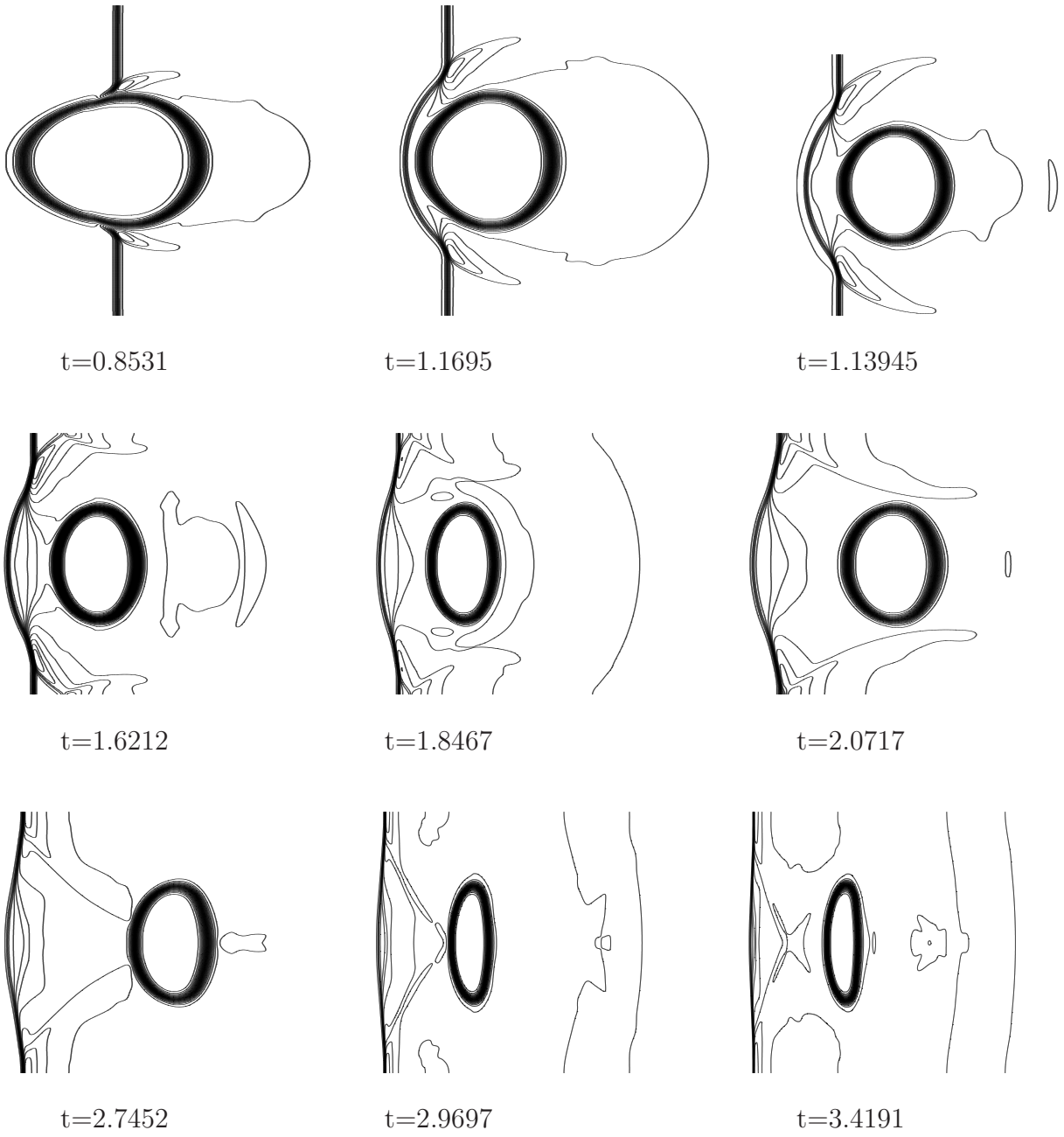


Figure 5.8: Results of heliumbubble interaction at different times.

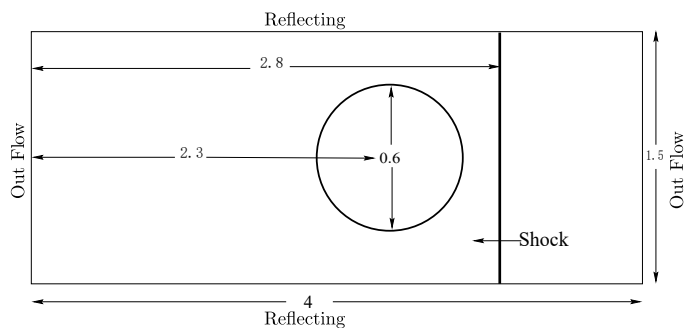


Figure 5.9: Computational domain for the shock wave.

### Problem 5: Explosion in the box

Initial conditions for the test problem are defined by the following equation

$$\begin{aligned}
 (\rho, v, p) &= (1.0, 0.0, 1000) & l = 0.2, \\
 (\rho, v, p) &= (1.0, 0.0, 10.0) & l = 1.0.
 \end{aligned}
 \tag{5.61}$$

Where  $l$  represents the length of the square boxes. The small box contains the helium gas at high pressure while the large box of length one contains air. Note that the small box having length 0.2 has taken placed at center of large box having length 1.0. Here, the numerical computational is set to be in the square region  $[0, 1] \times [0, 1]$  that is discretized by  $400 \times 400$  grid cells with reflecting walls. In this case, the specific heat of the air and helium at constant volume are equal to 0.72 and 2.42 whereas their specific heat ratios are 1.4 and 1.67, respectively. The proposed scheme is successfully applied to relativistic hydrodynamics as present in Figure 5.10.

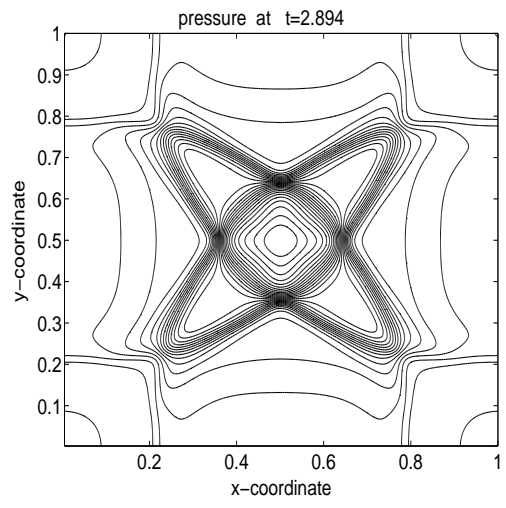
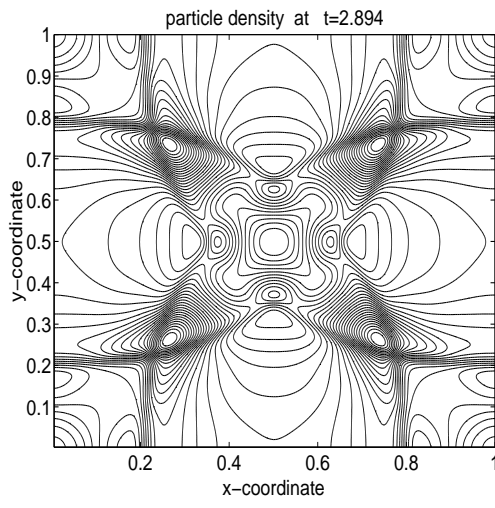
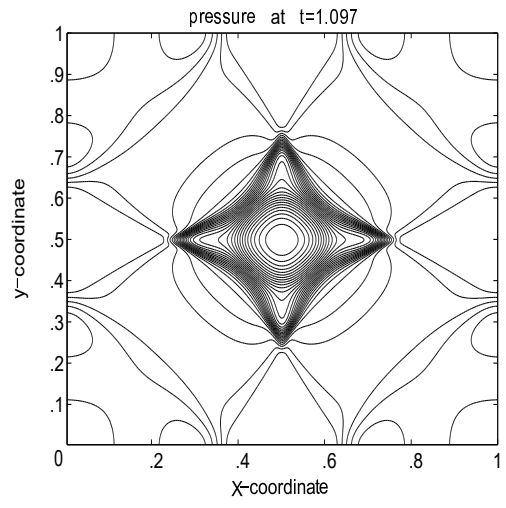
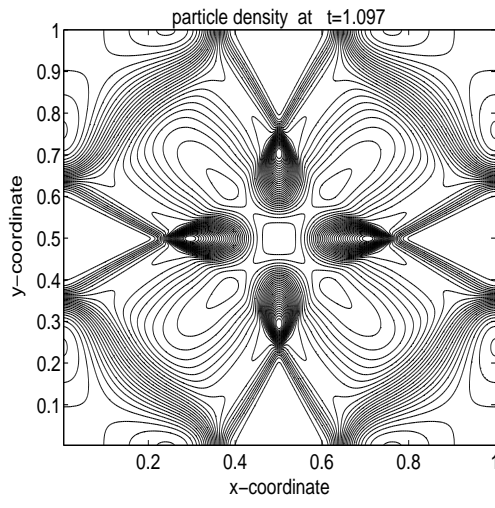


Figure continue...

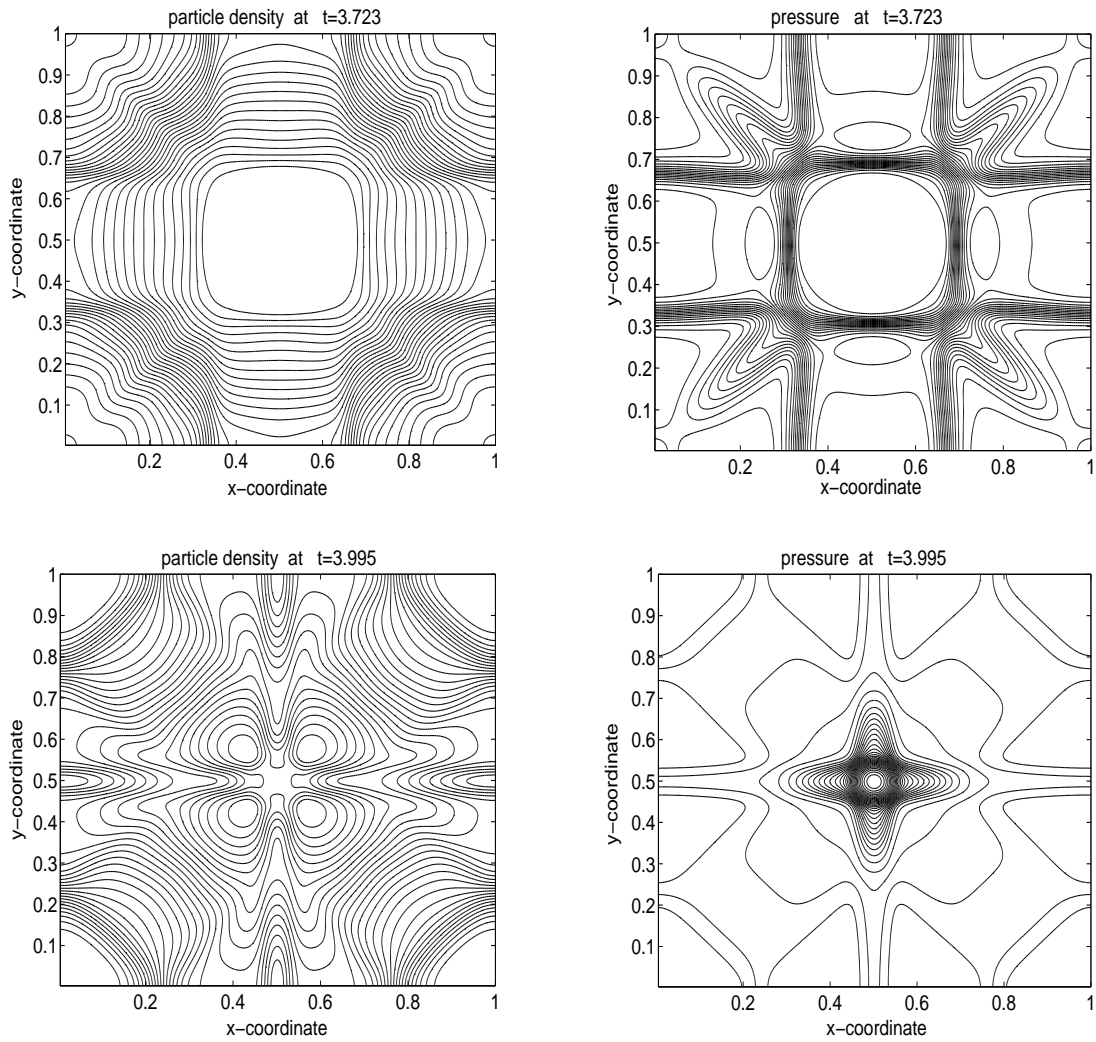


Figure 5.10: Results of explosion in the box at different times.

## 5.4 Summary

In our problem very high resolution scheme was implemented for the approximation of relativistic multi-component flow model equation. Similarly to non-classical case, the components in equilibrium state are coupled with space time possessing common velocity and temperature. For the validation of the schemes, several cases for one and two-dimensional problems were considered. Here, it was keenly observed that our suggested scheme has efficiently resolved such problems which have strong shocks removing the spurious oscillation. Therefore, the flow model is little complicated as compared to the classic case. In addition, due to relativistic effects narrower structures and higher jumps appear in the flow. The schemes ensure the exact conservation of mass for every integrant and also for the exact conservations of the total energy and momentum in the entire system of particles. It is observed that the execution of the central schemes through the computer machine are straightforward and compact. Although, the central schemes of second order are able to resolve contact discontinuity in a quite well manner. Moreover, central (NT) schemes do not require characteristic decomposition and Riemann solvers which makes them stable, reliable, simple and efficient.

## **Chapter 6**

### **Conclusions**



## 6.1 Evaluation of The Methods

In this thesis, the central upwind scheme was applied to numerically approximate the hyperbolic systems of special relativistic (SRHD) and ultrarelativistic hydrodynamic (URHD) models in one and two space dimensions. The suggested scheme has capability to capture the discontinues profiles of relativistic fluid flow with accuracy and avoids diffusion and dispersion in the solution numerically. It was found that the central upwind schemes are second-order accurate for smooth initial data in one and two space dimensions. The proposed scheme was found strongly connected to the analytical properties of the considered nonlinear equations that are designed for higher Lorentz factor with strong shocks. Furthermore, the central upwind schemes depends on the one-sided local speed of propagation that makes this scheme universal, accurate, simple and efficient.

The techniques were capable to simulate several complex and hard problems efficiently and precisely, corresponding to relativistic shock tube, perturbed shock tube, diffracting blast waves, explosion in the box, flow over the facing step, and cylindrical flow problem of both single and multi-dimensional SRHD model. Comparable set of numerical test cases were also conducted for URHD models. Reflecting, periodic, outflow and inflow conditions on the domain boundaries were applied in these test problems. The error analysis showed that central upwind scheme is second order accurate and produces less errors than the staggered central (NT) and KFVS schemes which were formulated for verifying the capability of the suggested scheme. Currently, only a few numerical schemes are available for relativistic hydrodynamics models. The suggested scheme has generated better results as compared to the schemes available in the literature [30, 56, 71, 72].

The central upwind scheme has capability to establish a considerable agreement between

the experimental and numerical results. The numerical approximated results of the KFVS and the staggered schemes are remarkable for the corresponding test problems. Although, in most of the cases solution profile of central upwind technique seemed to be more authentic than the others techniques [23, 55, 58]. Moreover, the computational costs of all schemes were of the order of few seconds in the one-dimensional case and of the order few minutes in a case of single dimension. Our numerical results have demonstrated the stability, high order accuracy of the suggested scheme.

The current dissertation was also concentrate on the analysis of one and two-dimensional relativistic hydrodynamic multi-component flow equations. Similarly to the non-classical case, the components in equilibrium state are coupled with space and time possessing common velocity and temperature. The same central upwind scheme was applied in order to solve corresponding model equations. For the current schemes validation, serval cases of one and two-dimensional problems where considered. It was observed that the suggested scheme has efficiently resolved the strong shocks and has avoided spurious oscillations. The multi-component relativistic flow model is more complicated as compared to classic one. In addition to relativistic effects, narrower structures and higher jumps appear in the flows. The schemes ensure the exact conservation of mass for every component and also the exact conservation of total energy and momentum in the entire particle system. It was also observed that computer programming of the central scheme is very simple and compact. The second order central upwind scheme has resolved the contact discontinuities quite well as compared to the central (NT) scheme which does not requires characteristic decomposition and Riemann solver.

We summarized that the results presented in this dissertation can be applicable for aca-

demic motivations, for understanding the considered complex processes, and could provide a doorstep for the future association with industry.

## 6.2 Future Considerations

In future, the current research analysis and investigation can be extended in various directions. The proposed models can be extended to special relativistic magnetohydrodynamic (SRMHD) models. The consequences of material parameters and of magnetic field can be investigated more rigorously through these extended models.

The current study can also be further extended to the theory of general relativistic hydrodynamic (GRHD) and to general relativistic magnetohydrodynamic (GRMHD) flow models. Implementation of the suggested numerical scheme for these models will be a new contribution in this area of research.

The theoretical results generated by suggested numerical schemes can be further validated via experimental results.

Finally, the considered scheme can also be extended and applied to other flow models arising in different science and engineering disciplines.

## Chapter 7

## References

1. Aloy, M. A., Ibáñez, J. M<sup>a</sup>., Martí, J. M<sup>a</sup>., Müller, E. (1999). GENESIS: A high-resolution code for 3d relativistic hydrodynamics. *Astrophys. J.* 122, 151-166.
2. Piran, T., Shemi, A., Narayan, R. (1993). Hydrodynamics of relativistic fireballs. *Mon. Not. R. Astron. Soc.* 263, 861-867.
3. Rodriguez, C. L., Amaro-Seoane, P., Chatterjee, S., Kremer, K., Rasio, F. A., Samsing, J., Ye, C. S., Zevin, M. (2018). Post-Newtonian Dynamics in Dense Star Clusters: Formation, Masses, and Merger Rates of Highly-Eccentric Black Hole Binaries. *arXiv preprint arXiv:1811.04926*.
4. Ma, T., Wang, S. 2014. Astrophysical dynamics and cosmology. *J. Math. Study.* 47(4), 305-378.
5. Csernai, L. P. (1994). Introduction to relativistic heavy ion collisions. *Wiley, Chichester, New York*.
6. Font, J. A., Ibáñez, J. M. (1998). A numerical study of relativistic Bondi-Hoyle accretion onto a moving black hole: Axisymmetric computations in a Schwarzschild background. *Astrophys. J.* 494(1), 297.

7. Wilson, J. R. (1972). A numerical method for relativistic hydrodynamics. In: Smarr, L. L., Ed., sources of gravitational radiation, Cambridge University Press, Cambridge, 423-446.
8. Tang, H. Z., Wu, H. M. (2000). Kinetic flux vector splitting for radiation hydrodynamical equations. *J. Comput. Fluids*. 29(8), 917-933.
9. Qamar, S., Warnecke, G. (2004). Simulation of multicomponent flows using high order central schemes. *App. Num. Math.* 50(2), 183-201.
10. Zeidan, D., Sekhar, T. R. (2018). On the wave interactions in the drift-flux equations of two-phase flows. *App. Math. Comput.* 327, 117-131.
11. Centrella, J., Wilson, J. R. (1984). Planar numerical cosmology II: The Difference Equations and Numerical Tests. *Astrophys. J.* 54, 229-249.
12. Hawley, J. F., Smarr, L. L., Wilson, J. R. (1984). A numerical study of nonspherical black hole accretion. II-Finite differencing and code calibration. *Astrophys. J. Supp. Series*. 55, 211-246.
13. Wilson, J. R. (1972). A numerical study of fluid flows in a Kerr space. *Astrophys. J.* 173, 431-438.
14. Bugner, M., Dietrich, T., Bernuzzi, S., Weyhausen, A., Brüggmann, B. (2016). Solving 3D relativistic hydrodynamical problems with weighted essentially nonoscillatory discontinuous Galerkin methods. *Phys. Rev. D.* 94(8), 084004.
15. von Neumann, J., Richtmyer, R. D. (1950). A method for the numerical calculation of hydrodynamic shocks. *J. App. Phys.* 21, 232-237.

16. Norman, M. L., Winkler, K.-H. A. (1986). Why ultrarelativistic hydrodynamics is difficult. In: Normanand, M. L. and Winkler, K.-H. A., Eds., *astrophysical radiation hydrodynamics*, reidel, Dordrecht, 449-476.
17. Martí, J. M<sup>a</sup>., Müller, E., Font, J. A., Ibáñez, J. M<sup>a</sup>. (1995). Morphology and dynamics of highly supersonic relativistic jets. *Astrophys. J. Letters*. 448, L105-L108.
18. Martí, J.M<sup>a</sup>., Müller, E. (1996). Extension of the piecewise parabolic method to One-dimensional Relativistic Hydrodynamics. *J. Comput. Phys.* 123, 1-14.
19. Kunik, M., Qamar, S., Warnecke, G. (2004). A BGK-type flux-vector splitting scheme for the ultrarelativistic Euler equations. *SIAM J. Sci. Comput.* 26(1), 196-223.
20. Qamar, S., Warnecke, G. (2005). A high order kinetic flux-splitting method for the special relativistic hydrodynamics. *IJCM*. 2(01), 49-74.
21. Kunik, M., Qamar, S., Warnecke, G. (2004). Kinetic schemes for the relativistic gas dynamics. *Num. Math.* 97(1), 159-191.
22. Nessyahu, H., Tadmor, E. (1990). Non-oscillatory central differencing for hyperbolic conservation Laws. *J. Comput. Phys.* 87(2), 408-463.
23. Jaing, G.-S., Tadmor, E. (1998). Nonoscillatory Central Schemes for Multidimensional Hyperbolic Conservation Laws. *SIAM J. Sci. Comput.* 19(6), 1892-1917.
24. Brysons, S., Kurganov, A., Levy, D., Petrova, G. (2005). Semi-discrete central-upwind schemes with reduced dissipation for Hamilton-Jacobi equations. *IMA J. of Num. Anal.* 25(1),

25. Ahmed, M., Saleem, M. R., Zia, S., Qamar, S. (2015). Central upwind scheme for a compressible two-phase flow model. *PloS one* 10(6), e0126273.
26. Qamar, S., Warnecke, G. (2006). Application of space-time CE/SE method to shallow water magnetohydrodynamic equations. *J. comput. Math.* 196(1), 132-149.
27. Qamar, S., Mudasser, S. (2010). On the application of a variant CE/SE method for solving two-dimensional ideal MHD equations. *J. Appl. Num. Math.* 60(6), 587-606.
28. Kurganov, A., Petrova, G. (2009). Central-upwind schemes for two-layer shallow water equations. *SIAM J. Sci. Comput.* 31(3), 1742-1773.
29. Qamar, S., Yousaf, M., Mudasser, S. (2011). The space-time CE/SE method for solving ultra-relativistic Euler equations. *Comput. Phys. Comm.* 182(4), 994-1004.
30. Qamar, S., Yousaf, M. (2013). Application of a discontinuous Galerkin finite element method to special relativistic hydrodynamic models. *Comput. Math. App.* 65(8), 1220-1232.
31. Friedrichs, K. O., Lax, P. D., (1971). Systems of conservation equations with a convex extension. *Proceed. Nation. Acad. Sci.* 68(8), 1686-1688.
32. Balbas, J., Karni, S. (2009). A central scheme for shallow water flows along channels with irregular geometry. *Math. Model Num.* 43, 333-351.
33. Nisar, U. A., Ashraf, W., Qamar, S. (2016). A splitting scheme based on the space-time CE/SE method for solving multi-dimensional hydrodynamical models of semiconductor devices. *Comput. Phys. Commun.* 205, 69-86.



34. Zeidan, D. (2016). Assessment of mixture two-phase flow equations for volcanic flows using Godunov-type methods. *App. Math. Comput.* 272, 707-719.
35. Kurganov, A., Noelle, S., Petrova, G. (2001). Semidiscrete central-upwind schemes for hyperbolic conservation laws and Hamilton–Jacobi equations. *SIAM J. Sci. Comput.* 23(3), 707-740.
36. Tang, H. Z., Xu, K. (2000). A high-order gas-kinetic method for multidimensional ideal magnetohydrodynamics. *J. Comput. Phys.* 165(1), 69-88.
37. Zanotti, O., Dumbser, M. (2015). High order numerical simulations of the Richtmyer–Meshkov instability in a relativistic fluid. *Phys. Fluids.* 27(7), 074105.
38. Eisberg, R., Resnick, D. (1985). Quantum physics of atoms, molecules, solids, nuclei and particles, second edition. Wiley, New York. 383-384.
39. Deshpande, S. M. (1986). A second-order accurate kinetic-theory-based method for inviscid compressible flows. NASA Langley Tech. 2613.
40. Mandal, J. C., Deshpande, S. M. (1994). Kinetic flux vector splitting for Euler equations. *Comput. Fluids J.* 23(2), 447-478.
41. Pullin, D.I. (1980). Direct simulation methods for compressible inviscid ideal gas flow. *J. Comput. Phys.* 34(2), 231-244.
42. Rietz, R. D. (1981). One-dimensional compressible gas dynamics calculations using the Boltzmann equation. *J. Comput. Phys.* 42(1), 108-123.
43. Perthame, B. (1992). Second-order Boltzmann schemes for compressible Euler equations in one and two space dimensions. *SIAM J. Numer. Anal.* 29(1), 1-19.

44. Croisille, J. P., Khanfir, R., Chanteur, G. (1995). Numerical simulation of the MHD equations by kinetic-type method. *J. Sci. Comput.* 10(1), 81-92.
45. Xu, K. (1999). Gas-kinetic theory based flux splitting method for ideal magnetohydrodynamics. *J. Comput. Phys.* 153(2), 334-352.
46. Tang, T., Xu, K. (1999). Gas-kinetic schemes for the compressible Euler equations: Positivity-preserving analysis. *Z. Angew. Math. Phys.* 50(2), 258-281.
47. Laney, C. B. (1998). Computational gasdynamics. Cambridge University Press, Cambridge.
48. Leveque, R. J. (2002). Finite volume methods for hyperbolic problems. Cambridge University Press, Cambridge.
49. Weinberg, S. (1972). Gravitation and cosmology: Principles and applications of the general theory of relativity. Wiley, New York.
50. Del Zanna, L., Bucciantini, N. (2002). An efficient shock-capturing central-type scheme for multidimensional relativistic flows. *I. Hydrodynamics*, A&A. 390, 1177-1186.
51. Kurganov A., Lin, C. (2007). On the reduction of numerical dissipation in central-upwind schemes. *J. Commun. Comput. Phys.* 2, 141-163.
52. Kurganov, A., Tadmor, E. (2000). New high-resolution central schemes for nonlinear conservation laws and convection-diffusion equations. *J. Comput. Phys.* 160(1), 241-282.

53. Yang, J. Y., Chen, M. H., Tsai, I. N., Chang, J. W. (1997). A kinetic beam scheme for relativistic gas dynamics. *J. Comput. Phys.* 136, 19-40.
54. Harutyunyan, A., Sedrakian, A., Rischke, D. (2018). Relativistic Dissipative Fluid Dynamics from the Non-Equilibrium Statistical Operator. *Particles.* 1(1), 155-165.
55. Zia, S., Qamar, S. (2014). A kinetic flux-vector splitting method for single-phase and two-phase shallow flows. *Comp. Math. Appli.* 67(6), 1271-1288.
56. Qamar, S., Yousaf, M. (2012). The space-time CESE method for solving special relativistic hydrodynamic equations. *J. Comput. Phys.* 231(10), 3928-3945.
57. Toro, E. F. (2013). Riemann solvers and numerical methods for fluid dynamics: a practical introduction. Springer Science & Business Media.
58. Kunik, M., Qamar, S., Warnecke, G. (2003). Kinetic schemes for the ultra-relativistic Euler equations. *J. Comput. Phys.* 187(2), 572-596.
59. Rao, P. L. (1981). Approximate Riemann solvers, parameter vectors and difference schemes. *J. Comput. Phys.* 43, 357-372.
60. He, P., Tang, H. (2012). An adaptive moving mesh method for two-dimensional relativistic hydrodynamics. *Commun. Comput. Phys.* 11(1), 114-146.
61. Nisar, U. A., Ashraf, W., Qamar, S. (2018). Application of kinetic flux vector splitting scheme for solving viscous quantum hydrodynamical model of semiconductor devices. *Result. Phys.* 11, 629-637.
62. Levy, D., Tadmor, E. (1997). Non-oscillatory central schemes for the incompressible 2-D Euler equations. *Math. Res. Lett.* 4, 321-340.

63. Aguayo-Ortiz, A., Mendoza, S., Olvera, D. (2018). A direct Primitive Variable Recovery Scheme for hyperbolic conservative equations: The case of relativistic hydrodynamics. *PloS one* 13(4), e0195494.
64. Bereux, F., Sainsaulieu, L. (1997). A Roe-type Riemann solver for hyperbolic systems with relaxation based on time-dependent wave decomposition. *Numerische Mathematik*. 77(2), 143-185.
65. Königl, A. (1980). Relativistic gas dynamics in two dimensions. *Phys. Fluids*. 23, 1083-1090.
66. Martí, J. M., Müller, E. (1999). Numerical hydrodynamics in special relativity. *Liv. Rev. Relativity*. 2, 1-101.
67. Thompson, K. (1986). The special relativistic shock tube. *J. Fluid. Mech.* 171, 365-375.
68. Schneider, V., Katscher, U., Rischke, D. H., Waldhauser, B., Maruhn, J. A., Munz, C.-D. (1993). New algorithms for ultra-relativistic numerical hydrodynamics. *J. Comput. Phys.* 105, 92-107.
69. Wu, K., Tang, H. (2018). On physical-constraints-preserving schemes for special relativistic magnetohydrodynamics with a general equation of state. *Z. Angew. Math. Phys.* 69(3), 84.
70. Ashraf, W., Qamar, S. (2013). Application of central schemes for solving radiation hydrodynamical models. *Comput. Phys. Commun.* 184, 1349-1363.

71. Zia, S., Ahmed, M., Qamar, S. (2014). A gas-kinetic scheme for six-equation two-phase flow model. *App. Math.* 5(03), 453.
72. Nisar, U. A., Ashraf, W., Qamar, S. (2017). Application of kinetic flux vector splitting scheme for solving multi-dimensional hydrodynamical models of semiconductor devices. *Result. Phys.* 7, 1915-1931.